Design, Fabrication, and Characterization of Controllable Conducting Polymer Actuation Systems

by

Eli Paster

B.S. Mechanical Engineering (2004)
University of Colorado at Boulder

Submitted to the Department of Mechanical Engineering
in Partial Fulfillment of the Requirements for the Degree of

Master of Science in Mechanical Engineering

at the

MASSACHUSETTS INSTITUTE OF TECHNOLOGY

June 2010

Signature of Author _____
Department of Mechanical Engineering
May 19, 2010

Certified by _____
Ian Hunter
Hatsopoulos Professor of Mechanical Engineering, Work Supervisor

Accepted by _____
David E. Hardt
Chairman, Department Committee on Graduate Students

Design, Fabrication, and Characterization of Controllable Conducting Polymer Actuation Systems

by

Eli Paster

Submitted to the Department of Mechanical Engineering
on 19 May, 2010 in partial fulfillment of the
requirements for the degree of
Master of Science in Mechanical Engineering

Abstract

The geometric, hierarchal, multifunctional composition of mammalian skeletal muscle and the neuromuscular system consists of actuation elements, length sensors, force sensors, localized energy storage, controlled energy delivery, computational components, and intercommunication pathways. Conducting polymer materials are versatile enough to perform all of the above functions. This work explores the design, characterization, and implementation of three conducting polymer components in building artificial muscle actuation systems: actuators, length sensors, and energy storage. The first systematic strain characterization of polypyrrole actuators at voltages above 1 V for a frequency range of 0.01 Hz to 100 Hz is reported. Material, mechanical, and electrical properties of polypyrrole length sensors are evaluated over the same frequency range. Polypyrrole supercapacitors are evaluated as a function of dopant, electrolyte, geometry, and mass, enabling the determination of their capacitance, charge-discharge lifetime, and self-discharge. Fabrication techniques for combining multiple conducting polymer components (actuators, length sensors, and energy storage elements) by means of electrically insulated, mechanical attachments are developed and demonstrated. An all-polymer, open loop linear contractile actuation system is presented, along with the first conducting polymer powered conducting polymer actuators, and the first tri-polymer system. These results build a foundation upon which large, scalable, self-powered, all polymer electro-chemo-mechanical actuation systems can be developed for a future set of conducting polymer artificial muscle systems.

Work Supervisor: Ian Hunter
Title: Hatsopoulos Professor of Mechanical Engineering

Acknowledgments

One of the most remarkable things about MIT is its community. There are world-class scientists, research laboratories par none, courses that cover even the most remote areas of science relevant to specialized disciplines, and an overall atmosphere of progress, work ethic, and teamwork. None of these elements have been lacking since the day I arrived.

I am grateful to Ian Hunter, who has provided a research laboratory in which, "anything can go from idea, to prototype, to reality, within a matter of weeks." There has never been a dearth scientific or intellectual resource in the BioInstrumentation Laboratory, and Ian has built both a research environment and a research group embodying this concept. In the study of science, sometimes we are searching for paths that have not yet been crossed, building bridges over rivers that run swiftly below our feet. Ian's steadfast vision and encouragement have been invaluable towards approaching these endeavors

I must thank my colleagues at the BioInstrumentation Laboratory, who have provided input that has both grounded and inspired me. Bryan Ruddy's long discussions on conducting polymers, chemistry, and science in general have helped me search for answers in places previously unbeknownst to me. Priam Pillai has provided the necessary skepticism in critiquing my experimental designs, always making them better, while being the cohesive force behind the conducting polymer group within the laboratory. Adam Wahab's resourcefulness, in turning any idea into reality with quick and clever solutions has helped me avoid several roadblocks. Brian Hemond's knowledge of electronics has helped point me in the right direction on more than one occasion. Scott McEuen's has been an excellent resource in contemplating and machining precision instrumentation. Cathy Hogan's knowledge of biology and experimentation has balanced the engineering aspects of my studies here. Jean Chang, Yi (Ellen) Chen, and Yenmei (Kerri) Keng have all made these first two years at MIT easier to navigate, and provided useful feedback and perspective. I am grateful to have had the opportunity to work alongside each member of the BioInstrumentation Laboratory, both inside and outside of the scientific discipline. I consider it honor to be in such good company.

Outside of the lab, Kurt Broderick and Vicky Diadiuk at the Microsystems Technology Laboratory have been excellent resources for turning substrates into devices.

The Department of the Interior deserves special thanks, for providing the financial support that has enabled this research to take place and take form.

Finally, I thank my wife, Zhang Xia, without which, none of this would be possible.

L'homme n'est rien d'autre que l'ensemble de ses actes,
rien d'autre que sa vie. *– Jean-Paul Sartre*

Table of Contents

List of Figures

Chapter 1 Overview

1.1 Introduction

If we examine the neuromuscular system of mammals, with consideration given to its hierarchal composition and each component's respective functionality, we cannot help but be astonished by its complexity, versatility, and adaptability across time and biological order. The skeletal muscle of the cheetah enables its rapid propulsion across the African desert. Not too a dissimilar muscle propels the blue whale through Antarctic waters. How can we engineer such a system and where should we begin?

A start would be to consider the actuation mechanism itself, a means by which we can artificially reproduce anisotropic strains and forces similar to the contractile subunit of mammalian muscle, the sarcomere. Not forgetting that energy must be stored, delivered, and controlled in order to regulate movement, we might consider the terminal cisternae and the sarcoplasmic reticulum, two components of the neuromuscular system that respectively store and regulate calcium ions that initiate muscle contraction. Since mammals have both capable and robust abilities to interact and move in precise and stable means within a variety of environments, muscle spindles and Golgi Tendon Organs (GTOs), which provide muscle length and local muscle tension feedback should also considered. Though the complexity of the mammalian neuromuscular system greatly exceeds this simple component breakdown, we have, at the very least, an idea of the building blocks out of which mammalian skeletal muscle is composed.

Conducting polymers are a versatile class of multifunctional materials that can be used to build artificial muscle systems. Conducting polymer actuators can be used to create linear contractile units, similar to the sarcomere. Depending on their geometry and configuration,

conducting polymer sensors can provide tensile or length measurements, much like the GTOs and spindles do. Conducting polymer supercapacitors, with large power densities, can provide localized energy storage, like the terminal cisternae and the sarcoplasmic reticulum. Conducting polymer transistors, wires, and electronic components can serve to regulate and deliver such energy. In short, though an artificial equivalent to the various components of the neuromuscular system differ in size, composition, and performance, through the multi-functionality of conducting polymers we may begin to develop the foundation from which artificial muscle systems can be realized.

1.2 Muscle and Artificial Muscle

Muscle is not the strongest, fastest, or most robust actuator known to exist, but a certain combination of performance metrics and versatile characteristics makes it suitable for both mammalian locomotion and desirable for man-made artificial systems. If one evaluates existing artificial muscle technologies with the same criteria as that of skeletal muscle, conducting polymers markedly stand out as viable candidates that may be able to replicate the full functionality of skeletal muscle and various components of the neuromuscular system. Since muscle is a complex, multi-component system, in designing artificial muscle systems one must consider the feasibility of combining components of varying functionalities that can interact on the same temporal and spatial realm as mammalian skeletal muscle. Here, conducting polymers and mammalian muscle share an important similarity: what they lack in superlative performance metrics is compensated for in versatility and girth.

From an engineering perspective, mammalian skeletal muscle typically produces strains up to 30%, with strain rates as fast as 100% per second [1]. While voluntary human skeletal muscle oscillates at frequencies below 20 Hz, skeletal muscle found in frogs can oscillate at up

to 200 Hz [2], and muscle in certain insects (such as the *Neoconocephalus robustus*) has be shown to produce synchronous contractions at up to 500 Hz [3]. Human muscular limbs can be held steady for extended periods of time, limited mostly by physiological tremor that occurs at a bandwidth between 7 and 12 Hz and is typically greater than 50 μm in amplitude [4]. In terms of force output, work density, and efficiency, skeletal muscle produces active stresses up to 0.35 MPa, work densities near 8 kJ/m^3, and efficiencies approaching 40% [1].

Various materials exist as potential choices for artificial muscles. A list of comparative artificial muscle technologies is shown in Table 1.

An examination of comparative technologies is necessary in the design of any new system. The actuators listed in Table 1 all carry certain merits in certain categories, but only a few of the materials are multifunctional. Ionic polymer metal composites can be used as actuators and sensors, but cannot store energy and are geometrically limited to bending applications [2]. Actuator materials limited solely to producing force or strain mandate that they be coupled with numerous external components (sensors, control electronics, batteries, etc.). While this is both feasible and employable, rarely are such systems compact or scalable over several orders of magnitude. With respect to artificial muscle systems, materials such as dielectric elastomers can provide significantly higher strains, strain rates, and work densities than skeletal muscle [5], but their high voltage requirements restrain them from many practical applications. Shape memory alloys offer significantly higher active stresses and faster contractile strain rates than mammalian skeletal muscle [6], but are more difficult to control and require high currents. Most importantly, however, is the concept that mammalian skeletal muscle, when considered as part of the central nervous system (CNS), requires integrated components.

Table 1: Comparison of artificial muscle actuators. From [1].

Actuator	Active strain	Active stress (MPa)	Work density (KJ/M^3)	Strain rate (%/s)	Efficiency	Operating voltage	Advantages	Disadvantages
Mammalian skeletal muscles	20	0.35	8	>50	40	N/A	Integrated system of energy storage, delivery, waste and heat removal; highly conserved	Yet to be man-made, requires specific thermal and chemical environment
Dielectric elastomers	up to 380	1	up to 3400	4500	30-90	< 1 kV	High stress and strain	High voltage requirements
Liquid crystal elastomers	0.5 -3	0.01 - 0.5	20	30-1000	75	1 to 25 MV/m	Relatively large strain (when thermally actuated), fast strain (electrically actuated)	Slow (when thermally actuated), high electric field requirements
Polypyrrole	39, 5 repeatable	up to 30	100	12	20	1 to 3 V	Low voltage, high stress, moderate strain	Slow, requires specific chemical conditions
Ionic polymer metal	0.5 - 3	3	up to 5	3	1.5-3	< 10 V	Low voltage,	Non-linear, only bending
Carbon nanotube actuators	< 1	up to 30	2	20	0.1	up to 30 V	Large operating temperature and range	Expensive, low active strains
Shape memory alloys	5	up to 200	>1000	300	<0.5	~ 25 V	High power requirement, low operating voltage	Difficult to control

From an economic perspective as well, multi-material systems require varied manufacturing processes, controlled tolerances, and assembly procedures. The cost of implementing these systems quickly increases with respect to the number of different components, required tolerances and production variations [7]. In this regard, conducting polymers are the most versatile artificial muscle technology [8]. With conducting polymers, fewer fabrication and combination techniques are required to produce devices with versatility on par with mammalian skeletal muscle, at a fraction of the manufacturing cost. For this reason, conducting polymers where chosen as the substrate from which the artificial muscle systems considered in this work were developed.

1.3 Organization of Work

Chapter 2 will give a brief overview of mammalian skeletal muscle and various building blocks of the neuromuscular system. **Chapter 3** presents the general mechanical, electrical, and chemical properties of conducting polymers. **Chapter 4** presents an evaluation of the performance of polypyrrole actuators, with emphasis on the relationships between actuation amplitude, bandwidth, energy and power requirements. **Chapter 5** presents the examination of polypyrrole length sensors with respect to material properties, lifetime, bandwidth and repeatability. **Chapter 6** discusses the investigation of polypyrrole supercapacitors, presenting studies on how polymer dopant, electrolyte, mass, and substrate affect overall capacitance, energy density, power density and self-discharge rates. **Chapter 7** focuses on fabrication techniques that enable the combination of conducting polymer components, investigating the material, electrical, and mechanical properties of adhesives, insulators, and thin films mechanical attachments. **Chapter 8** presents a combination of the research in Chapter 4 through Chapter 7,

in designing, fabricating, and testing all-polymer, multi-component, conducting polymer actuation systems. **Chapter 9** is a brief summary of the work presented and suggestions for further development.

Chapter 2 Muscle

2.1 Introduction

The neuromuscular system is an anisotropic, complex, hierarchal arrangement of components that allows molecular conformational changes occurring on the order of angstroms to synergistically produce macroscopic movement, ten orders of magnitude higher. Any attempt to mimic muscle from a systematic approach requires an understanding of its component mechanisms, the integration of these components, and the means by which they scale.

The biological system of muscle is not addressed here as a point of study, but as a point of departure, in an attempt to replicate some of muscle's functionality by creating analogous individual building block from which the neuromuscular system is composed. The organization of this chapter is therefore based on the study of each equivalent component in the neuromuscular systems that are replicated with conducting polymers in this work.

2.2 Energy: Storage, Regulation, and Delivery

Muscle observed on a macroscopic scale is composed of bundles of muscle fibers, each fiber containing myofibrils that are repeated in a longitudinal pattern along the muscle [9]. Each myofibril in turn consists of a bundle of myofilament. Each myofilament is composed of sarcomeres, cylindrical contractile units which repeat along the myofibril's length (Figure 1).

Integrated within the myofibril are terminal cisternae, discrete regions surrounding the myofibril that store the calcium necessary to excite muscle contraction upon the transduction of neural signals induced through action potentials from the CNS. Along the exterior of the myofibril are transvers tubules, deep invaginations of the sarcolemma which allow it to open

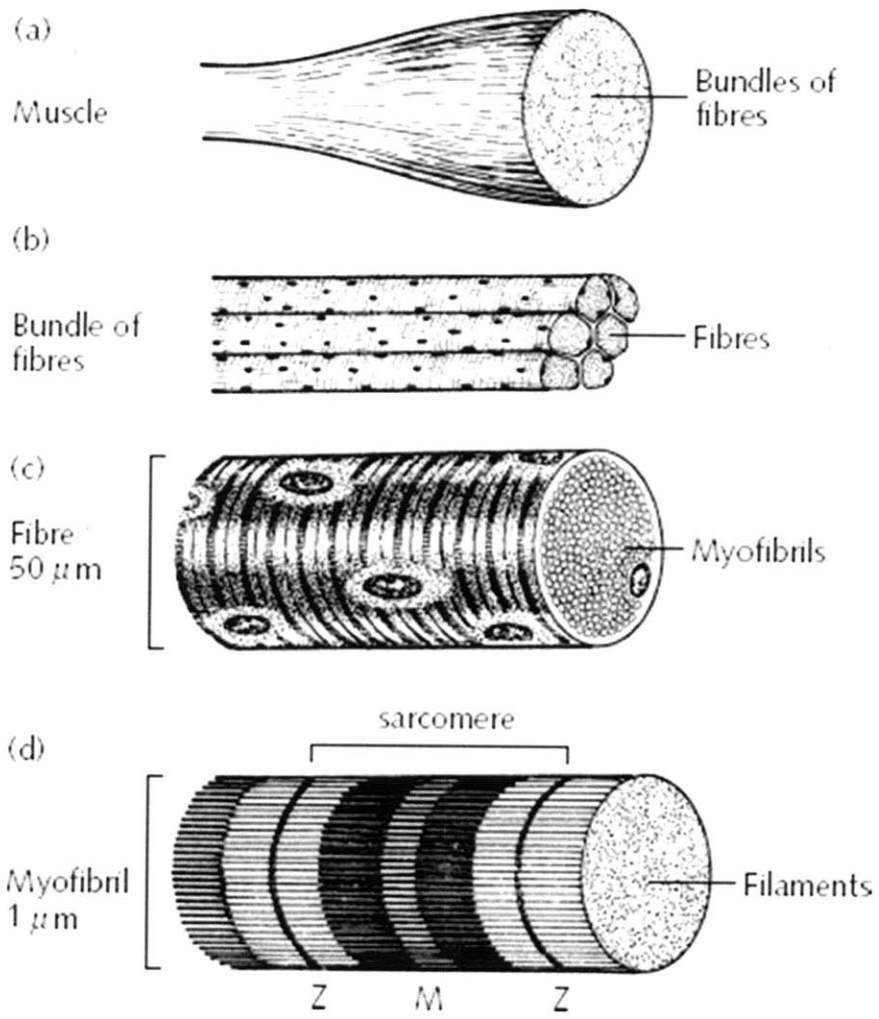

Figure 1: Hierarchal configuration of mammalian skeletal muscle. From [11].

and close [10]. The transvers tubules gate the flux of calcium into and out of the muscle, thereby regulating muscle contraction. Also along the perimeter of the myofibril are the sarcoplasmic reticulum, which serve to store and pump calcium ions (by release or absorbance) during muscular excitation and relaxation. Considered on the scale of myofibrils, muscle contraction is controlled by these embedded elements (terminal cisternae, transvers tubules, sarcoplasmic reticulum, etc.) which provide localized energy storage, delivery, and regulation (Figure 2).

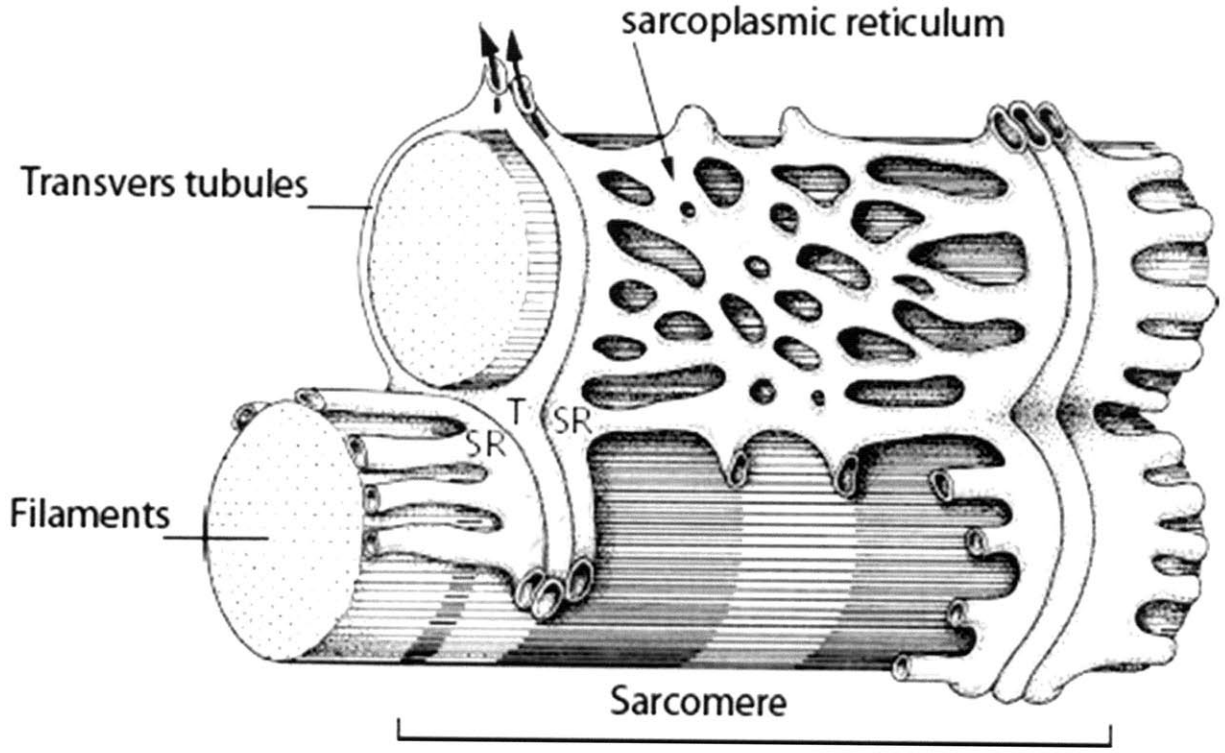

Figure 2: Localized energy storage and delivery components in mammalian skeletal muscle. From [11].

2.3 Actuators: The Sarcomere as the Contractile Unit

The digitized entity of muscle contraction is the sarcomere, the repetitive unit from which the myofibrils are composed [12]. The sarcomere is comprised of thick and thin filaments (Figure 3). The thin filaments primarily consist of filamentous actin, known to exist primarily as a helix of rotating subunits [13]. The thick filaments (floating in the middle of the sarcomere) are composed of type II myosin, helically wound chains with globular heads [14]. The commonly accepted theory of muscle contraction occurs by the interaction between actin and myosin filaments, where, through a cycle of chemical reactions, the thick and thin filaments "slide" past each other, causing sarcomere contraction [15]. Sarcomeres make up the bulk of the myofibril, which, when bundled together, form muscle fibers. By this means of scaling (in series and

parallel), the coordinated contraction of sarcomeres, that actuate due to allosteric changes, results in muscular actuation ten orders of magnitude higher.

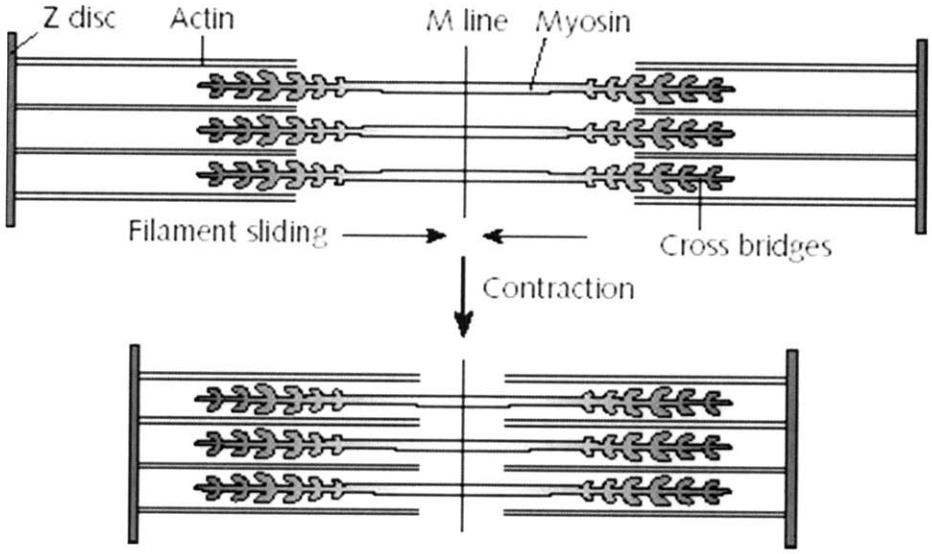

Figure 3: Diagram of the sarcomere, the contractile unit of mammalian skeletal muscle. The myosin thick filaments float in the center of the sarcomere while the actin thin filaments attach to the sarcomere's outer edges (the Z-disk). From [11].

2.4 Feedback: Length and Tension Sensors

The contractile components of muscle generate motion, however, it is the sensory components embedded within the neuromuscular system, interacting with the CNS, that allow motile organisms to understand and control the force and movement which they produce. The length and tension sensory components of the neuromuscular system are primarily composed of muscle spindles and Golgi Tendon Organs (Figure 4), measuring length and tension, respectively.

Muscle spindles are made up of distinct components that allow for accurate length measurement under different conditions of movement [10]. Spindles are composed of intrafusal muscle fibers, large-diameter myelinated sensor endings, and small diameter myelination endings. Nuclear bag fibers within the intrafusal muscle fibers are separated into two types, dynamic or static, depending on their form and function [16]. Dynamic nuclear bag fibers are

sensitive to rate changes in muscle length while static nuclear bag fibers are sensitive to the steady state length of the muscle. A contractile element within muscle spindles allows it to modify the feedback gain that muscle spindles provide to the CNS over a wide range of length states. Feedback in muscle is a multi-sensory combination of length measurements and accounts for both steady-state and dynamic conditions. This steady-state and time-varying feedback of muscular contraction enables the CNS to control the neuromuscular system with a remarkable degree of accuracy and robustness.

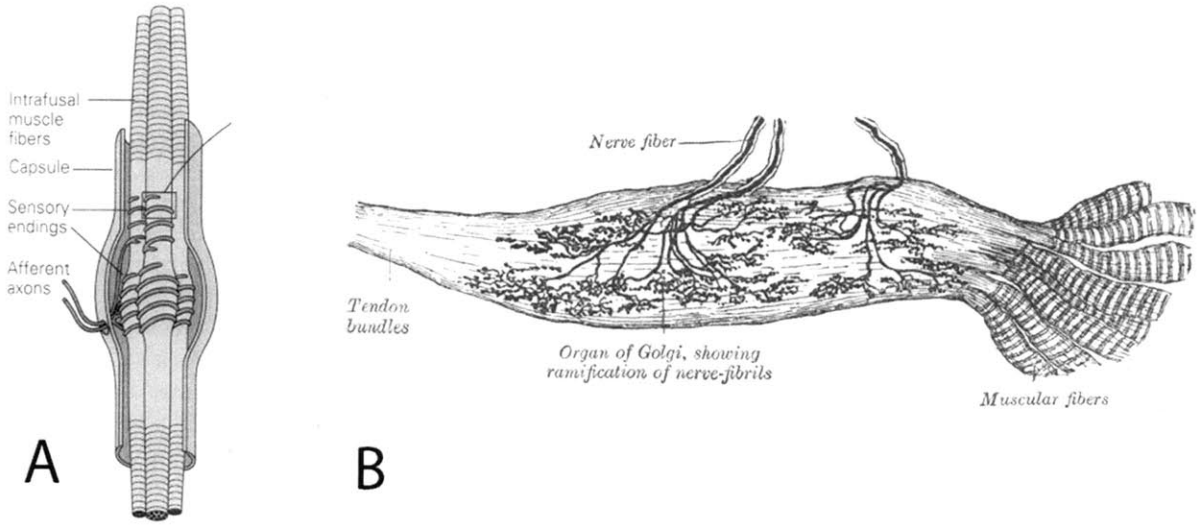

Figure 4: Length and tension sensors in mammalian skeletal muscle. (A) The muscle spindle, which measures dynamic and static length changes. (B) The Golgi Tendon Organ, which measures muscle tension. From [10].

Golgi Tendon Organs (GTO) are encapsulated structures that are intertwined among braided collagen fascicles that allow the measurement of muscle tension [17]. The GTOs are situated in series between the muscle fibers and tendons. Under strain, the GTOs straighten out the collagen fibers in which they are embedded, causing the compression of nerve endings which subsequently fire stimuli indicating increased or decreased muscular tension [18]. The integrated geometry of GTOs and collagen is such that small longitudinal strain (experienced under tension)

results in significant transverse compression, thereby allowing GTOs to maintain high sensitivity to small changes in length. GTOs provide feedback information about muscles state of tension, but do so only on a local scale with respect to the CNS. From a neural-sensory perspective, muscular movement and control is thus regulated in part by feedback provided from the static and dynamic length states of the muscle, in addition to the instantaneous tension a group of muscle fibers is subject to.

2.5 Summary

Mammalian skeletal muscle and the associated components of the neuromuscular system can be thought of as a compact system of power supplies, gates, and switches which regulate energy delivery, actuators, sensors, and computational elements. Neuromuscular control can be both open-loop, such as reflexive systems, or closed-loop, such as maintaining a steady posture, which occur through lower and higher neural operations respectively. Such complexity, integration, and conservation across thousands of biological orders beg the question: if the basic components of skeletal muscle are conserved (functionally and temporally) across enormous spans, what can we learn from each component and the system as a whole, if we attempt to mimic it? As we observe these molecular mechanisms that induce force and length changes ten orders of magnitude higher than the individual elements alone, where millions of muscular subunits are regulated by tens of thousands of individual sensors, energy storage areas, and controlled delivery mechanisms, we must approach such complexity with humility.

Chapter 3 Conducting Polymers

3.1 Theory of Conductivity

Since their inception in the early 19th century, polymers were believed to have a fundamental limitation in their chemical composition which prevented them from conducting electricity. In 1977, Heeger, MacDiarmid, and Shirakawa [19] demonstrated for the first time that polymers could conduct electricity if the synthesis and resultant chemical composition met certain criteria. These criteria for polymer conductivity are: (1) a conjugated backbone that runs along the polymer chain, consisting of a series of single and double bonds, and (2) a dopant.

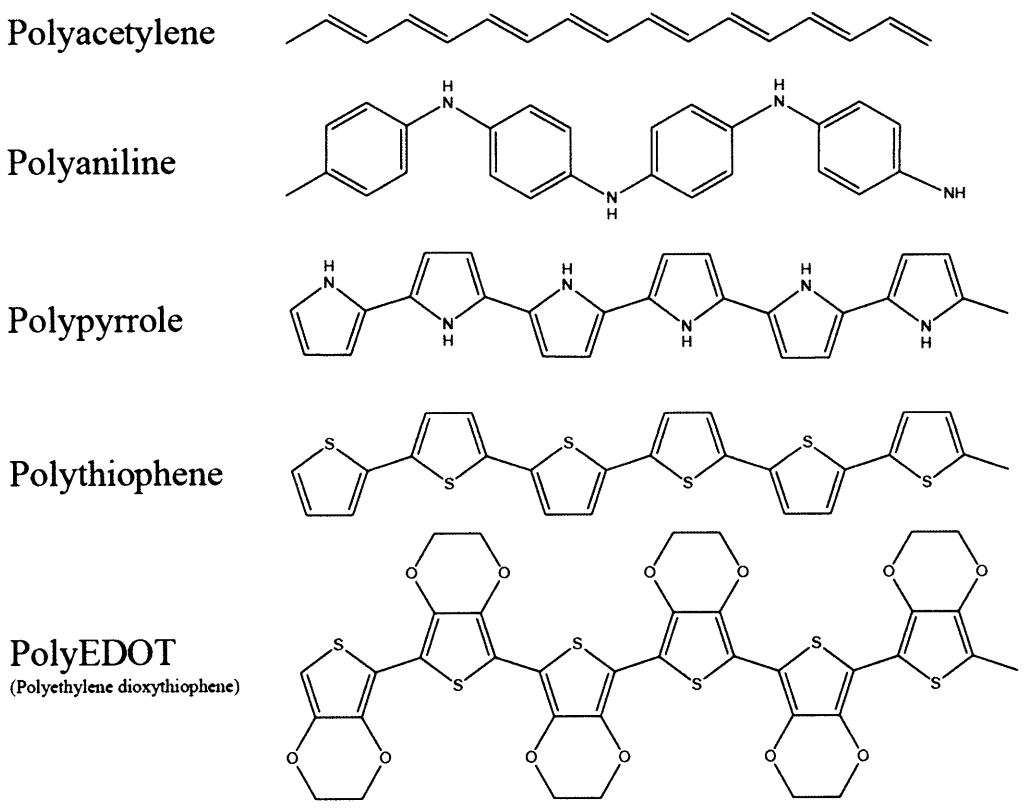

Figure 5: Conjugated backbone structures of various conducting polymers. From [29].

The conjugated backbone structure in conducting polymers enables electrons associated with the backbone's double bonds to become delocalized and therefore have increased mobility [20]. A series of conducting polymers with their associated conjugate backbones is shown in Figure 5. A dopant, normally incorporated into the polymer during fabrication, provides extra electrons that serve as charge carriers. Dopant molecules [21], monomer type, synthesis conditions [22], polymer structure [23, 24], etc., can all lead to varying polymer conductivities, with values approaching 10^4 S/m [25].

3.2 Synthesis through Electropolymerization

The conducting polymer polypyrrole has one of the highest conductivities among conducting polymers, is mechanically robust, and can be grown into free-standing thin films. For these reasons, polypyrrole has been chosen as the main conducting polymer used throughout this work.

Polypyrrole can be synthesized from the pyrrole monomer through chemical or electrochemical deposition. To date, electrochemical deposition yields higher film conductivities [24], and was therefore selected as the sole means of polymer growth and exploration within this work. While there are still unanswered questions regarding the exact polymerization process, a generally accepted set of mechanisms is shown in Figure 6.

The electrochemical deposition process begins in an electrochemical cell where at least two conducting electrodes are separated by an electrolyte that contains the pyrrole monomer and a dopant. The oxidation of the pyrrole monomer is initiated by applying a potential or a current between the working and counter electrodes. When the working electrode becomes positively charged with respect to the counter electrode, the monomer solution in contact with the working

electrode begins to oxidize, forming cations which can exist in several resonant modes. As cations join into pairs and form dimers, the polymer grows.

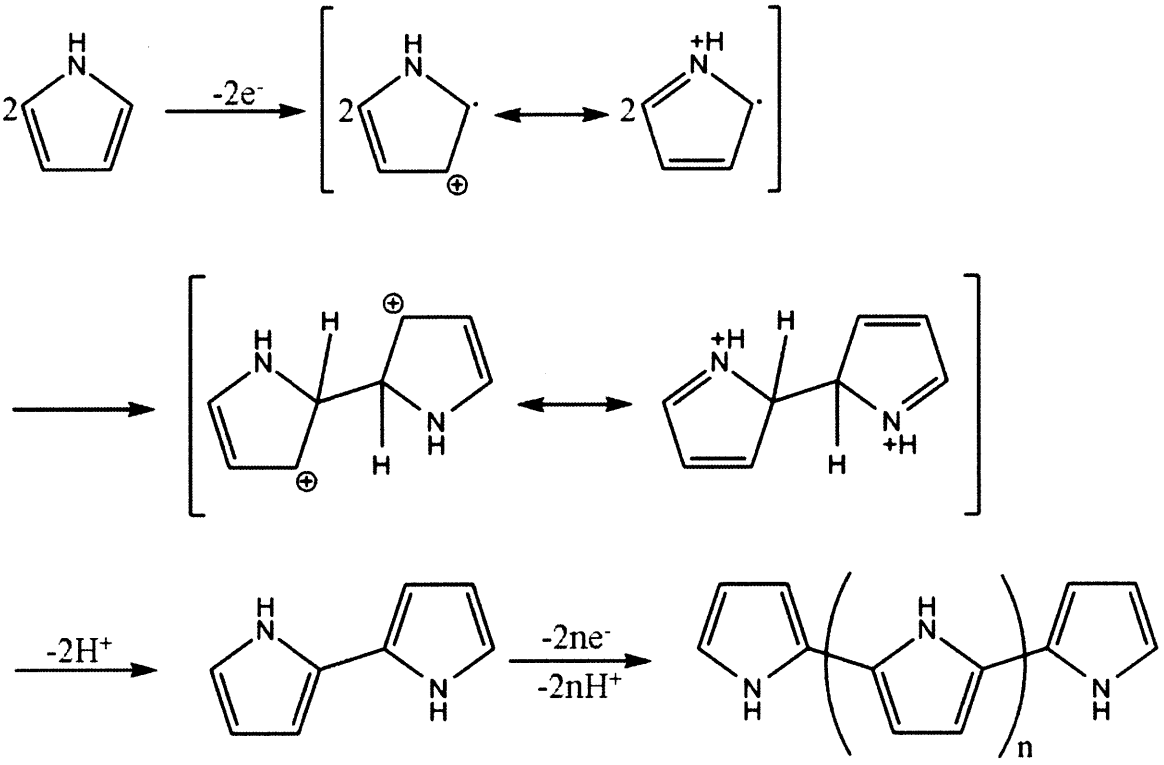

Figure 6: Molecular steps involved in the synthesis of polypyrrole. From [24].

During this cycle, the positively charged surface (working electrode) also attracts negatively charged ions from the dopant within the electrolyte solution. As these ions are attracted to the working electrode, they are incorporated into the polymer film. It is this intercalation of ions that makes the polymer conductive [26]. This process continues upon itself, thereby growing a doped polymer.

During electropolymerization, there is a breadth of variables that can be modified to affect the resultant polymer's conductivity, morphology, mechanical properties, chemical properties, growth rates, etc. A non-exhaustive list is presented in Table 2.

Table 2: Variables that affect the conductivity of electrochemically deposited polypyrrole films.

Chemical	Environmental	Material
Dopant concentration	Growth temperature	WE surface pattern
Monomer concentration	WE*/CE* separation distance	WE surface area
Solvent	Potential	CE surface area
Dopant type	Sweep rate	WE material
Distillation quality	Current density	CE material
	Time	

*WE = working electrode; CE = counter electrode

Electrochemical deposition of polypyrrole is often done in a two or three electrode cell as shown in Figure 7. The working electrode is a conductive surface, preferably one that is both chemically inert and stable. The counter electrode, also a conductive surface, is separated by some distance from the working electrode. Depending on the growth method, an independent reference electrode may or may not be used. An electrolyte containing both the pyrrole monomer and the dopant fills the space between the working electrode and the counter electrode. Films can be deposited galvanostatically (constant current), potentiostatically (constant potential), or through a cyclic variation of controlled potentials or currents.

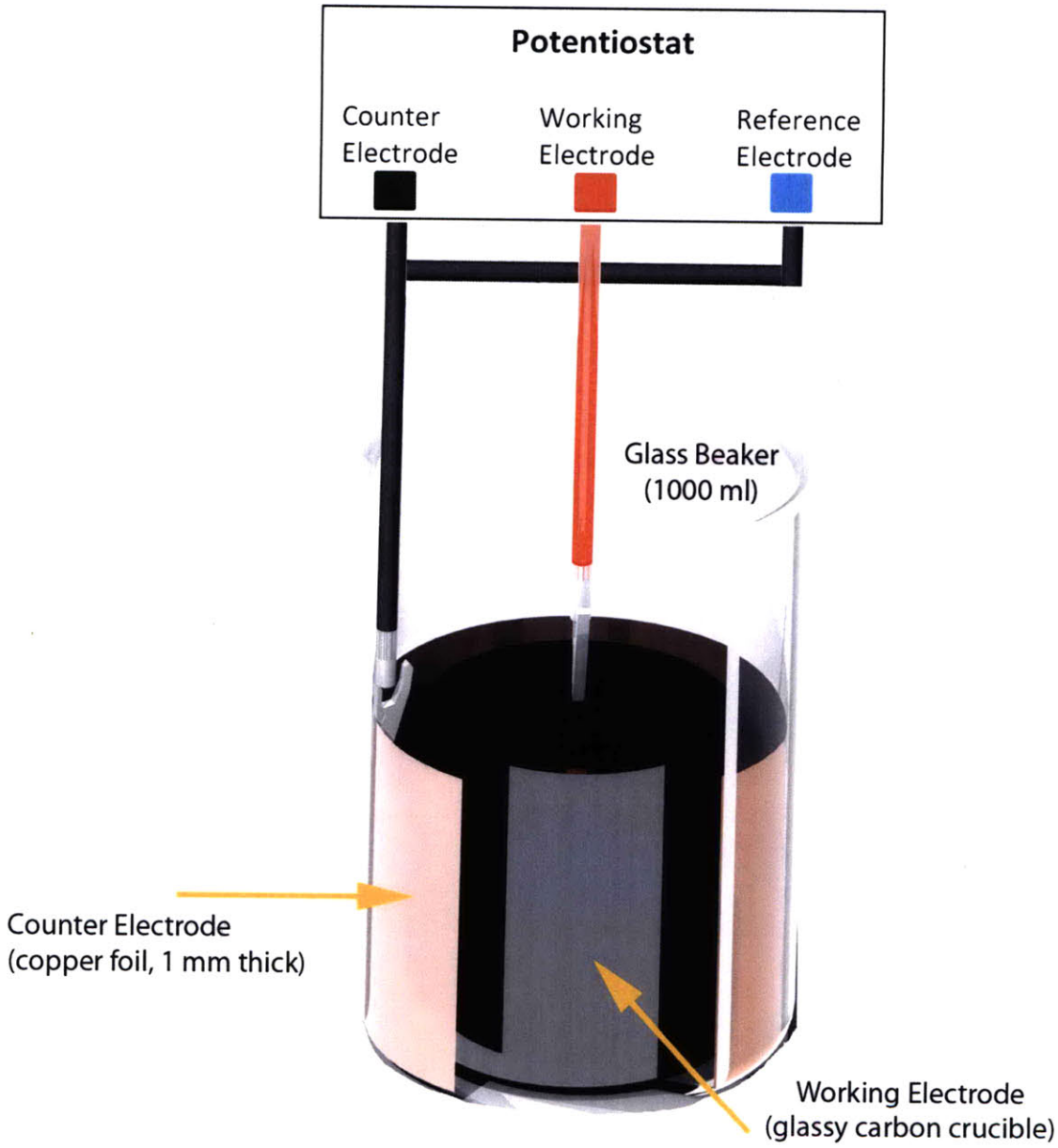

Figure 7: Two electrode, electrochemical cell used in the electropolymerization of polypyrrole.

3.3 General Properties

The conducting polymer polypyrrole has a versatile set of material properties that makes it an attractive choice when building artificial muscle systems. When polypyrrole is held under tension, submerged in an electrolyte, and electrically excited, it performs as an actuator (see

Chapter 4). In comparison to mammalian skeletal muscle, polypyrrole actuators can produce one hundred times the active stress, ten times the work density, and one third the strain of mammalian skeletal muscle. As a surface coating or as a compliant free standing film, polypyrrole can be used as electrical conduits or wires, respectively, the latter of which can be manufactured with dimensions in the nanometer range [27, 28]. As wires, polypyrrole can withstand potentials of several volts and tolerate peak current densities approaching that of copper [29]. When conducting polymers such as polypyrrole are deposited as thin films and are partially exposed to an electrolyte, they can be cycled through states of oxidation and reduction, thereby acting as semi-conductors [30, 31] that can be used to make transistors, logic gates, diodes, amplifiers, etc. (see Chapter 7). Free-standing polypyrrole films that are subject to small mechanical strains will deform elastically. During this strain the resistance between two points on the film will change depending on the point locations and their geometric relationship to strain, enabling polypyrrole to be used as variable resistance length sensors, force sensors, or pressure sensors (see Chapter 5). When two polypyrrole substrates are separated by an electrically insulating but ionically conducting porous membrane, a potential can be stored by reducing and oxidizing the opposing substrates, enabling polypyrrole to volumetrically store energy as a redox supercapacitor (see Chapter 6).

Numerous applications outside of the scope of this work (microphones, chemical sensors, electro-chromic displays, etc.) can be made from polypyrrole or other conducting polymers. In building artificial muscle systems, the focus here on polypyrrole's multi-functionality will be limited to energy storage, actuation, and force and length sensors. In the future, artificial muscle systems based off conducting polymers will evolve to include control electronics, non-volatile memory, energy harvesting and added chemical, thermal and electrical sensing capabilities.

Chapter 4 Actuators

4.1 Introduction

Polypyrrole actuators were first examined in the 1990s as novel materials for generating strain through electrochemical mechanisms. Since their inception, research has steadily improved the maximum strain output, stress output, mechanical properties, and chemical properties [32]. As research, knowledge of chemistry, and fabrication techniques progress, stress and strain rates will continue to improve, and a plethora of applications will undoubtedly emerge. Polypyrrole actuators have already been employed in both liquid and air environments to drive numerous devices [33, 34, 35].

4.2 Theory of Actuation

Actuation in linear contractile polypyrrole actuators occurs by the flux of counterions in and out of the polymer. This flux occurs when polymer films are submerged in an electrolyte solution and electrically excited with a power source (*e.g.* a potentiostat). Solid electrolytes and localized electrolyte-soaked membranes, such as those seen in bending tri-layer polypyrrole actuators [36], are also possible, but remain outside the scope of this work. The actuation mechanism, however, for both linear and bending actuators remains the same.

Linear contractile polypyrrole actuators are commonly driven using a three-electrode electrochemical cell, where the polypyrrole actuator acts as the working electrode, a conductor (*e.g.* gold, stainless steel, polypyrrole) physically isolated from the polypyrrole actuator serves as the counter electrode, and a third conductor (*e.g.* a silver wire or a calomel electrode) located in

close proximity to the polypyrrole actuator behaves as the reference electrode. A diagram of this configuration is shown in Figure 8.

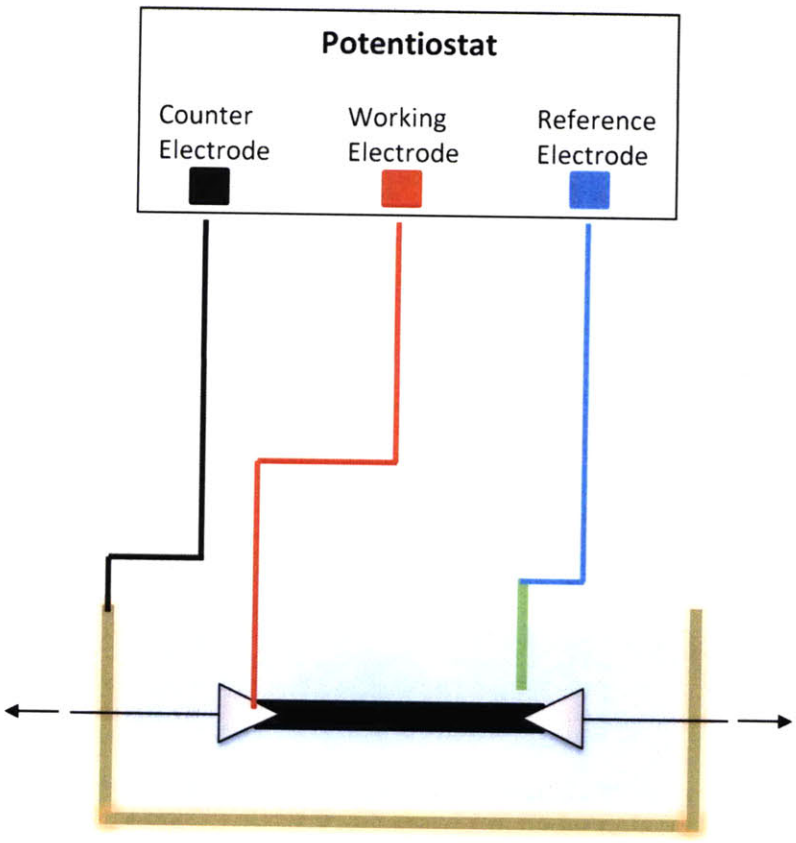

Figure 8: Three-electrode setup for electrochemical excitation of polypyrrole actuator. The actuator (center, black) is preloaded in tension by two conductive clamps (grey, triangles) while submersed in an electrolyte (light blue). The outer walls of the bath (gold) serve as the counter electrode. The reference electrode (green) is placed near the polypyrrole actuator.

To initiate actuation, a potential is applied across the polypyrrole actuator (*i.e.* the working electrode) and the counter electrode. As charge builds up inside the polypyrrole actuator, counterions from the surrounding electrolyte accumulate near its surface. A capacitive double layer is thus formed at the polymer-electrolyte interface, within a matter of hundreds of milliseconds, depending on the conditions of the actuator and the electrolyte. This this process is commonly referred to as double layer charging.

The migration of counterions towards the charged polypyrrole actuator surface during and after double layer charging creates an ionic gradient at the polymer-electrolyte interface. In the presence of this gradient, counterions will begin to diffuse into the polymer, after which they couple with opposite polarity charge carriers to maintain charge neutrality within the polypyrrole actuator. It is this uptake of ions by the polymer that leads to the volumetric expansion of polypyrrole actuators, where strain is roughly proportional to the amount of charge entering the film [29]. A diagram of this actuation process is shown in Figure 9.

If the actuator's potential is positive with respect to the counter and reference electrode, the film undergoes an oxidation reaction and cations will flux out of the polymer while anions flux into the polymer [25]. If the actuator's potential is negative with respect to the counter and reference electrode, the film undergoes a redox reaction, where cations are intercalated in the solution and anions are de-intercalated in the polymer.

As the polypyrrole film is held under tension, the uptake of counterions during oxidation results in volumetric expansion. When the counterions are expelled during reduction, the polymer will contract.

4.3 Actuator Geometries

Polypyrrole actuators are typically fabricated into two geometries: linear contractile or bending (trilayer) actuators. An electrolyte is required for either geometry, and comes in the form of a solid, gel, or liquid. Without an electrolyte, no appreciable (>0.1%) actuation occurs [29]. To date, the majority of linear contractile actuators operate while submersed within a liquid electrolyte. Bending actuators, in contrast, can operate in air if the electrolyte is stored in a gel or porous membrane that remains in mechanical contact with the actuator. Bending actuators, though outside the scope of this work, are briefly discussed for reference.

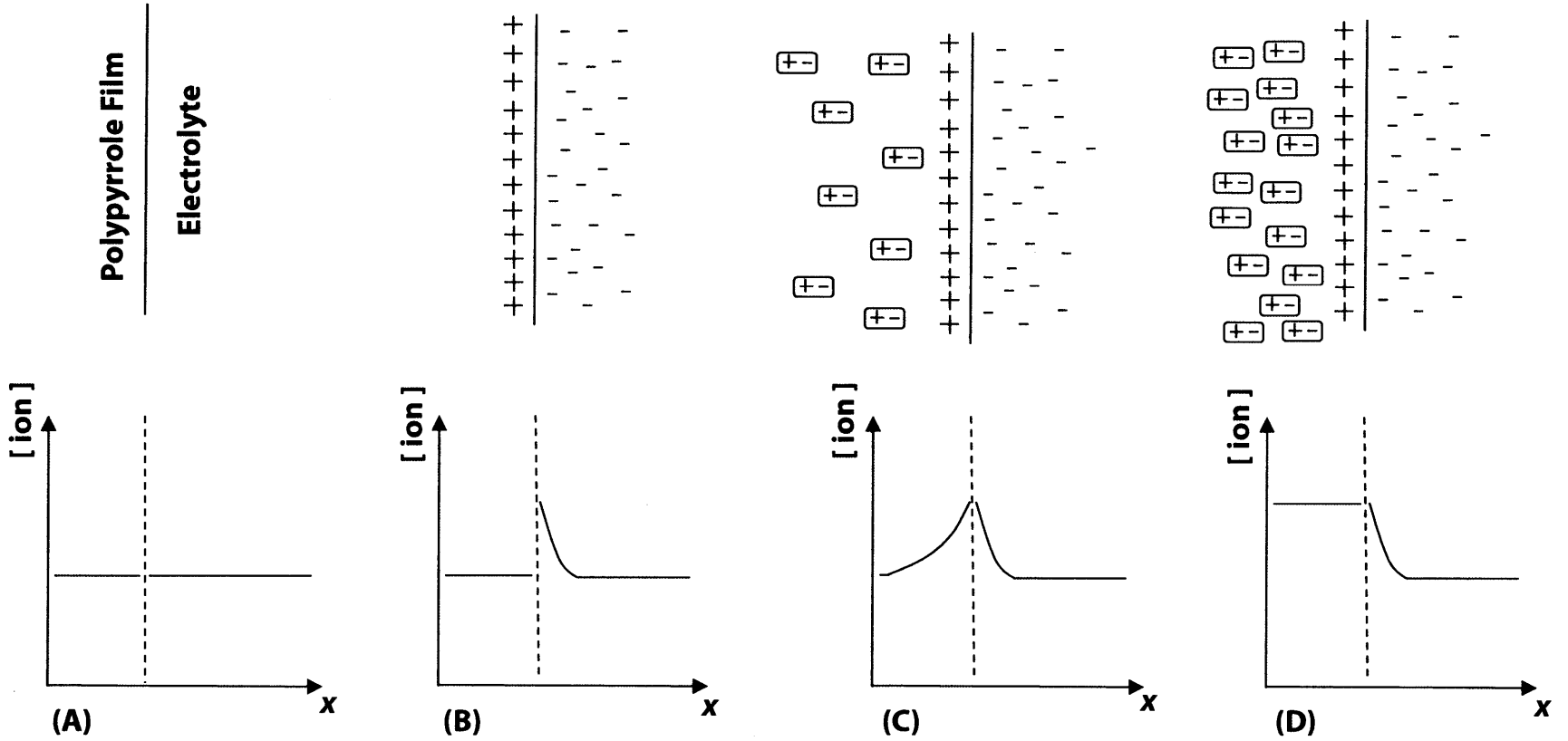

Figure 9: Illustration of ion movement during polypyrrole actuation. (a) Polymer-electrolyte interface at equilibrium. (b) After a potential is applied to the polymer, charge builds up inside the polymer while counterions from the electrolyte accumulate at the polymer-electrolyte interface. (c) The concentration gradient of counterions across the polymer-electrolyte interface drives counterions into the polymer, causing actuation. (d) Counterions continue to diffuse into the polymer until there is no ionic gradient across the polymer-electrolyte interface. The polymer is now fully actuated.

Bending actuators are commonly produced by combining a stack of two layers of conducting polymer with a non-conducting, ionically porous membrane or gel separator (see Figure 10). Because the two layers of conducting polymer are only joined through an ionic medium (*i.e.* an electrolyte), the application of a potential (voltage) across the two opposing conducting polymer layers will cause one layer to undergo a redox reaction while the other layer undergoes oxidation. This leads to the simultaneous contraction and expansion of the two opposing layers, resulting in a bending motion of the stack [37].

Bending actuators can produce significantly larger displacements than their linear counterparts, because strain is amplified by the mechanical interface that exists between the contracting and non-contracting layers. At the same time, bending actuators generate significantly lower forces [38].

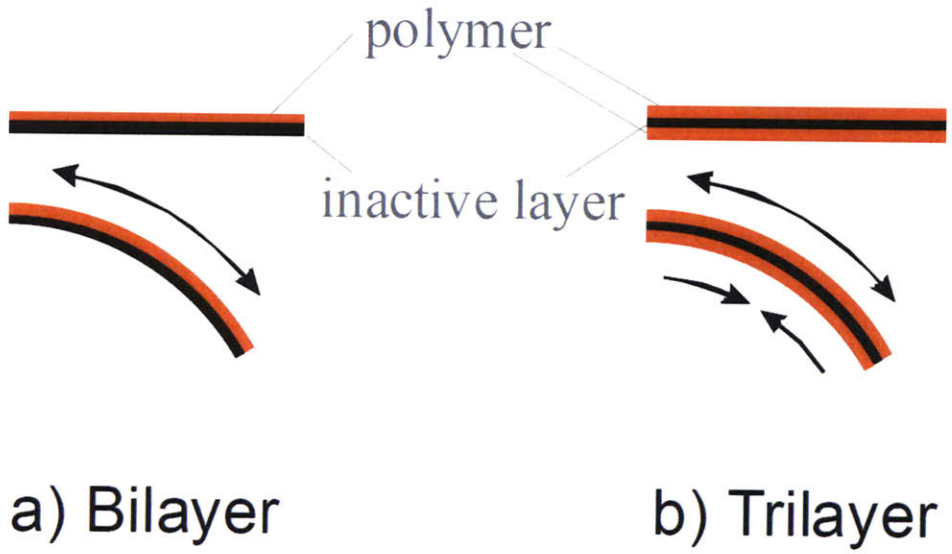

Figure 10: Polypyrrole bending actuators. The active material (red) undergoes a change in strain while the inactive material (black) causes the bilayer or trilayer to bend. From [37].

This work focuses primarily on linear contractile actuators for several reasons. First, linear actuators yield significantly higher stresses and therefore, per unit area, can produce

significantly higher forces. This is important for any system which wishes to replicate the performance metrics of mammalian skeletal muscle. Secondly, while bending actuators produce higher displacements, their motion occurs along the bending path of the actuator itself. Therefore, the total volume required to enable actuation is significantly larger. This is of concern when considering the closely-packed, hierarchal configuration of mammalian skeletal muscle (see Chapter 2). Finally, linear contractile actuators more accurately represent the contractile unit of mammalian skeletal muscle, the sarcomere, in the sense that displacement occurs linearly, in a contractile manner, along a straight line of action. This enables such actuators to be easily joined together or scaled to build artificial muscle systems. While studies on the scaling of bending actuators have been performed with certain degrees of success [39], the combination of linear contractile actuators, both in series and in parallel configurations, is less convoluted geometrically. To date, experimental results in scaling linear contractile actuators have also shown significant promise [40].

4.4 Previous Actuator Performance Studies

Since their inception, numerous studies have been performed to understand, quantify, and improve conducting polymer actuators. Synthesis conditions, electrolyte choice, geometry, mechanical configurations, and thermal and electrical stimulation have all been explored in some detail with the goal of improving actuation performance.

The performance of conducting polymer actuators can be considered from two major metrics: the active stress which the actuator produces and the strain that it is able to generate. There are numerous sub-categories to these two metrics, such as stress and strain rates, lifetime, repeatability, power consumption, and efficiency, along with mechanical characteristics such as yield stress, yield strain, viscoelasticity, and creep.

Metallic Backings

One manner of increasing polymer actuation speed is to increase the conductivity of the film by coating it with a thin layer of highly conductive metal during synthesis. While polypyrrole has conductivities near 10^4 S/m, there is still a significant potential drop that occurs along the polymer, even for distances on the order of millimeters [37, 40]. Increasing the effective film conductivity reduces this potential drop, allowing double layer charging to occur faster and more evenly along the actuator's length. This directly results in faster, more uniform actuation [40]. Films can be co-synthesized with highly conductive metallic backings (*e.g.* copper, gold, platinum) by electroplating substrates prior to electrochemical deposition [40] or through sputter coating substrates before or after electropolymerization (see Chapter 7).

Metallic-backed polymers have certain drawbacks, however, such as increased fabrication times, material costs, processing steps, and material complexity and visibility. Furthermore, while conducting polymers may be feasible for biocompatible actuation systems, metallic backing can peel or flake away from the polymers they are attached to, thereby requiring actuator encapsulation.

Thermal Stimuli

Polypyrrole actuator performance also changes depending on thermal stimuli [25, 41, 42], where increasing the heat input will result in larger strains. A recent systematic study of thermal stimulation has shown that both strain rate, maximum charge rates, and peak stresses increase with temperature, while stiffness decreases [43].

It is unclear how increased thermal stimulation over time will affect the lifetime of the polypyrrole actuators, but spectroscopic studies of polypyrrole at elevated temperatures have shown that polypyrrole does not degrade appreciably in a nitrogen environment until 375°C.

Fluorine and hydrogen fluoride, however, have been detected at temperatures near 110 °C, suggesting that dopant ions may decompose at relatively lower temperatures [29].

Ionic Matching

Several studies have been performed to increase the performance of polypyrrole actuators by modifying dopants in either the polymer or electrolyte. Controllable properties such as the diffusion constant, cation-ion pair matching [26] and ion sizes have been shown to enable both faster actuation and larger strains.

Trade-offs exist when searching for the appropriate actuation ions. Reducing the ion size will increase ionic mobility, thereby enabling faster actuation (caused by faster diffusion), but at the expense of producing smaller strains. Conversely, larger ions will enable a greater range of expansion and contraction, but increasing the ion size increases the diffusion rate and therefore, reduces the resultant strain rate as well. Depending on the size and doped composition of both the polypyrrole actuator and the electrolyte, single or multiple ions may cause actuation, which affects the maximum resultant strain, strain rate, and stress.

Actuation Voltage

Changing the actuation voltage can also affect the performance of polypyrrole actuators. Polypyrrole has an oxidation peak near 1 V, and is typically excited at voltages less than or equal to this value so as not to degrade the polymer. A few studies, however, have looked at high voltage actuation [29, 34]. In terms of strain, one study has shown that increasing the actuation voltage will increase the speed of actuation and therefore, the strain rate. A second study showed that increasing the voltage will also increase the actuator's ability to generate stresses at higher frequencies.

4.5 Frequency and Voltage Dependent Actuator Characterization Study

In order to design artificial muscle systems, it is important to know the performance metrics of each respective component. While performance studies on polypyrrole actuators have been broad and varied, almost all of them have limited actuation tests to a small, discrete number of frequencies over a limited range of voltages. A more systematic understanding polypyrrole actuator strain performance is needed if polypyrrole is to be used in designing artificial muscle systems. A systematic study is also important when designing closed-loop control actuation systems, in order to predict actuation capabilities and bandwidth.

If we recall the performance metrics of mammalian skeletal muscle (see Chapter 2), and wish to replicate its bandwidth, then it will be important to understand actuation in polypyrrole actuators over the same range of frequencies over which skeletal muscle has been observed operate. This, however, presents a significant challenge: polypyrrole actuation amplitude decreases as a function of frequency, making relatively high-frequency difficult to observe. To date, actuation measurement made above 3 Hz have only been accomplished by measuring the displacement of trilayer actuators [36, 45], where displacements are significantly amplified and are therefore, easier to measure. For linear actuators, strains have not been characterized above 3 Hz [36]. For bending actuators, strains have been observed up to 150 Hz [45]. In the latter case, however, the observation of strain at 150 Hz arose solely from the fact that the bending actuator had a resonant mode at this frequency. The amplitude was therefore not a measure of polypyrrole actuation capabilities, but rather the system's actuation capabilities. Therefore, the lack of understanding the actuation capabilities above 3 Hz led to the first systematic study of polypyrrole strain over a broad range of frequencies and voltages.

4.5.1 High Frequency Test Apparatus Design

Amplitude and Strain Resolution

The first criterion established in the design of a high-frequency, thin-film actuator test apparatus was the consideration of relating actuator frequency and strain. Linear contractile actuators typically exhibit strains between 2% and 5% repeatedly, but can reach up to 12% with modified manufacturing techniques [24]. All of these maximum strain values occur at low frequencies (less than 0.1 Hz). Because the ohmic potential drop across the polymer can become significant for longer films [40], films are typically evaluated at lengths less than 50 mm. At strains less than 5%, this corresponds to upper displacement limits near 2.5 mm.

Depending on the frequency, displacement resolution requirements may vary. At low frequencies where peak-to-peak strain is maximized, moderate resolution is possible with a variety of length measurement techniques. At higher frequencies (greater than 1 Hz), peak-to-peak strain decreases significantly, making displacement measurements more difficult to attain. Strain amplification techniques have been used in the past to make low-strain measurements possible [29]. From previous experiments, at frequencies above 10 Hz, strain was predicted to be less than 0.1%. This corresponds to a lower displacement limit, of 50 μm for a 50 mm film. As it was desired to test frequencies above 10 Hz, and to most likely use samples as short as 10 mm, a strain resolution in the 100 nm range was desirable.

Quasi-Isometric Testing

Strain actuation tests are typically evaluated in an isometric configuration, where the stress of the polymer is held constant during cycles of contraction and expansion and the strain is measured independently. Constant stress is usually maintained during isotonic tests by using a

mechanical stage [25, 46], or a mass/pulley or tilting system [47]. Masses and pulleys, however, introduce friction and inertia into the measurements, and may appreciably effect measurements at high frequencies or low-strains. Mechanical stages, on the other hand, require relatively fast closed-loop control to maintain isometric conditions, thereby significantly increasing the cost and complexity of the test bench. Ideally, a parallel drive, high dynamic range, high bandwidth system, such as those used to test single living cells and muscle tissues [48], should be used to obtain the best results.

To minimize friction and inertia within the test bench, and to avoid closed-loop control challenges at higher frequencies, the high-frequency actuation test bench in this work was designed to hold actuators under quasi-isotonic tension by means of a low spring-constant extension spring or an elastic band. Using an elastic member to preload the sample under tension reduced the friction and inertia associated with pulleys. It did, however, add a small amount of damping to the system.

In order to maintain quasi-isotonic tension, the force that the elastic band exerts on the polypyrrole actuator should remain relatively constant over the entire range of actuation strain. The change in force of the elastic band as a function of actuator strain can be calculated by recognizing that the displacement of the actuator, x, is a function of the actuation strain, ϵ, and the sample length L, as describe by:

$$x = \epsilon L \quad . \tag{4-1}$$

The reaction force of the elastic band, F, is a function of its spring constant k, and the displacement of the actuator, as:

$$F = kx \quad . \tag{4-2}$$

The total change in the reaction force over the entire range of actuation is therefore a combination of Equations 4-1 and 4-2, and will be a function of the total change in strain of the actuator (ϵ_{max} - ϵ_{min}), where ϵ_{max} and ϵ_{min} are the maximum and minimum strains of actuation, respectively. This range can be written as:

$$F = k(\epsilon_{max} - \epsilon_{min})L \quad . \tag{4-3}$$

Equation 4-3 can be applied to the high frequency actuation test bench once the spring constant is known for the elastic band. The stress-strain curve of the elastic band used for the high-frequency test bench is shown in Figure 11.

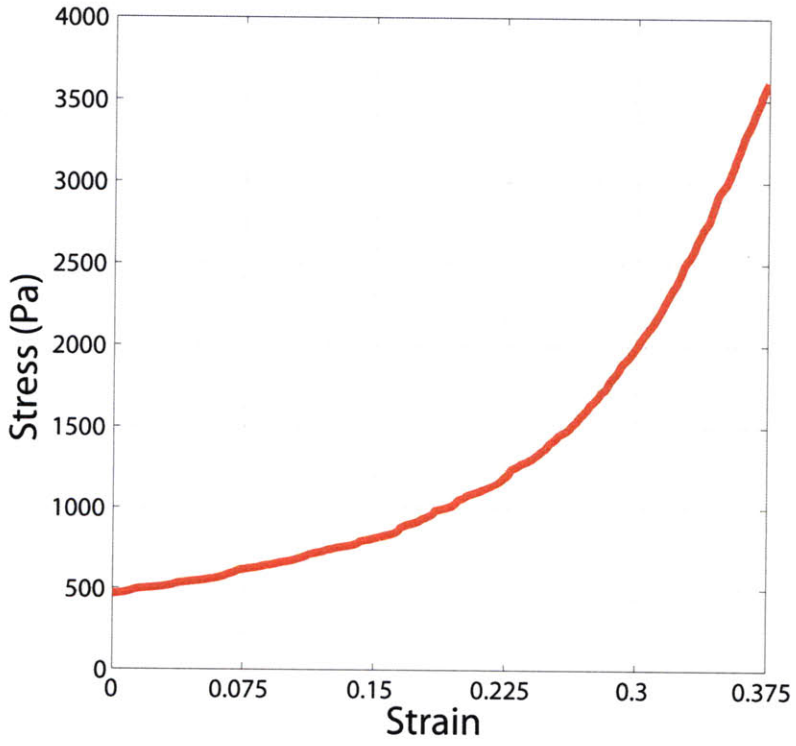

Figure 11: Stress versus strain curve of elastic band used in the high frequency polypyrrole test apparatus. For any small region of strain, the curve can be considered approximately linear. Since actuator displacements are relatively small, changes in stress from the reaction force of the elastic band are minimal.

Although the stress-strain relationship shown in Figure 11 is non-linear, for any strain range less than 5%, the stress-strain relationship can be approximated as linear. One specific 5% strain region is shown in Figure 12.

The change in reaction force exhibited on the polymer during actuation can then be approximated by (4-3), knowing that the cross-sectional area of the elastic band was 10^{-6} m^2 and assuming the actuator and the elastic band are of equal starting lengths. At a maximum strain range of 5% (all data presented in this work are below 4% strain) the change in stress from the reaction force of the elastic band will be 0.6 kPa. This corresponds to a change in reaction force of 0.6 mN. The typical cross-sectional area of polypyrrole actuators used in this work were $0.06 \cdot 10^{-6}$ m^2, (3 mm by 0.020 mm). While polypyrrole typically generates active stresses

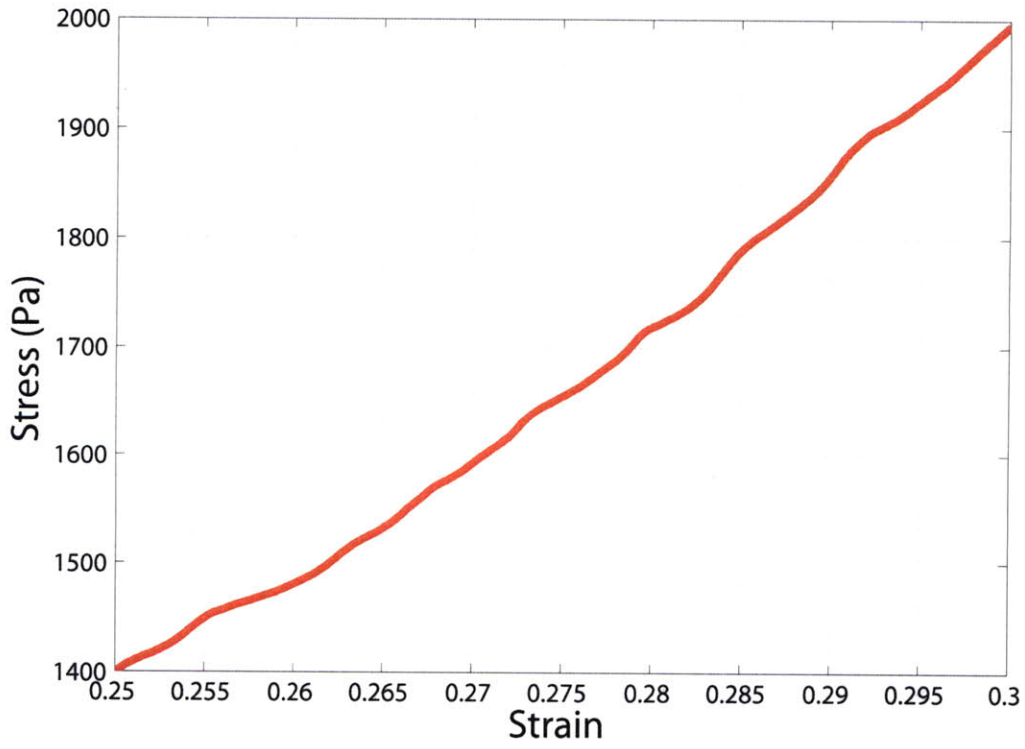

Figure 12: Example 5% region of the elastic band. Over small changes in strain, the stress versus strain curve is approximately linear, as shown above.

between 5 and 10 MPa, a typical actuator used in this work generates about 0.3 N of force, five hundred times higher than the total change in reaction force.

Test Apparatus Geometry

Using the maximum strain and minimum strain resolution as design criteria, along with the goal to create a quasi-isotonic test bench, an actuator test bench was designed to measure the strain of polypyrrole actuators at frequencies up to 1 kHz. An image of the high-frequency test bench is shown in Figure 13.

The high frequency actuation test bench works by holding a polypyrrole actuator under quasi-isotonic conditions, exciting the actuator using a potentiostat (Amel, 2053), and measuring the change in strain over time. Film samples are held under tension along a single line of action using a combination of flexure clamps, non-elastic Spectra® line, and an elastic band. At one end of the line of action, a force sensor (Futek, LSB200) measures the tension under which the sample is held. At the other end of the line of action, the elastic band holds the sample taught. Actuator samples are submersed in an electrolyte bath that sits collinear with the line of action.

Two AC/AC linear variable differential transformers (LVDT) (Measurement Specialties, MHR-025) are positioned at the outer, lateral edges of the bath and encased within a custom-machined aluminum housing. Compact LVDTs were chosen with ultra-lightweight cores (~ 400 mg) to reduce line sag under horizontal tension. The cores of the LVDTs are mounted concentrically on the Spectra® cable, such that any change in displacement resulting from strain generated by the polymer or environmental vibration is measured. Ideally, all strain changes occur at the elastic end of the line of action (*i.e.* on the right side). In practice, however, small strains also occur at the non-elastic end of the LVDT, due in part to line sag, elasticity, and

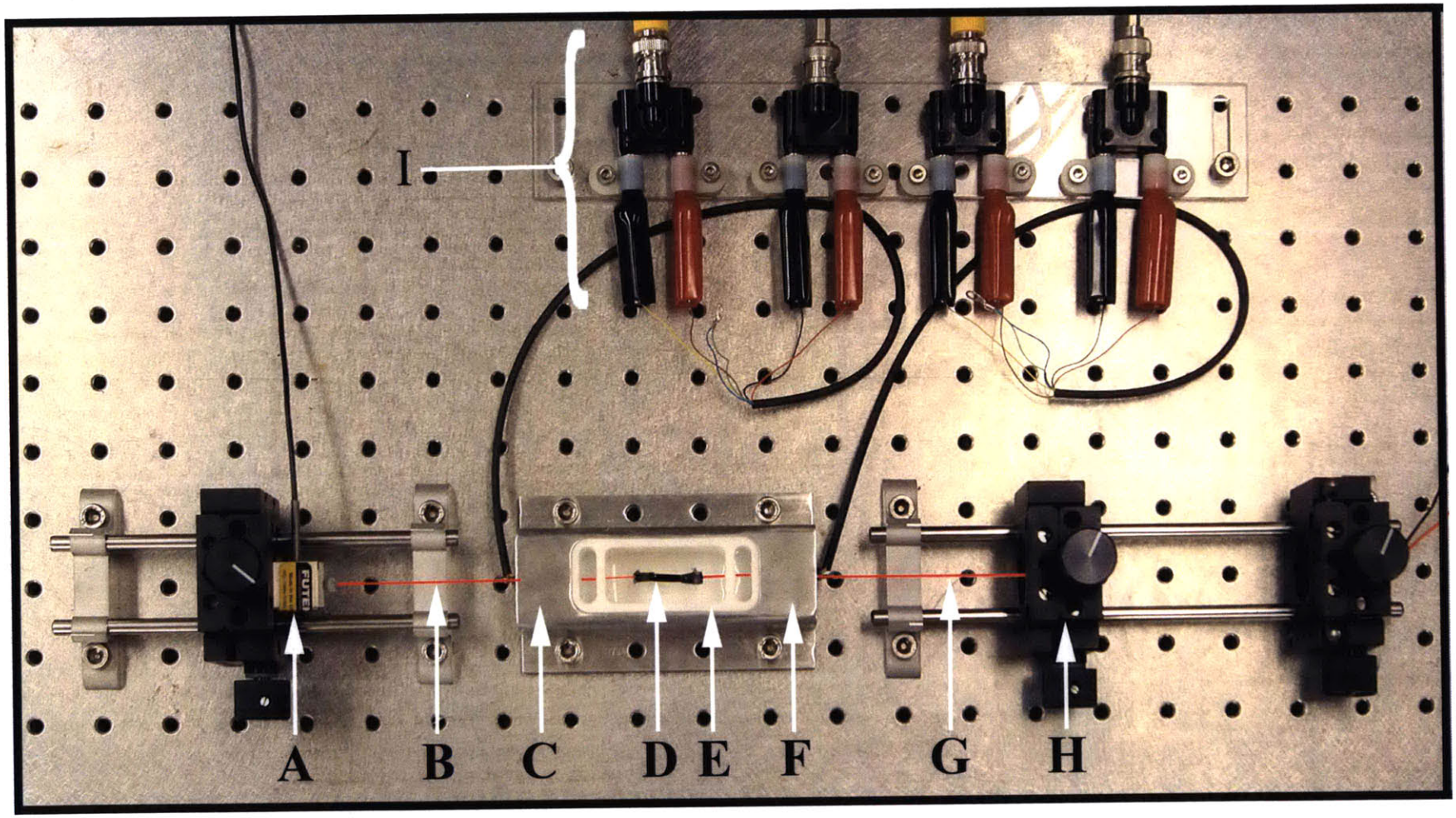

Figure 13: High-frequency actuation test bench (A) Force sensor (B) Non-elastic Spectra® line (C) Left LVDT (D) Polypyrrole sample held in tension between two flexure clamps (E) Teflon bath (F) Right LVDT (G) Elastic band (H) Two-axis positioner (I) I/O Lines for LVDTs. The line of action (not labeled) is shown in red, between points (A) and (H).

environmental disturbances. The dual LVDT arrangement enables the measurement of actuator strain that is isolated from the environment, and is computed by subtracting the difference between the right and left LVDT displacement measurements, respectively. The displacement from the right LVDT, connected to the elastic band, was about two orders of magnitude higher than the displacement from the left LVDT, connected to the non-elastic Spectra® cable.

The electrolyte bath was fabricated from Teflon®, which provided excellent resistance to chemical degradation over time and electrical insulation from the surrounding aluminum housing. The bath was lined with gold-plated, 40 μm thick, stainless steel foil (not shown) which served as the counter electrode of the electrochemical cell. Concentric holes were drilled laterally through the bath, along the line of action of the entire test bench, such that the samples could be held under tension, submersed in an electrolyte, yet never make physical contact with the bath. In this manner, friction was almost entirely eliminated from the system.

The bath was divided into three compartments: a center compartment, filled with electrolyte, where actuation occurred, and two outer compartments. The two outer compartments collected any liquid that seeped out from the concentric holes, in the space between the Spectra® cable and the hole walls.

Flexure Clamp Design

Polypyrrole actuator samples were mounted along the line of action by a set of custom designed flexure clamps (see Figure 14). Design criteria in this high-frequency electrochemical system required that the clamps be:

1. Electrically conductive so that they could be used for both clamping and electrical excitation.
2. Lightweight, in order to minimize inertia effects and line sagging.

3. Electrochemically inert.
4. Reusable.

In order to satisfy criteria 1, 3, and 4, 1095 blue spring steel was chosen as the flexure clamp material. Although steel is not completely electrochemically inert, its high yield stress and resistance to fatigue enables the steel clamps to be used repeatedly.

To satisfy criteria 2 and 4, the clamp geometry was designed to minimize the total clamp mass while considering the maximum force the clamp could exert and the compressive force required to open and close the clamps. A simple finite element simulation was run on solid model designs of several proposed clamp geometries to estimate the opening and closing forces. The flexural member (label B, Figure 14) was cut to around 225 μm, such that less than 2 N of force was required to open or close the clamp. The 225 μm flexural member was also thick enough to maintain the clamps structural integrity, even after the repeated bending.

The yield stress of polypyrrole is above 100 MPa. Typical samples used within the clamps were 3 mm by 0.02 mm. From these specifications, the clamps were required to hold the actuator sample with at least 6 N of force, so that any strain measurement could be attributed to active or passive properties of the actuator sample itself, and not slippage in the clamps. A set screw was therefore integrated into the design to ensure that the flexure clamping force greatly exceeded the tensile force corresponding to the actuator sample yield stress.

The flexure clamps were cut using Wire-EDM micromachining after several design iterations were made to minimize the mass while maintaining clamping forces and structural integrity during repeated opening and closing. At the outer edge of the clamps, small holes were drilled such that the clamps could be mounted concentrically along the system's line of action. At the distal end of the screw that holds the clamp closed, a small angled ridge was added to

ensure that the screw made sufficient contact with the flexure end. Soft materials such as aluminum and copper were determined, through finite element simulation and empirical tests, to plastically deform and lose shape after less than three opening and closing cycles.

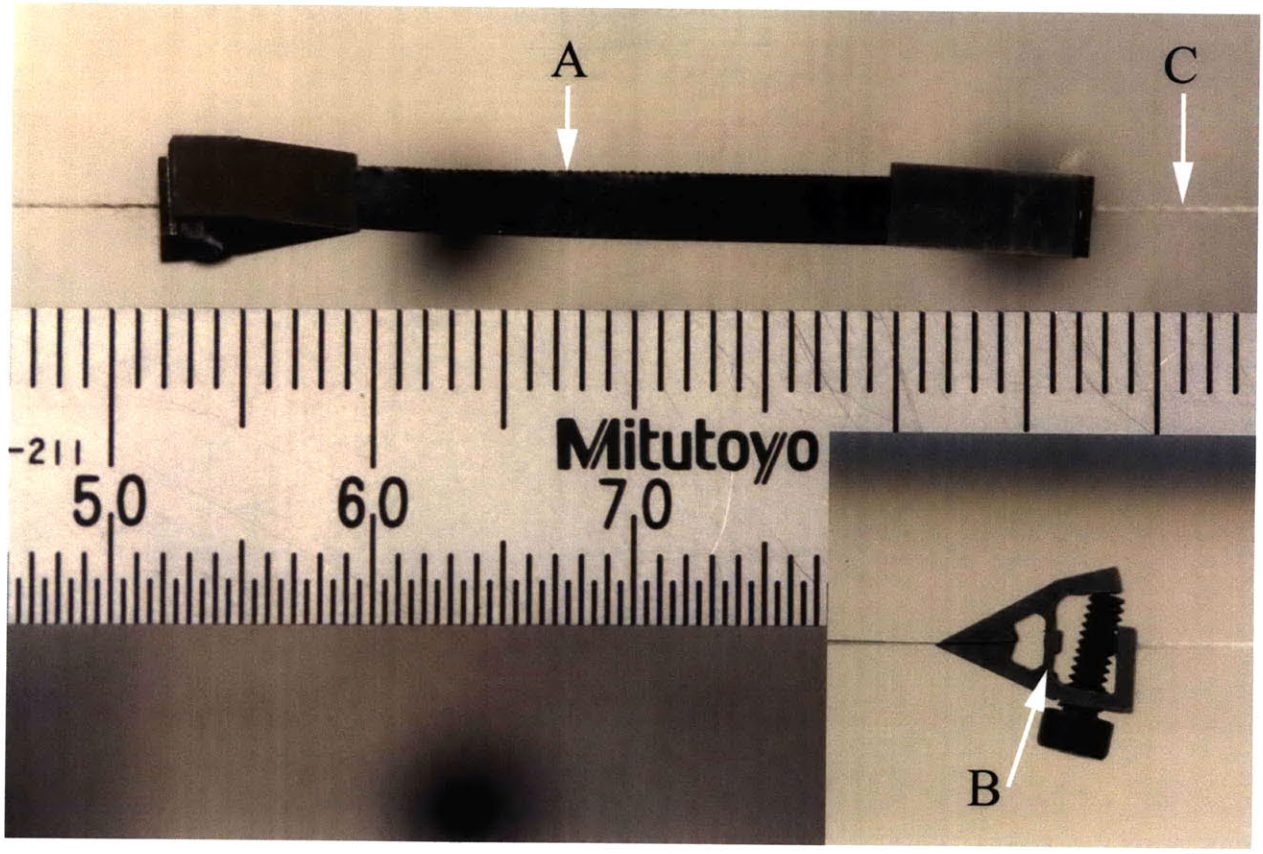

Figure 14: Flexure clamps to hold polypyrrole actuator samples. (A) A polypyrrole actuator sample, held under tension between two flexure clamps. (B) Flexural member of the clamp which determines the required opening the closing forces. (C) The line of action can be seen as the white Spectra® cable, holding the outer portions of the clamps under tension.

4.5.2 Data Acquisition Hardware

A brief discussion of the data acquisition hardware and software programming is discussed here, while detailed code can be found in the Appendix.

Position Measurements

Bandwidth and positioning resolution are of primary importance when attempting to characterize the actuation of polypyrrole actuators at relatively high frequencies. Using AC/AC LVDTs, the systems resolution is limited by the quality of the measurement hardware along with the data acquisition and signal excitation setup. Modern day signal generators such as the Agilent 33220A Arbitrary Waveform Generator have a frequency stability specification of 20 ppm + 3 pHz, and amplitude stability specification of ± 1 mV_{PP}. While these limits may be acceptable for many amplitude-insensitive measurements, in order to take full advantage of the positioning resolution of the LVDTs and be able to measure down into the nanometer range, a function generator with greater amplitude stability needed to be used. After an experimental comparison of many candidates, the best performing waveform generator was an HP 3245A Universal Source. The Universal Source was programmed to output a 24-bit resolution, 3 Vrms, 10 kHz sine wave that excited both LVDTs in parallel. The input signal amplitude and frequency corresponded to the calibrated manufacturer excitation characteristics.

The output of the LVDTs were collected on a 24-bit, 8 channel, data acquisition card (PCI-4472) from National Instruments. This particular card was chosen for its ability to simultaneously sample multiple channels, at frequencies up to 104 kHz per channel. Position measurements were computed from the output of the LVDT signals by computing the RMS voltage of the LVDTs, in real-time through a data acquisition script.

Actuator Excitation

Actuators were excited in a three electrode electrochemical cell using a computer controlled potentiostat (AMEL, 2053). During testing, DC or AC command voltages were generated programmatically and output to the potentiostat. The potentiostat then regulated the flow of current between the counter electrode and the working electrode, such that the potential

difference between the working electrode and the reference electrode was equal to the input command voltage. As the potential across the actuator changed, the polymer was driven through cycles of oxidation and reduction, leading to actuation.

Software

All data were collected using custom-designed Virtual Instrument (VI) scripts written in LabVIEW 8.5 through LabVIEW 2009. Voltage measurements from the LVDTs were synchronously recorded using virtual streaming channels with buffered configurations that enabled sampling up to the maximum hardware limit of 104 kHz. Signal measurements such as the potentiostat output voltages and currents, along with the force sensors were collected with streaming channels at lower sampling rates (1 kHz), since no RMS calculation was required.

Characterizing the frequency response of polypyrrole actuators at relatively high voltages presents a considerable challenge because of actuator degradation. At low frequencies (less than 0.1 Hz) and higher voltages (greater than 5 V), the actuator degrades considerable faster than when it is excited at lower voltages (less than 1 V). While the precise cause of degradation is unclear, one possible explanation is that holding the polymer at relatively high voltages near full oxidation results in an excessive amount of current passing through the polymer. High currents lead to Joule heating within the polymer, and mechanical failure. A polypyrrole actuator that has degraded due to high voltages will exhibit signs of melting.

While it is worth noting that at relatively high voltages, low frequency actuation is unrealistic, it was still desired to characterize the strain properties of polypyrrole actuators, consistently, for the frequency and voltage ranges tested. Therefore, in order to maintain the same testing parameters for all actuators regardless of the potential applied in the low frequency regime, the total number of cycles was limited, thereby reducing each actuator's exposure time to

higher voltages. At higher frequencies where over-oxidation was less of an issue, the total number of frequencies tested was increased. See Table 3 for a distribution of testing frequencies.

Table 3: Distribution of frequencies used for actuator characterization with the high frequency test apparatus. Frequencies were chosen after experimentally determining the maximum number of cycles at which a polypyrrole actuator degrades for a given frequency and voltage.

Start Freq. (Hz)	Stop Freq. (Hz)	# of Increments	Periods per Freq.
0.01	0.1	25	2
0.1	1	50	2
1	10	100	2
10	100	100	10
100	1000	100	10

4.5.3 Test Protocol

An example plot of a frequency sweep from 0.01 Hz to 100 Hz is shown in Figure 15. The initial strain offset has been removed during data processing for the ease of computing amplitude information. Sections of the graph in the subplots (B), (C), and (D) show the slight change in shape of the actuation curve as the input frequency increases. At low frequencies, polypyrrole is shown to take on a sinusoidal shape, similar to that of the input waveform. As the frequency increases, the upper and lower lobes of the curve begin to flatten out. This can be attributed to the non-linear characteristics of polypyrrole actuators and the diffusion-limited mode of actuation. When the change actuation excitation frequency is sufficiently low, the actuator output follows the input excitation waveform because diffusion-dependent limitations of counterion flux in and out of the polymer are minimal, *i.e.* the gradient across the polymer-electrolyte interface is small. At higher frequencies, the change in potential occurs faster than

the rate at which counterion flux occurs across the interface. Therefore, the polymer is essentially under-actuated for its given instantaneous potential and therefore, and has reduced (flatter) actuation strains for a given voltage.

4.5.4 Frequency Dependent Amplitudes

Tests similar to Figure 15 were performed for voltages ranging between 0 and 8 V in order to quantity the actuation performance of polypyrrole actuators. The peak to peak strains were then computed and plotted as a function of frequency, as shown in Figure 16.
Several important observations can be made from these frequency sweeps.

From Figure 16 it can be noted that as excitation voltage increases, the actuation strain increases over the entire range of frequencies. Also, the relationship between voltage and actuation strain changes as a function of frequency. At frequencies less than 1 Hz, the strain to voltage relationship is approximately constant, while at higher frequencies, the difference in strain as a function of voltage is highly non-linear.

There also appears to be two distinct regimes of actuation, which can be visually differentiated by examining the slopes of the log-log plot of strain versus frequency. At lower frequencies, strain decays as a function of frequency with a slope near -1 on a log-log plot. In impedance analysis, this is equivalent to the behavior of an ideal capacitor. At higher frequencies, starting near 1 Hz, the slope decreases dramatically, as shown by the sharp decay in peak-to-peak strain amplitude. This transition might be attributed to the non-linear charging effects of the polymer; at sufficiently high frequencies, the rate of change in actuation excitation is much faster than the flux of counterions into and out of the polymer, and therefore, much less actuation is observed.

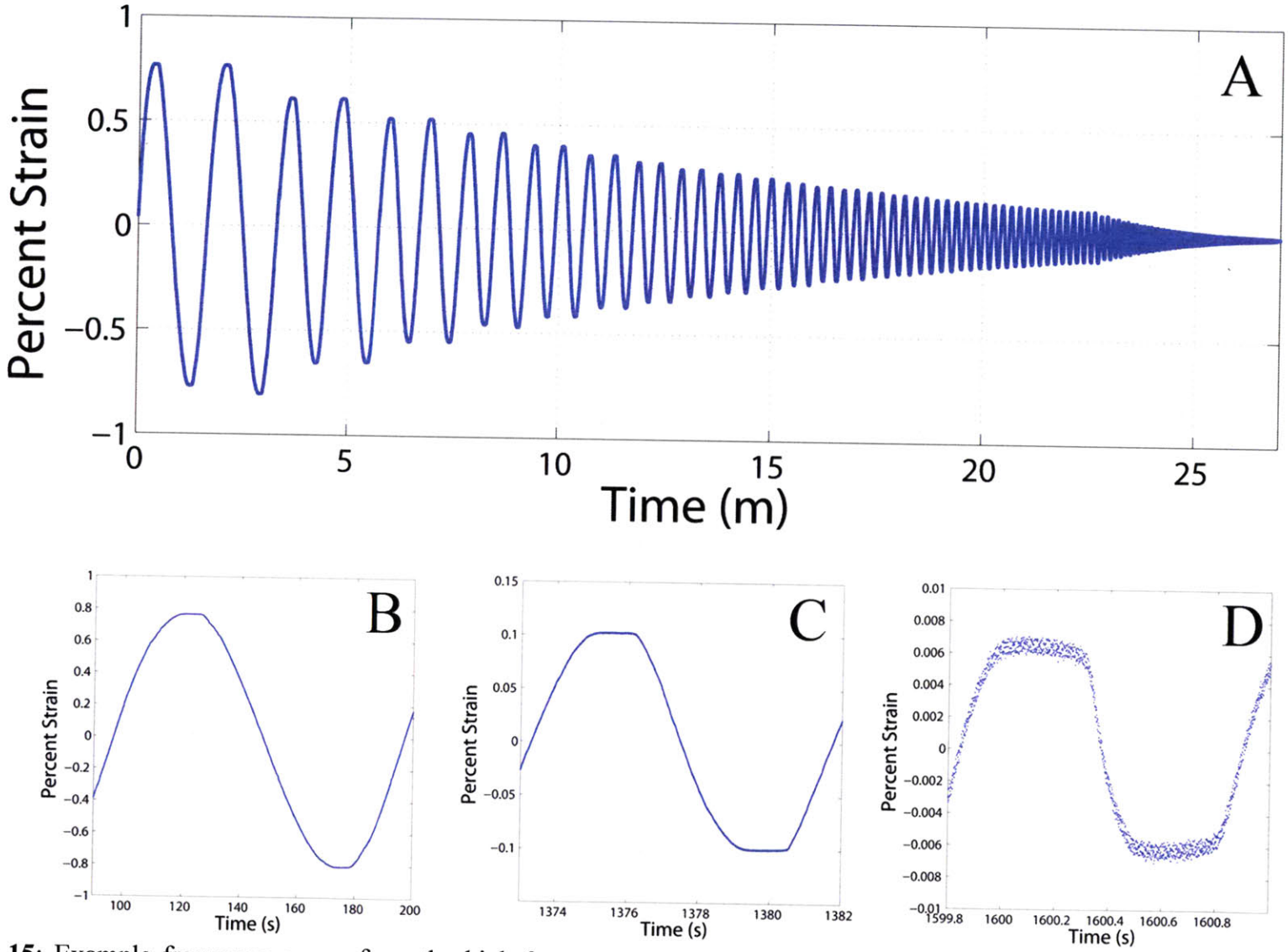

Figure 15: Example frequency sweep from the high frequency test apparatus. Plots show actuation in response to a frequency-varying, 3.0 V sinusoidal input. (A) Single, continuous frequency sweeps and example subsections near (B) 0.01 Hz, (C) 0.1 Hz, and (D) 1 Hz.

A few discrepancies that exist in Figure 16 can be attributed to experimental errors. The small fluctuations of amplitude at lower frequencies, such as that of 3 V, may be attributed to the fact that poor electrical contact was made between the polymer and one of the flexure clamps. At 8 V, a small resonant peak is observed near 5 Hz. This resonance is a function of the elastic band's spring constant and the flexure clamp mass, both existing along the actuator line of action, and is discussed in further detail in the proceeding section.

There does not appear to be a consistent relationship between the excitation voltage and the frequency at which the transition between the two regimes of actuation occurs. Experimental variations in the pre-stress, the starting length of the actuators, the length of the elastic band and the age of the electrolyte, however, can all affect this value.

Figure 16 is also exceptionally important for the design of polypyrrole artificial muscle systems because it enables the designer to predict the actuation strain for a given set of system specifications. For example, if one wishes to develop an artificial muscle actuation system built from polypyrrole that is capable of a given displacement at a given frequency, the initial polymer length and voltage ranges can be chosen to meet design requirements.

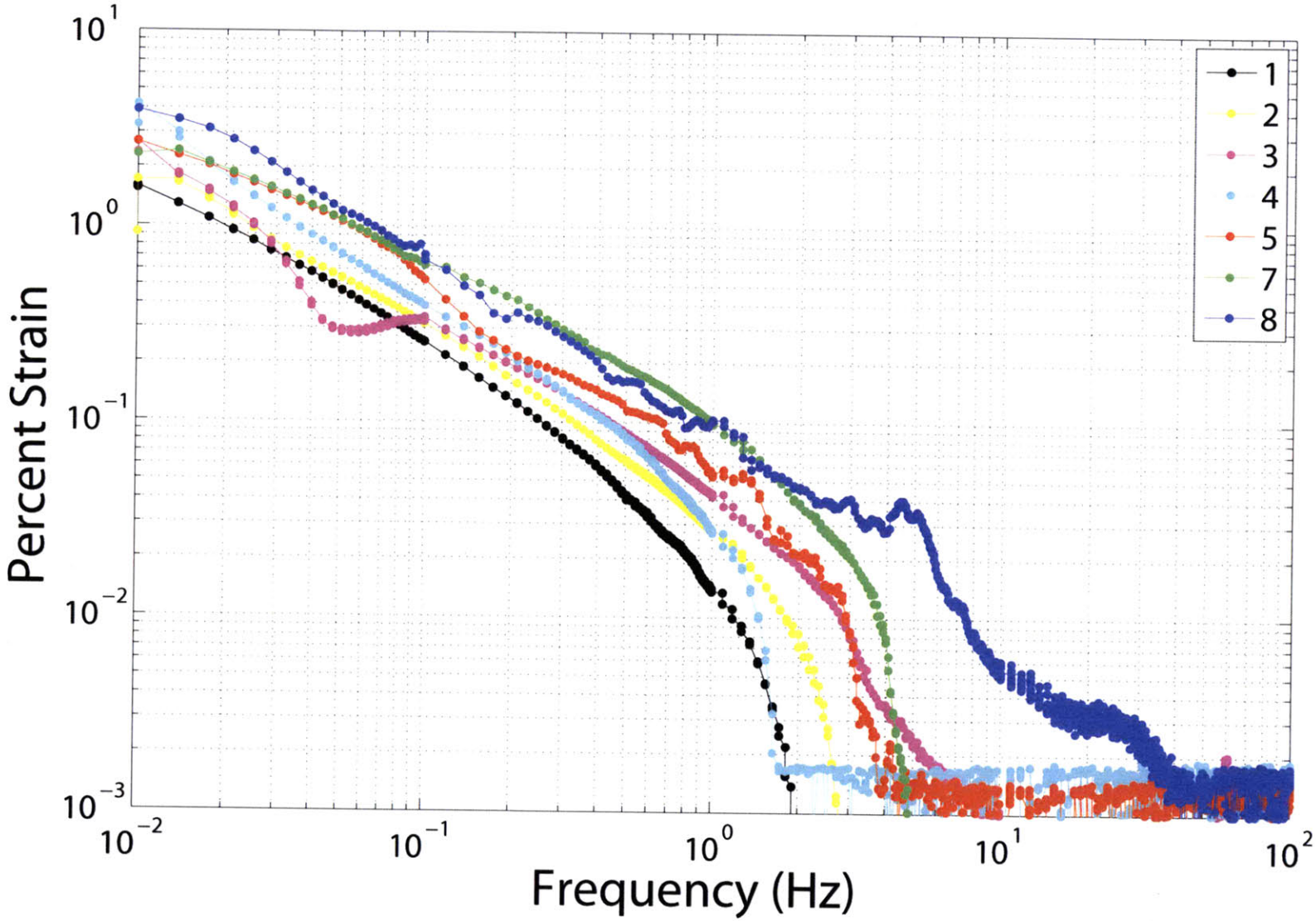

Figure 16: Strain output of polypyrrole actuators at frequencies varying between 0.01 Hz and 100 Hz. All input signals were sinusoidal waveforms, of varying amplitude, from 1.0 V to 8.0 V. Legend entries have units of volts.

4.5.5 Power Consumption

Power consumption is also of interest when seeking to understand the frequency-dependent actuation characteristics of polypyrrole. The mode of actuation in polypyrrole actuators is non-linear in time. If one examines the strain, voltage, and current of an actuator for a given input square wave, these nonlinearities become apparent. Consider, for example, the plot shown in Figure 17.

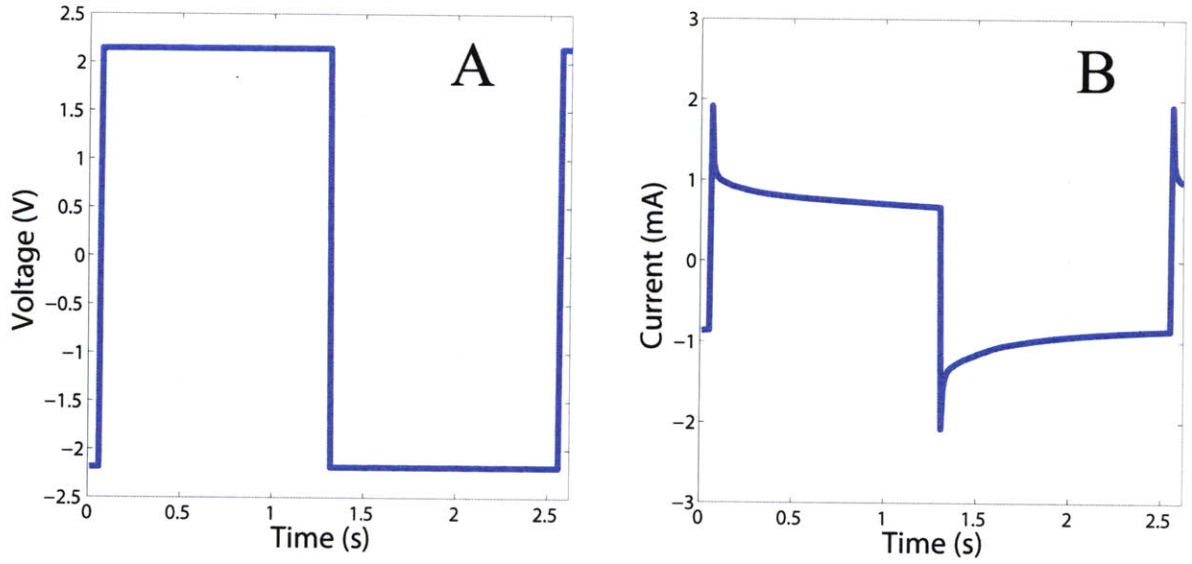

Figure 17: Voltage and current characteristics for a typical actuation cycle of polypyrrole when driven in potentiostatic mode. Double layer charging can be seen by the initial spike in current.

When the excitation voltage is set at a constant value, the current is non-linear in time. Initially, a jump in current is observed, which can be attributed to double layer charging of the actuator. As counterions begin to diffuse into the polymer and charge neutrality is approached, the current decays with time. For long periods, the current eventually approaches a steady state value.

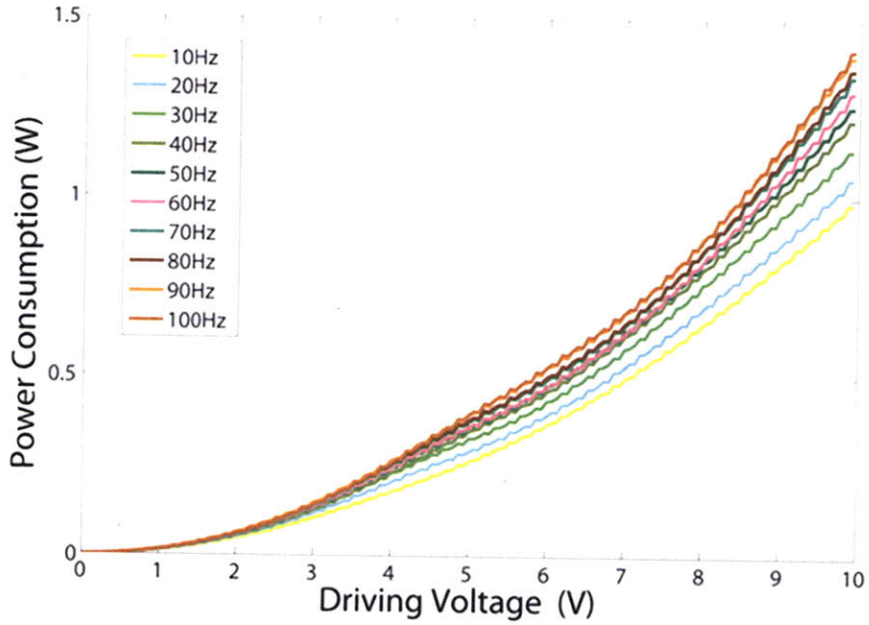

Figure 18: Power consumption of polypyrrole actuators as a function of voltage and frequency. Samples were driven at fixed frequency, amplitude-varying, sinusoidal inputs from 0.0 to 10.0 V over 120 s sweeps. Power consumption was determined from the RMS values of current and voltage.

Power consumption in polypyrrole actuators is also dependent on input voltage and frequency. The change in power consumption as a function of frequency (Figure 18) can be attributed to the non-linear aspects of polypyrrole actuation. As the double layer charges, an initially high flux of current drives the actuator, followed by a gradual decay over time. While the shape of this curve will change for a sinusoidal waveform (as compared with the square wave excitation shown in Figure 17), the actuation mechanism remains unchanged. At higher frequencies, double layer charging still occurs, and the peak input current during double layer charging will affect the overall power consumption of the actuator. The amount of time at which the polymer experiences the decaying current, however, will be shortened for higher actuation frequencies and therefore, the total average current (per cycle) that flows through the actuator increases.

The curves in Figure 18 can be fit with a second order, quadratic polynomial, as described by:

$$P = Af^2 + Bf + C \quad , \tag{4-4}$$

where *A, B,* and *C* are coefficients, *f* is the frequency, and *P* is the observed power consumption.

For all of the data shown, second-order polynomial fits agreed well with the experimental values, with R-square coefficients above 0.9975. The initial curve offset (coefficient *C*) was close to zero for each curve and the linear coefficient *B* was approximately constant, independent of frequency. The second order coefficient, *A,* increased as a function of frequency and is shown in Figure 19.

This result indicates that at low frequencies, the power consumption increases more dramatically as a function of frequency, as indicated by the initial rise in the curve at frequencies between 10 and 60 Hz. At high frequencies, the change in the power consumption as a function of frequency becomes less pronounced (*i.e.* flattens out). This is consistent with the previous explanations of double layer time-dependent charging affects, and further suggests that as some threshold frequency is approached, which will most likely occur when actuation due to counterion flux ceases to occur, the power consumption will reach some fixed value.

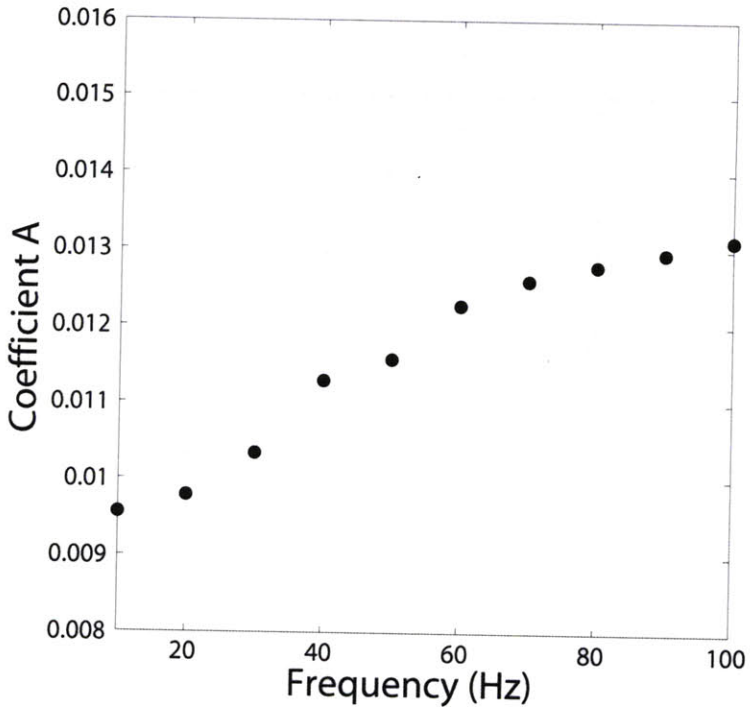

Figure 19: Quadratic coefficient "A" from second order fits applied to the power consumption of polypyrrole actuators at time-varying voltages (Figure 18).

4.5.6 Resonance Exploitation

System resonance is a characteristic undesirable for quantifying actuator properties, but can be exploited in the design of polymer actuation systems to amplify the strain at which a polymer actuates. In the case of the current high frequency tests, resonance can occur because of the mass-spring-damper characteristics of the system. The polymer mass itself is small, but the flexure clamps along the line of action are significantly more massive (see Figure 13). The elastic band will affect the spring constant of the system, as well as contribute to damping. Furthermore, as the polymer is actuated in a viscous electrolyte medium, drag on the polypyrrole actuator and the flexure clamp may also contribute to system damping. If we assume that system

damping is relatively small, the system can then be approximated as a spring and mass in series.

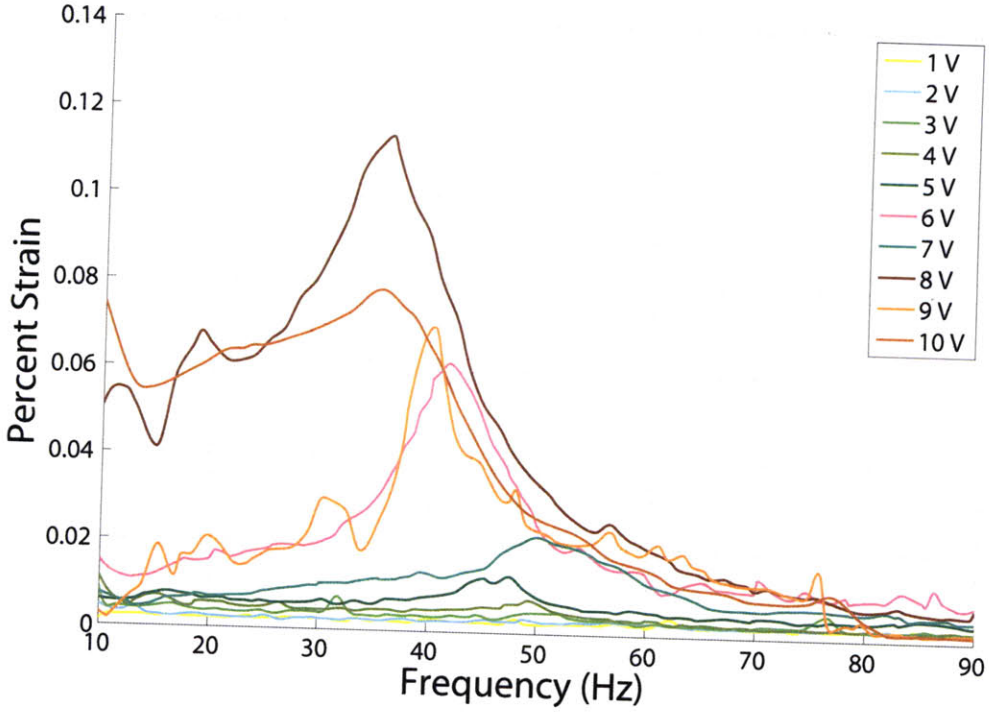

Figure 20: Peak-to-peak strain amplitude of high frequency polypyrrole linear contractile actuators. Actuators were driven on potentiostatic mode with square wave inputs of fixed amplitudes and frequencies that ranged between 10 and 90 Hz. A resonant peak is visible near 33 Hz.

Since the stiffness of the system can be modified by changing the stiffness of the elastic element that holds the polymer under tension, the system resonance can be altered such that it falls within the range of actuation frequencies tests (0.01 to 100 Hz). Figure 20 shows a set of experiments in which the spring constant has been modified such that system resonance occurs near 30 Hz. For the plot presented, a continuous, time-linear frequency sweep excited the actuator between the frequencies of 10 and 90 Hz. The strain values for a given frequency and excitation voltage are significantly higher than those shown in Figure 16 because of the system

resonance.

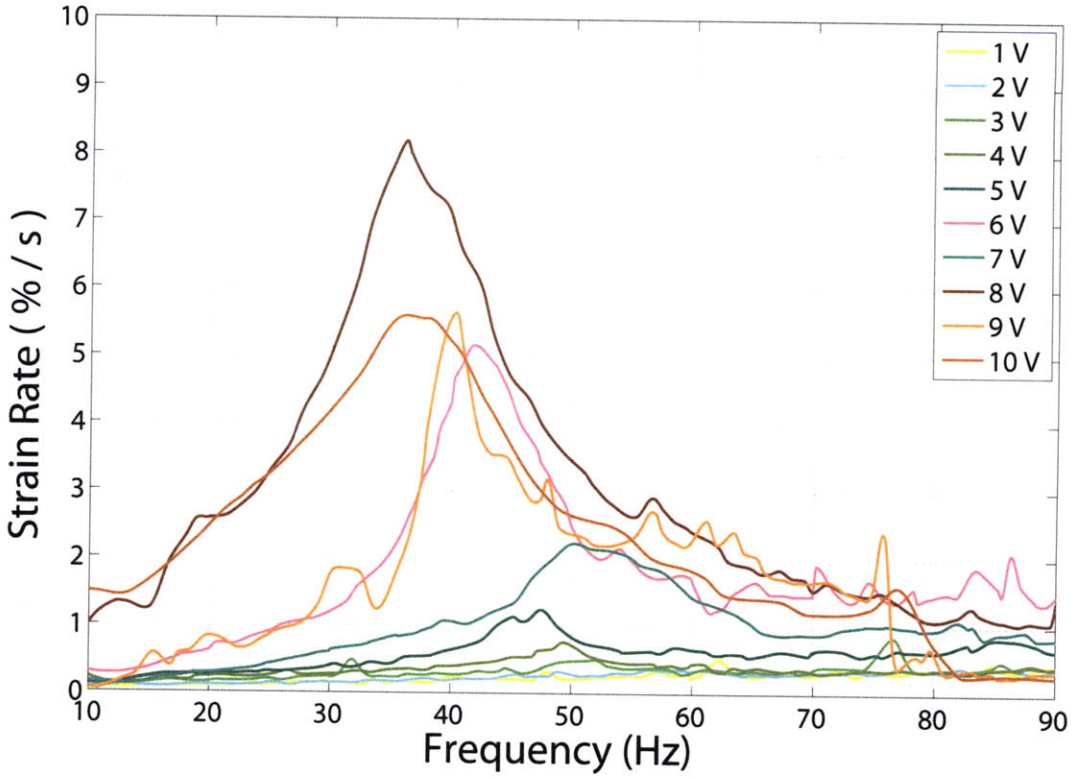

Figure 21: Computed strain rates from the peak-to-peak strains shown in figure 20. Strain rates were determined by dividing the instantaneous peak-to-peak strain at a given frequency by half the period.

Resonance actuation systems can also be used to generate higher strain rates. While the strain values in Figure 20 are still relatively low for polypyrrole actuators, it is important to consider that such strains are occurring at relatively high frequencies. Therefore, an important metric to consider is the strain rate of the actuator. Here, the strain rate is determined by dividing the peak to peak amplitude, as shown in Figure 20, by the time interval over which actuation occurs (in this case, one half of the actuation period). A plot of the strain rate as a function of frequency is shown in Figure 21.

The strain rate of polypyrrole actuators is typically less than 1% per second, and in certain cases, has been reported up to 6% per second through the exploitation of resonance. Here

the resonant system has caused a strain rate of 8.3% per second, near 33 Hz. While this is still far lower than the strain rate of mammalian skeletal muscle (up to 100% per second), it opens up the possibility for actuation systems that are designed to exploit resonance in order to achieve either high strain rates of significantly higher strains at relatively high frequencies.

Chapter 5 Length and Tension Sensors

5.1 Introduction

Stain gages are used to measure the mechanical length changes of a material. Commercial strain gages commonly used in civil engineering are made from copper, nickel, or platinum alloyed thin metallic films, that, when undergoing strain, change their electrical resistance. Metallic strain gages are susceptible to environmental conditions (e.g. temperature, humidity), but various measurement and signal processing techniques have been developed to accommodate for these sources of environmental noise.

In practice, however, strain gages (or mechanical length sensors) need not be limited to a specific metallic compound or thin film configuration, so long as length transduction occurs in some measureable, repeatable form. Other materials such as piezoelectric substrates and conducting polymers can also be used as length sensors or strain gages.

Conducting polymer length sensors have primarily been investigated in two configurations. In the first configuration, non-modified free-standing conducting films have been shown to exhibit a change in resistance as they are stretched [29]. The resultant change in resistance occurs in part because of geometric changes that the film undergoes during stretching [49]. In the second configuration, a fibrous, elastic material such as Lycra® is coated with a conducting polymer. As the material stretches, the distance between individual strands of the interwoven fiber mesh mechanically slide past each other, thereby increasing the total distance from the two points of tension. As the mesh stretches, the resistance between these points increases [37]. Examples of conducting polymer coated elastic materials have been used in a wide variety of applications [8, 37, 49].

5.2 Design Considerations

Several important considerations must be taken into account when considering the type of conducting polymer length sensor that should be used for artificial muscle actuation systems. Some critical criteria include:

- resolution (gage factor)
- measurable range of strain
- repeatability
- lifetime
- mechanical properties of the length sensor (e.g. elastic range, elastic modulus, yield stress)
- sensor geometry

The resolution of a strain gage is commonly denoted by its gage factor, which is a measure of the sensor's change in resistance for a given strain. The gage factor (GF) is commonly denoted by the equation:

$$GF = \frac{\Delta R/R_G}{\varepsilon} \quad , \tag{5-1}$$

where ΔR is the change in resistance of the strain gage for a given strain, ε, and R_G is the resistance of the strain gage under no strain. Metallic strain gages typically have gage factors near 2. Polypyrrole coated elastic fibers have gage factors which range from 2.5 to 10 [37]. Free-standing polypyrrole films have been previously reported to have gage factors near 2.5 [49].

The strain range over which strain gages are able to render repeatable measurements varies distinctly between the two common conducting polymer length sensor configurations. Length sensors fabricated from conducting polymer coated elastic fabrics have been shown to have measureable strains up to 100% [37]. Free-standing conducting polymer films, however,

can only measure strain accurately if they do not exceed the elastic region of the material, which typically ranges between 2 and 4% [29].

The repeatability and lifetime of conducting polymer length sensors is a factor of the material composition and the maximum strain it experiences. One critical hindrance to conducting polymer coated elastic fabrics is that the number of cycles in which strain can accurately be measured is limited. One set of studies, for example, demonstrated that strain repeatability for polypyrrole coated elastic Lycra® was limited to 15 cycles [37]. No lifetime studies prior to this work have been performed on free-standing films.

Some final design considerations for conducting polymer length sensors are the passive mechanical properties of the length sensors and the geometry under which they will operate. In a conducting polymer actuation system, where the dimensions of the length sensor may be of the same order of magnitude as the dimensions of the actuator, if the length sensor is too stiff, it will impede the actuator's performance. Also, if the length sensor does not geometrically scale such that it can be reduced in size yet maintain its measurable strain range, then the sensor will be limited only to large displacement applications.

Taking these design consideration into account, this work pursues the investigation of free-standing polypyrrole films as the length sensor of choice. Free-standing films are mechanically compact, can be reduced in size yet maintain moderate gage factors, and will be shown to have a longer lifetimes than conducting polymer coated elastic materials.

5.3 Mechanical Testing of Polypyrrole Length Sensors

Polypyrrole length sensor tests were performed on a modified version of the electrochemical dynamic mechanical analyzer [25, 46]. Films were held under tension by electrically conducting mechanical clamps that had gripping forces exceeding 20 N. A

mechanical stage stretched the polypyrrole films at computer-controlled strain rates, frequencies, and amplitudes while a force sensor measured the sample stress.

The change in resistance of the polypyrrole length sensor as a function of strain was determined by incorporating the polypyrrole length sensor into a Wheatstone bridge, shown in Figure 22. The signal output from the Wheatstone bridge was passed through a signal conditioning amplifier (Vishay, 2311) with a bridge excitation voltage of 0.7 V, a gain of 100, and a 100 Hz cutoff low-pass filter. All films presented in this work were tested under the same electrical configurations. Film samples were cut to standard lengths (3 mm x 15 mm) and typically had thickness between 20 and 25 μm.

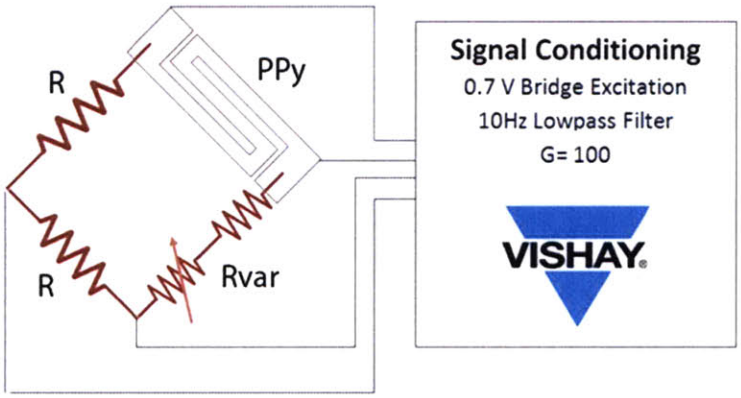

Figure 22: Wheatstone bridge configuration used for testing polypyrrole length sensors. The Wheatstone bridge is composed of fixed value resistors (R), a potentiometer (Rvar) and a polypyrrole length sensor (PPy).

From the Wheatstone bridge, the change in resistance was determined by the equation:

$$V_{Ex} = V_{out}\left(\frac{R_g}{R_g+R_s} - \frac{1}{2}\right), \tag{5-2}$$

where V_{Ex} is the excitation voltage, V_{out} is the recorded output voltage, R_g is the length sensor's resistance, and R_s is the resistance of the fixed resistor.

5.4 Mechanical and Electromechanical Properties of Polypyrrole Films

Dry polypyrrole films typically have an elastic modulus near 800 MPa and tensile strengths as high as 150 MPa [29]. Figure 23 shows a typically stress-strain curve for a polypyrrole length sensor. This particular sample has an elastic modulus of 794 MPa. The area indicated in red shows the linear-elastic region of the material, which is limited to slightly less than 5% strain. Above 5%, polypyrrole begins to permanently deform, as indicated by the change in slope of the stress-strain curve.

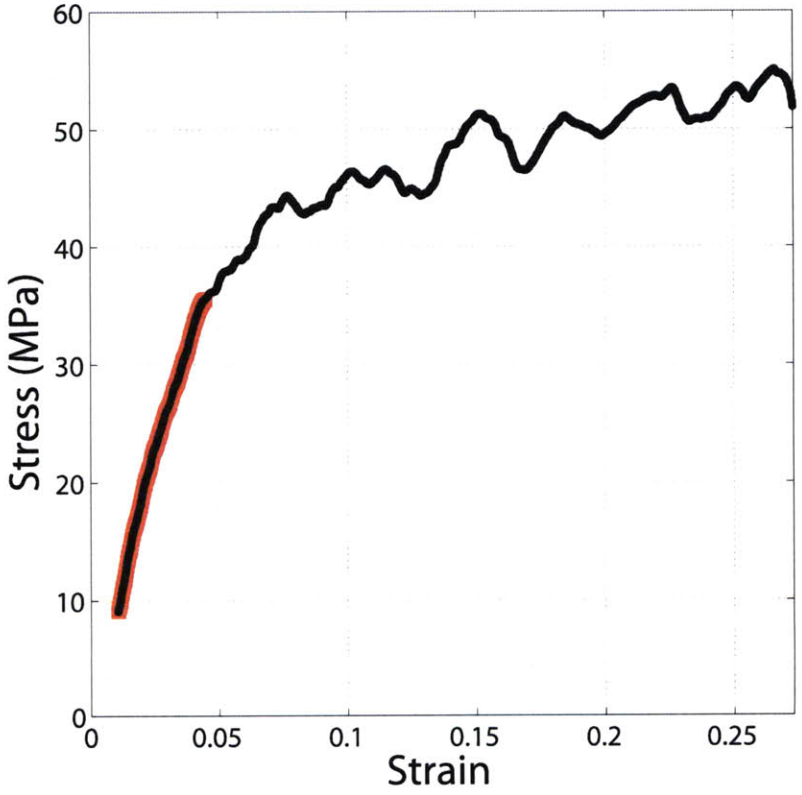

Figure 23: Stress-strain curve of polypyrrole length sensor. The region in red indicates the linear elastic region of the sample.

During the stretching of polypyrrole films, the change in resistance was measured at a sampling rate of 100 Hz from the output of the signal conditioning amplifier. Using Equation 5-2 the resistance of the length sensor as a function of strain was determined. One example plots is

shown in Figure 24. The red highlighted region in this plot indicates the region of elasticity. The small fluctuation in resistance, seen at about 2.5% strain, is due to noise in the system and is discussed in more detail in the next section.

From Figure 24 the gage factor can also be determined using Equation 5-1. For this particular sample, the gage factor was 4.0. Over the course of this work, gage factors varied from 0.5 to 8. Although no systematic study has been performed to determine what parameters affect the gage factor of polypyrrole, one contributing factor is the film's age. Over the course of this work, freshly deposited films tended to exhibit higher gage factors and larger elastic regions of strain, while older films were more brittle and exhibited less changes in resistance as a function of strain.

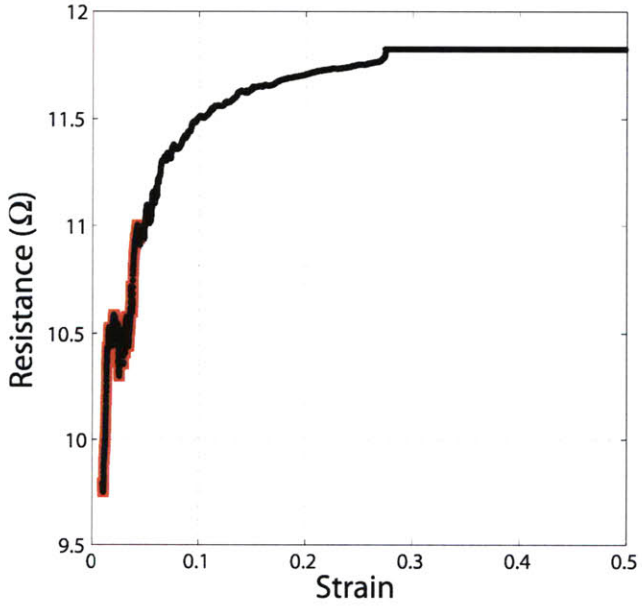

Figure 24: Change in resistance of polypyrrole length sensor as a function of strain.

One drawback to using free-standing polypyrrole films as length sensors is the viscoelastic behavior the films exhibit under large stresses. Previous researchers have developed viscoelastic models to simulate this aspect of polypyrrole length sensors [49]. Figure 25 shows

the viscoelastic behavior of a free-standing polypyrrole film subject to a constant, 1.5 MPa load over a period of 4 hours. The change in strain over time shows that the polymer will exhibit viscoelastic behavior when subject to sufficiently high pre-loads.

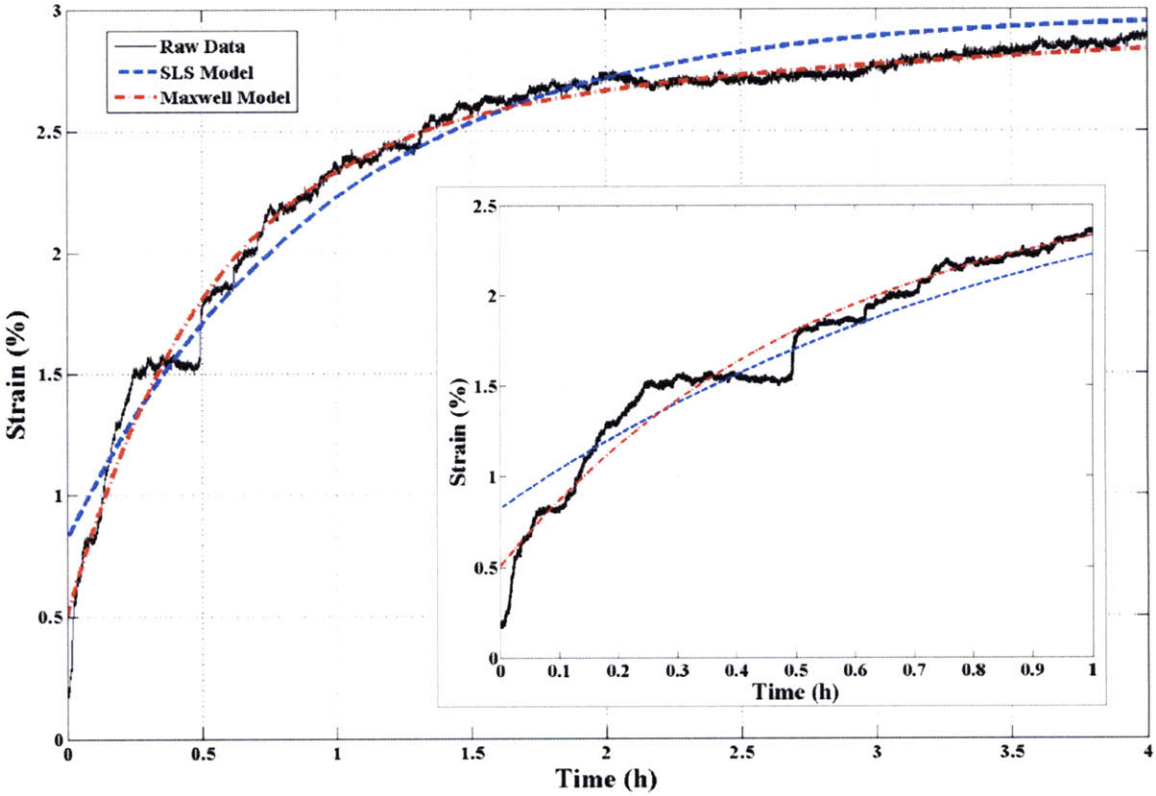

Figure 25: Viscoelastic behavior of polypyrrole length sensor when subject to a constant 1.5 MPa stress. From [49].

5.5 Length Sensor Bandwidth

The bandwidth limitation of free-standing polypyrrole length sensors was characterized in order to determine whether frequency affected length sensor performance. For this study, films were subject 2% sinusoidal strain inputs over frequencies ranging from 0.01 Hz to 30 Hz. The distribution of frequencies tests was similar to those discussed in Table 3.

Figure 26 shows the change in resistance of a polypyrrole length sensor when subject to a sinusoidal, 2% strain input of 0.01 Hz. At this low frequency, the change in resistance roughly

follows the shape of input strain, but environmental noise is clearly visible. Low frequency tests at various strain amplitudes (1%, 2%, and 3%) all showed this characteristic fluctuation in the output signal, which appears to occur on the order of seconds.

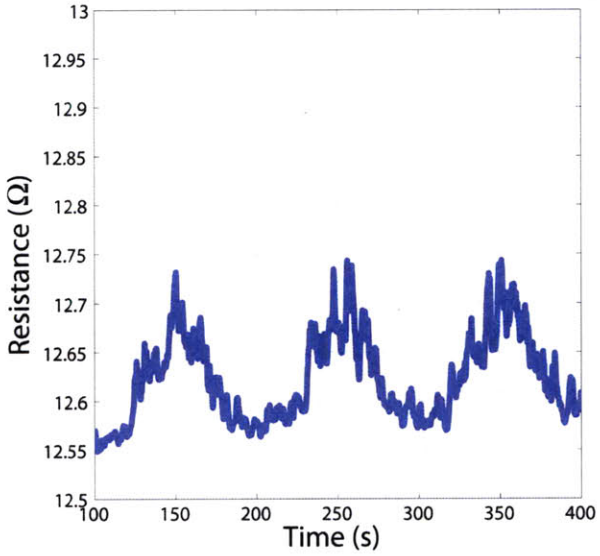

Figure 26: Change in resistance of polypyrrole length sensor when subject to a 2% strain, sinusoidal input at 0.01 Hz.

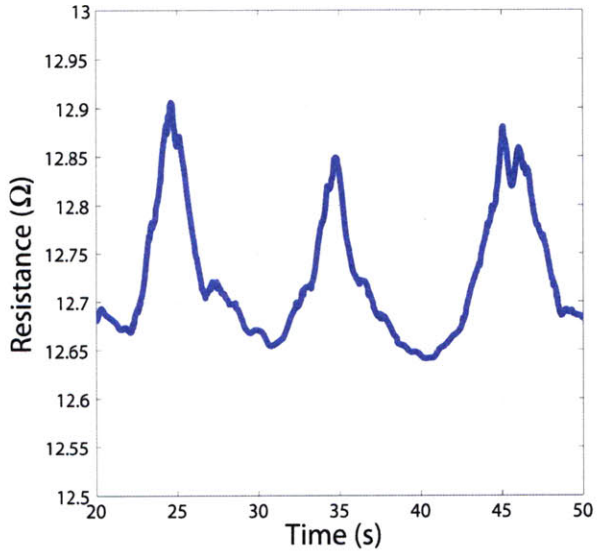

Figure 27: Change in resistance of polypyrrole length sensor when subject to a 2% strain, sinusoidal input at 0.1 Hz

Figure 27 shows the change in resistance of a polypyrrole length sensor when subject to a 2% sinusoidal strain at a frequency of 0.1 Hz. The noise here is slightly less apparent than at 0.01 Hz, and can be attributed to the fact that the graph shows a shorter period of time. The total change in resistance (peak-to-peak) as a function of strain is slightly larger than that at 0.01 Hz.

At 1 Hz (Figure 28), the change in resistance closely follows the sinusoidal shape of the input strain. Small fluctuations in noise are only slightly visible, and could be due to electrical characteristics of the system or thermal fluctuations.

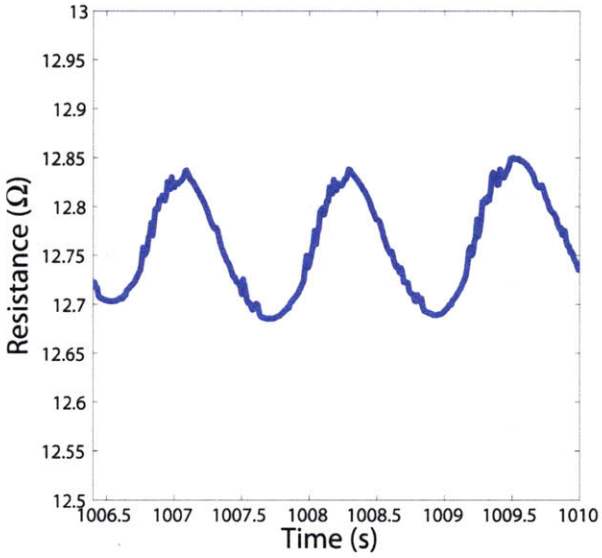

Figure 28: Change in resistance of polypyrrole length sensor when subject to a 2% strain, sinusoidal input at 1 Hz.

At 10 Hz (Figure 29) the change in resistance again takes on a slightly distorted version of the input sine wave, this time with a slightly larger peak-to-peak amplitude. Noise is almost entirely absent over the time frame of a single cycle.

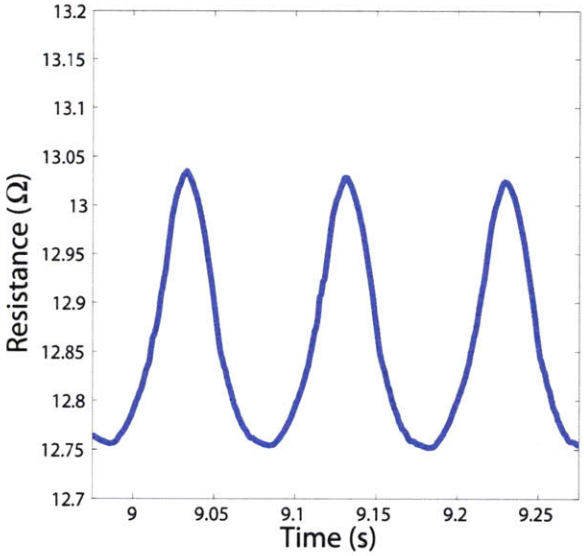

Figure 29: Change in resistance of polypyrrole length sensor when subject to a 2% strain, sinusoidal input at 10 Hz.

After examining individual frequencies, the peak-to-peak change in resistance as a function of a 2% strain sinusoidal inputs was also measured across the entire frequency range. The result, shown in Figure 30, suggests that the change in resistance for constant amplitude, 2% strain sinusoidal inputs fluctuates between about 0.1 and 0.4 Ω over the frequency range tested, with an average change in resistance near 0.2 Ω. There is an observed, fluctuating noise amplitude of 0.2 Ω along the entire frequency range. The fluctuation does not appear to be frequency dependent, except perhaps at very low frequencies where the resistance appears more stable.

Polypyrrole length sensors also appear to have a time dependent modulus of elasticity, something that becomes apparent when examining the stress response of a polypyrrole length sensor when subject to a constant amplitude strain at various frequencies. Figure 31 shows the peak-to-peak stress experienced by the polymer when subject to a constant 2%, sinusoidal strain at frequencies ranging from 0.05 to 30 Hz. The discontinuities at each order of magnitude (0.1

Hz, 1 Hz, 10 Hz) are an artifact of the testing protocol, where films were allowed to relax for 60 seconds while the data were being saved.

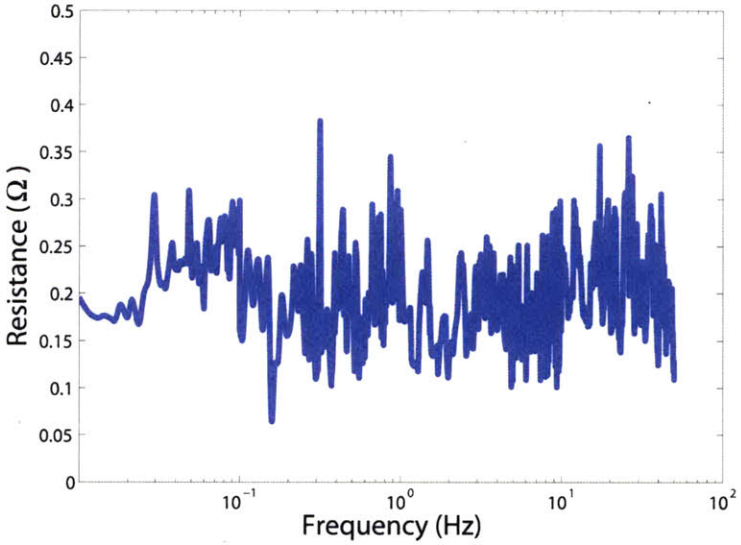

Figure 30: Peak-to-peak change in resistance of polypyrrole length sensor when subject to a 2% strain, sinusoidal input at frequencies ranging from 0.01 Hz to 30 Hz.

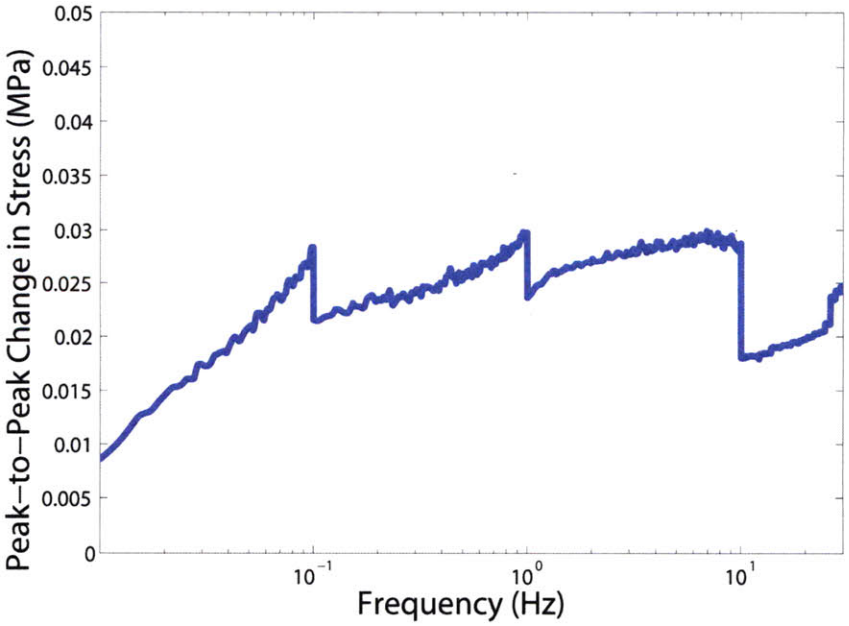

Figure 31: Peak-to-peak change in stress of polypyrrole length sensor when subject to a 2% strain, sinusoidal input at frequencies ranging from 0.01 Hz to 30 Hz. The discontinuities at 0.1 Hz, 1 Hz, and 10 Hz are from relaxation intervals in which the system was saving the experimental results.

From the Figure 31, a slight increase in the stress response to a constant sinusoidal strain appears markedly at low frequencies (0.01 to 0.1 Hz) and then levels off at higher frequencies. Over each interval, however, the stress response increases as the frequency increases. This increase in stress may be due to repeated cycling or increased frequency excitation.

5.6 Summary

From this set of length sensor tests, several conclusions can be drawn. First, noise within the system is preventing polypyrrole length sensors from being used to measure stable, steady-state lengths. Further work needs to be performed in order to determine whether the source of system noise is related to the environment, the instrumentation, or is an inherent property of polypyrrole length sensors. Regardless of noise, however, polypyrrole length sensors do show viscoelastic behavior, which at the moment excludes them from being used for high stress, steady state length measurements. While one way to improve the viscoelastic behavior may be to synthesize polypyrrole-carbon nanotube composite films [25, 42], viscoelasticity does not exclude free-standing polypyrrole length sensors from being used in artificial muscle actuation systems. The dynamic nuclear bag fibers that make up part of the muscle spindle are sensitive to rate changes in muscle length, not steady state conditions. Free-standing polypyrrole films have been shown to operate over a wide bandwidth, and, at short time intervals, accurately measure the change of strain. For these reasons, polypyrrole length sensors may be employable as dynamic length sensors in artificial muscle actuation systems.

Chapter 6 Energy Storage

6.1 Introduction

Energy storage is a fundamental component necessary for creating integrated artificial muscle actuation systems. Within the mammalian biological system, energy storage is integrated within the mechanical structure of muscle; it is localized, scalable, regenerative, and mechanically flexible. Considering these criteria led to the investigation of the conducting polymer supercapacitors.

As energy storage devices, polypyrrole supercapacitors are rechargeable, up to at least 1000 cycles, have energy densities near 89 kJ/kg and have high power densities approaching 2 kW/kg [50]. Several important questions concerning the performance of polypyrrole supercapacitors, however, remain unanswered. First, are polypyrrole supercapacitors scalable? Secondly, can polypyrrole supercapacitors operate on flexible substrates, so that they can be integrated into soft actuation systems? Finally, what are the performance metrics of polypyrrole supercapacitors for various electrolytes and dopants, and are there means to improve metrics such as power density, energy density, and self-discharge so that they can be used in actuation systems? This chapter seeks to answer these questions by investigating various properties of polypyrrole supercapacitors through various electrochemical analysis techniques.

6.2 Theory of Energy Storage in Electrochemical Conducting Polymer Redox Supercapacitors

Electrochemical supercapacitors are commonly classified into two categories: double layer supercapacitors and redox supercapacitors. In double layer supercapacitors, charge is stored by the accumulation of an ionic double layer on the surface of the capacitor's electrodes.

Whereas electrostatic capacitors have a dielectric separator between two parallel plates of opposite charge, the plates of a double layer supercapacitors are separated by a non-conducting membrane soaked in an electrolyte or a solid electrolytic material. Carbon-based materials (e.g. carbon fiber matrices, carbon nanotube sheets, paste/resin combinations) are the most common electrode material in such capacitors. With double layer supercapacitors, charge is stored as a function of surface area, and current research is focused on increasing the surface area of various carbon substrates [51, 53, 54, 55]. Double layer supercapacitors can already be found in commercial applications such as computer battery backup systems and certain electrical systems where high power densities are required.

Redox supercapacitors differ from electrochemical double layer capacitors in several regards. First, the mechanism of charge storage does not occur at the electric double layer, but through a faradaic reaction of charge transfer occurring between the electrolyte and the electrode. This process of charge transfer has been previously discussed in Chapter 3 and Chapter 4, and is sometimes referred to as doping and un-doping, or oxidation and reduction.

The kinetics of electrochemical charge and discharge in redox supercapacitors are reversible, relatively fast (depending on various system parameters), and scales by means of material volume or mass, as opposed to surface area. In this work, all specific results are presented with respect to mass.

Electrochemical redox supercapacitors can be further categorized depending on the chemical composition of the opposing electrodes. Three common redox supercapacitor configurations are (a) symmetric electrodes that have identically doped polymers, (b) un-symmetric electrodes that have two different doped polymers, each of which operates (oxidizes and reduces) over a different voltage range, (c) un-symmetric electrodes that have non-

identically doped plates, where one plate is a p-doped polymer while the other plate is an n-doped polymer. This work only deals with capacitors of type (a).

Conducting polymer redox supercapacitors transfer charge in a manner similar to batteries. The process of doping and un-doping is described through Equations 6-1a and 6-1b as:

$$(M)_n + nyA^- \underset{\text{undoping}}{\overset{\text{p - doping}}{\rightleftharpoons}} (M^{y+}A^-_y)_n + nye^- \quad , \qquad (6\text{-}1a)$$

$$(M)_n + nye^- + nyC^+ \underset{\text{undoping}}{\overset{\text{n - doping}}{\rightleftharpoons}} (M^{y-}C^+_y)_n \quad , \qquad (6\text{-}1b)$$

Where M is the monomer unit, A^- and C^+ are anions and cations respectively, e^- is the electron and n and y are integer values [56].

6.3 Electrochemical Testing Background

There are several electrochemical techniques that can be used to evaluate redox supercapacitors. A short description of the techniques used in this work, along with relevant equations are presented here.

6.3.1 Impedance Spectroscopy

Impedance analysis is commonly used with electrical circuits to analyze the gain and phase information of passive electronic components. For a simple resistor, the impedance value is the ratio of the voltage to the current passing through the resistor over a given frequency range. All electrical components, however, do not behave as ideal resistors. Impedance therefore is best expressed by being written in its complex form, defined by the ratio of voltage to current at a particular frequency, where its value contains both a magnitude and an associated phase.

The magnitude of a system's impedance is defined at the ratio of the voltage magnitude to the current magnitude. The phase of the system's impedance (its complex component) is the

phase shift by which the current passing through the system leads the voltage. Systems are also sometimes described by admittance, which is the reciprocal of impedance, and carries the units of Siemens or 1/ohm.

A log-log plot of the gain versus frequency data from impedance analysis enables a quick estimation of a component's (or combination of components) behavioral characteristics as a function of frequency. For example, an ideal resistor will show a constant gain, with a phase of 0^{o}. An ideal capacitor will have a slope of -1, with a phase at -90^{o}, where the voltage leads the current.

In electrochemical systems, the concept of impedance analysis remains the same. Electrochemical impedance measurements, also referred to as electrochemical impedance spectroscopy, apply the concept of impedance analysis to an electrochemical system. Electrochemical impedance spectroscopy can be performed by applying a set of sinusoidal frequencies across an element with a fixed potential (Potential Electrochemical Impedance Spectroscopy, PEIS), or, (2) a fixed current (Current Electrochemical Impedance Spectroscopy, CEIS). The former, PEIS, was used for all of the tests in this work.

Low voltage signals are normally used in PEIS analysis, under the assumption that at small signal amplitudes the system can be approximated as linear. Ideally, in a linear system, the output current will be a sinusoidal pattern of the same frequency but a different phase than the input potential. In most cases, an electrochemical systems' response is pseudo-linear, i.e., it is linear only for small input voltages (normally less than 50 mV) [57].

A mathematical representation of impedance can be represented in its complex form by representing the input and output signals as periodic functions. The potential excitation signal can be expressed in the time domain as:

$$E(t) = E_0 \cos(wt) \quad , \tag{6-2}$$

where *E(t)* is the potential, *t* is time, E_o is the amplitude of the input signal, and *w* is the radial frequency. The relationship between the radial frequency and the frequency, *f*, in Hertz can be written as:

$$w = 2\pi f \quad . \tag{6-3}$$

In a linear system, the response of the system will be a current of a different amplitude I_0, and a shifted phase ϕ as described by:

$$I(t) = I_0 \cos(wt - \emptyset) \quad . \tag{6-4}$$

Similar to Ohm's law, the impedance of a time-varying system can be described by the ratio of current to voltage as:

$$Z = \frac{E(t)}{I(t)} = \frac{E_0 \cos(wt)}{I_0 \cos(wt - \emptyset),} = Z_0 \frac{\cos(wt)}{\cos(wt - \emptyset)}, \tag{6-5}$$

where the impedance, *Z*, is expressed in terms of a magnitude, Z_0.

For an electrochemical capacitive system, the value of capacitance can be determined from PEIS by the equation:

$$C = -\frac{1}{Z_{im} * w} \quad , \tag{6-5}$$

Where C is the capacitance and Z_{im} is the imaginary component of impedance [60].

6.3.2 Cyclic Voltammetry

Cyclic voltammetry is another method of characterizing electrochemical supercapacitors. In cyclic voltammetry, the capacitive system is excited with a time-linear voltage ramp over a specific voltage range. The shape of the current response from this ramp is then used to estimate the capacitance (and capacitive behavior) of the system. An example cyclic voltammogram from a polypyrrole supercapacitor is shown in

Figure **32**.

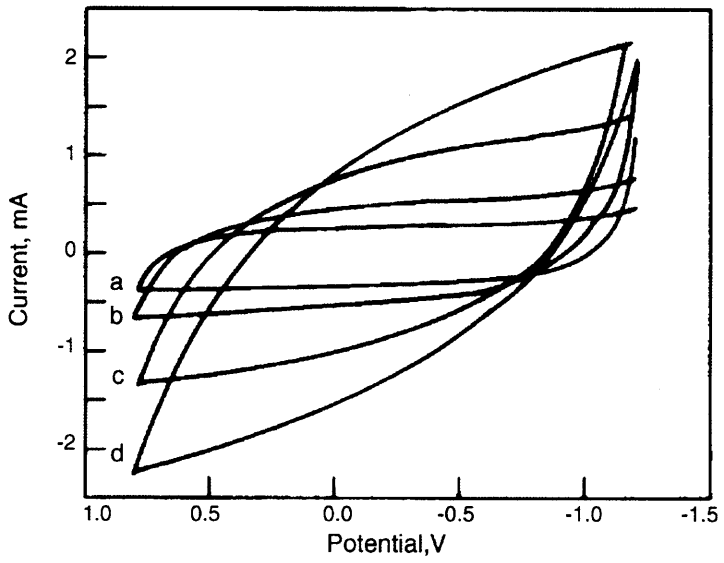

Figure 32: Example cyclic voltammogram of polypyrrole electrochemical redox supercapacitor. Letters indicate the various scan rates of (a) 1 mV/s (b) 2 mV/s (c) 10 mV/s (d) 20 mV/s. Taken from [61].

Ideally, the cyclic voltammogram for a redox supercapacitor will be a perfect square, where the current remains constant across the entire voltage ramp. While

Figure **32** is not ideal, as the scan rate is reduced, the supercapacitor behaves more and more like the ideal case.

From the cyclic voltammogram, the capacitance of the system can be estimated by the equation:

$$C = \frac{i}{s} \ , \tag{6-6}$$

where C is the capacitance, i is the average current, and s is the scan rate [57].

6.3.2 Galvanostatic Charge Discharge

Galvanostatic charge discharge tests are useful for estimating the specific capacitance, the power and energy densities, the columbic efficiency and the cycling lifetime of a system. As the name suggests, galvanostatic tests are performed by charging and discharging the capacitive system with a constant current. Normally, this current is reported as a current density, (i.e. A/kg or A/m^2). For the tests reported here, all current densities have been reported with respect to mass.

From galvanostatic charge discharge curves the discharge capacitance C_d can be determined using the equation:

$$C_d = \frac{i\Delta t}{\Delta V} \ , \tag{6-8}$$

where i is the current density, Δt is the change in time over a specific interval, ΔV is the change in voltage over a specific interval, and $\Delta V/\Delta t$ is the slope of the linear portion of the charge discharge curve.

The energy density can also be determined from the charge discharge curves by the equation:

$$E = i \int \frac{V dt}{m} \ , \tag{6-9}$$

where i is the current, m is the mass of the electrode, t is time and V is the voltage. From the energy density, the power density, P, can also be determined by considering the ratio of the energy density E to discharge time t_d as:

$$P = \frac{E}{\Delta t_d} \quad . \tag{6-10}$$

A final measure of performance in electrochemical redox supercapacitors is the coulombic efficiency, which is defined as the ratio of discharge times, t_D, to charge times, t_C, and can be represented by the equation:

$$\eta = \frac{t_D}{t_C} \quad . \tag{6-11}$$

6.4 Fabrication Technology

Polypyrrole supercapacitors were fabricated from polypyrrole thins films using the recipe discussed in Chapter 7. Capacitors were made by separating two polypyrrole substrates with a thin PVDF membrane (Millipore, IPVH 00010). The membrane was soaked in electrolytes composed of tetrabutylammonium hexafluorophosphate (TBAP), tetraethylammonium hexafluorophosphate (TEAP), or tetramethylammonium hexafluorophosphate (TMAP). For all polypyrrole supercapacitors, 0.3 M concentrations of the above salts in propylene carbonate were used for all of the tests performed.

Supercapacitors were made in rigid, flexible, and rolled configurations. In the rigid configuration (Figure 33), polypyrrole was deposited directly onto gold coated glass microscope slides (CA134, EMF Corporation). The slides were then separated with porous membranes, soaked in electrolyte, and wrapped in Parafilm® to prevent them from drying out. Flexible substrates (Figure 34) were made by encapsulating two polypyrrole electrodes (separated with a

membrane) in a sealable, polyethylene container. Rolled substrates (Figure 35) were fabricated with the same process as flexible substrates, except that the films were rolled and then sealed in Parafilm®. Polypyrrole supercapacitors do not have a polarity associated with the electrodes, but the samples in the Figures 34 and 35 have polarity marks, to keep track of electrode testing conditions.

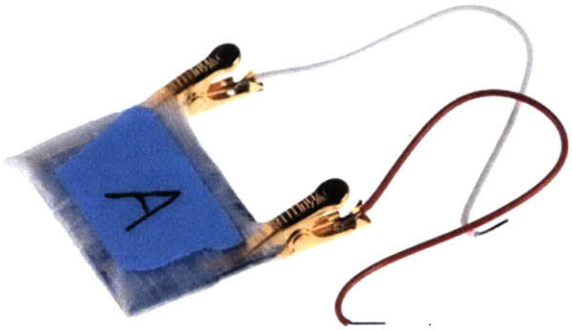

Figure 33: Polypyrrole supercapacitor fabricated from rigid, gold plated microscope slide. The supercapacitor is wrapped in Parafilm® to prevent the liquid electrolyte from evaporating

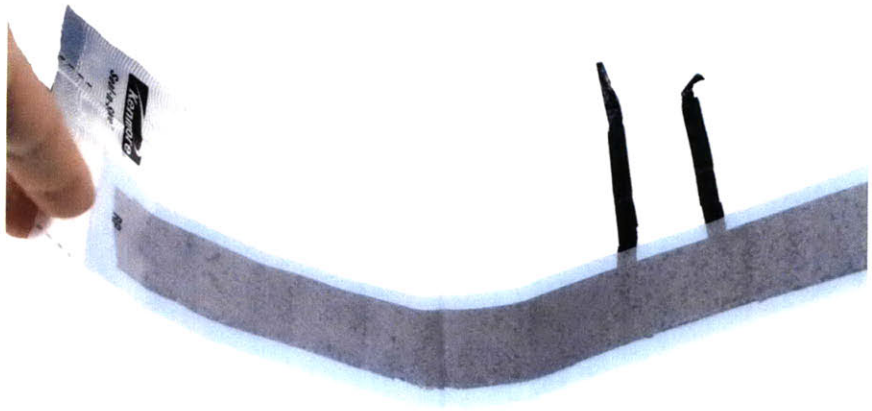

Figure 34: Flexible polypyrrole supercapacitor fabricated from free-standing polypyrrole films that are encapsulated in a sealable plastic casing. The two electrical contacts are black strips of polypyrrole films.

Figure 35: Rolled polypyrrole supercapacitor wrapped in Parafilm® to prevent evaporation. Although polypyrrole supercapacitor do not have polarity, electrodes were marked with "+" and "-" to keep track of the polarity of applied potential and current during testing.

6.5 Performance at Various Scan Rates

From cyclic voltammetry, the performance of a redox supercapacitor can be assessed by examining the shape of the curve, and by using Equation 6-6. The polypyrrole supercapacitor shown in Figure 32 is far from an ideal square shape. The sloped regions of the cyclic voltammogram indicate that the capacitor has a significant amount of resistance associated the system. While the average current over such sweeps indicate that the polypyrrole substrate will hold charge, actual implementation of such a polypyrrole supercapacitor is limited. This limitation is due to the face that larger internal resistances will result in larger current leaks. The protocols developed in this work have enabled significantly better capacitive characteristics for polypyrrole redox supercapacitors. One performance increase can be seen in Figure 36.

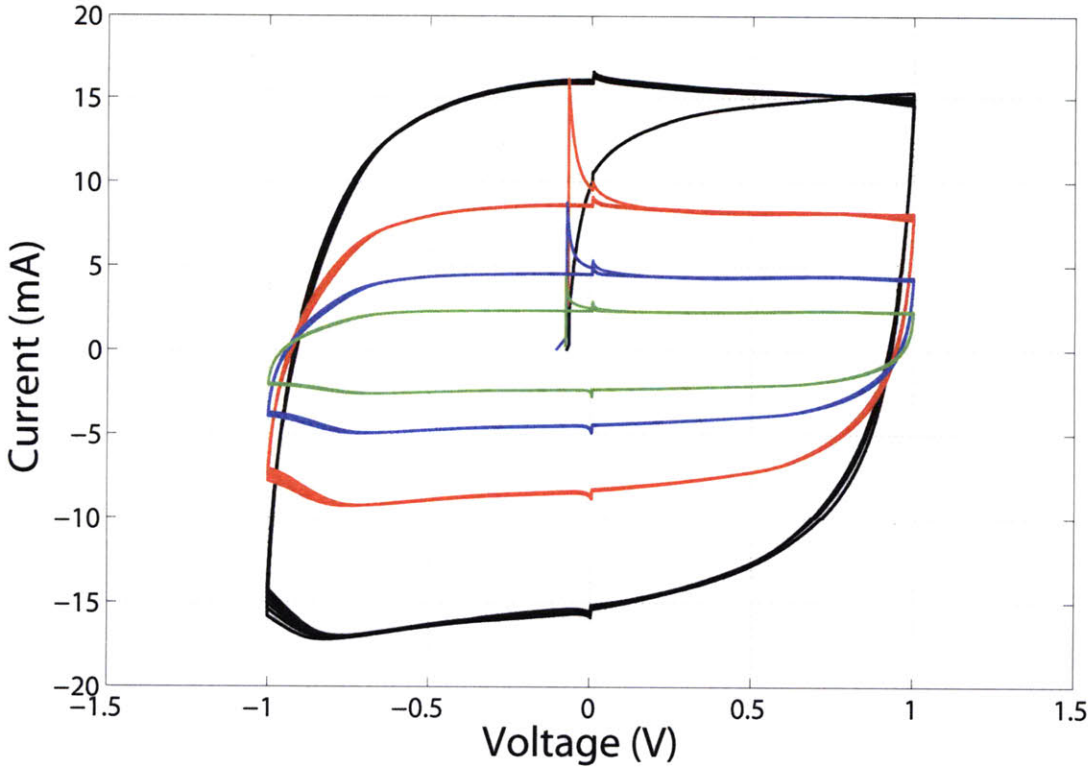

Figure 36: Cyclic voltammograms of rigid polypyrrole supercapacitors doped with TBAP and using a TBAP electrolyte. Scan rates vary by color: black (100 mV/s), red (50 mV/s), blue (25 mV/s), green (12.5 mV/s).

Figure 36 shows a variety of scan rates for a TBAP doped polypyrrole supercapacitor. The cyclic voltammogram shows remarkably flat regions of current flow between voltages of -0.5 V and 0.5V. As the scan rate decreases, the center regions flatten out slightly, which corresponds to lower excitation frequencies. Table 4 summarizes the specific capacitance for the scan rates presented in Figure 36.

Table 4: Capacitance values for TBAP doped polypyrrole supercapacitors in TBAP electrolyte at various scan rates.

Scan Rate (-1.0 V to 1.0V)	Capacitance x 10^4 (F/kg)
100 mV/s	2.07
50 mV/s	2.24
25 mV/s	2.35
12.5 mV/s	2.45

Cyclic voltammograms are also useful for estimating the voltage range over which a polymer supercapacitor can operate. Figure 37 shows the cyclic voltammogram of a TBAP doped polypyrrole supercapacitor at voltages of ± 1.0 V, ± 1.5 V, and ± 2.0 V. The resultant current characteristics for a ± 1.0 V scan suggest stable capacitive behavior below 0.5 V, with a small amount of degradation visible at the current peaks near -1.0 V and 1.0 V. At 1.5 V, this degradation becomes more visible, as the cyclic voltammogram deviates more and more from an ideal square shape. At 2.0 V, the polypyrrole supercapacitor degrades significantly.

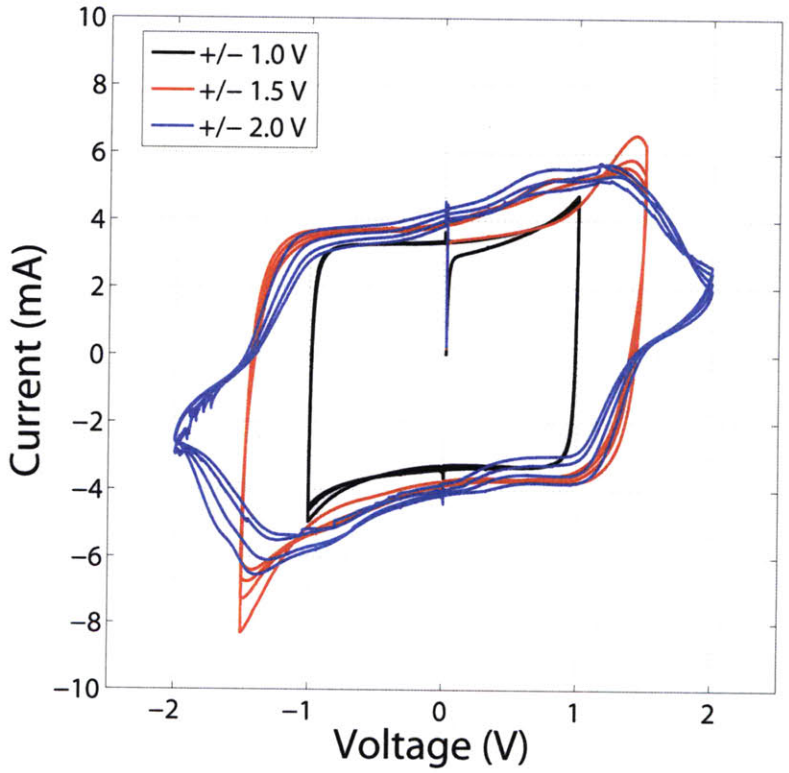

Figure 37: Cyclic voltammograms of rigid polypyrrole supercapacitors doped with TBAP and using a TBAP electrolyte. The supercapacitor was scanned at a constant 25 mV/s over various voltage ranges. Colors indicate the range: black (± 1.0 V), red (± 1.5 V), blue (± 2.0 V).

One possible cause of degradation is the fact that polypyrrole typically oxidizes around 1.0 V [62]. If the polymer has reached full oxidation, yet is brought to increasingly higher voltages, an excess of current will flow through the polymer substrate, causing it to degrade over

time. Repeated scans at higher voltages also increase this amount of degradation. For example, at scans of ± 1.0 V in Figure 37, the current follows the same curve each time. In each successive scan at ± 1.5 V and ± 2.0 V, the current increases on each successive scan.

6.5.1 Mass Scaling

When building artificial muscle actuation systems, it is important to determine whether a proposed power source will be able to scale with mass or volume. Muscle, as discussed in Chapter 2, has localized energy storage that scales up several orders of magnitude. An investigation of polypyrrole supercapacitors has been undertaken to see whether the performance metrics of the material also scale with size. As polymer-based redox supercapacitors store charge through a faradic reaction in the polymer matrix, scaling occurs not as a function of surface area, but as a function of the mass.

Mass scaling studies of polymer supercapacitors involved the investigation of two criteria: the capacitance as function of mass and the self-discharge as a function of mass. The samples for this study were all grown on glassy carbon crucibles, according to the protocol discussed in the previous section. PEIS characterizations were performed at 20 mV amplitudes, between the frequencies of 1 mHz and 200 Hz at a spacing of 25 points per decade.

Figure 39 shows the computed specific capacitances for each substrate, while Figure 38 shows the imaginary impedance and phase information of polypyrrole supercapacitors of different masses. Specific capacitances fell within the range of $1.25 \cdot 10^5$ F/kg to $1.75 \cdot 10^5$ F/kg. The close range of the specific capacitance suggests that the polymer is able store a specific amount of energy, independent of mass.

Experimental methods may have caused the slight variation in specific capacitances between samples, as all capacitors did not come from the same electrochemical deposition of

polypyrrole because of the required substrate sizes. The largest capacitor was made from two full glass carbon crucibles, while the smallest capacitor was made from 1/30 of a crucible. Slight variations in deposition conditions may have affected the material properties of the polypyrrole and therefore, the capacitance.

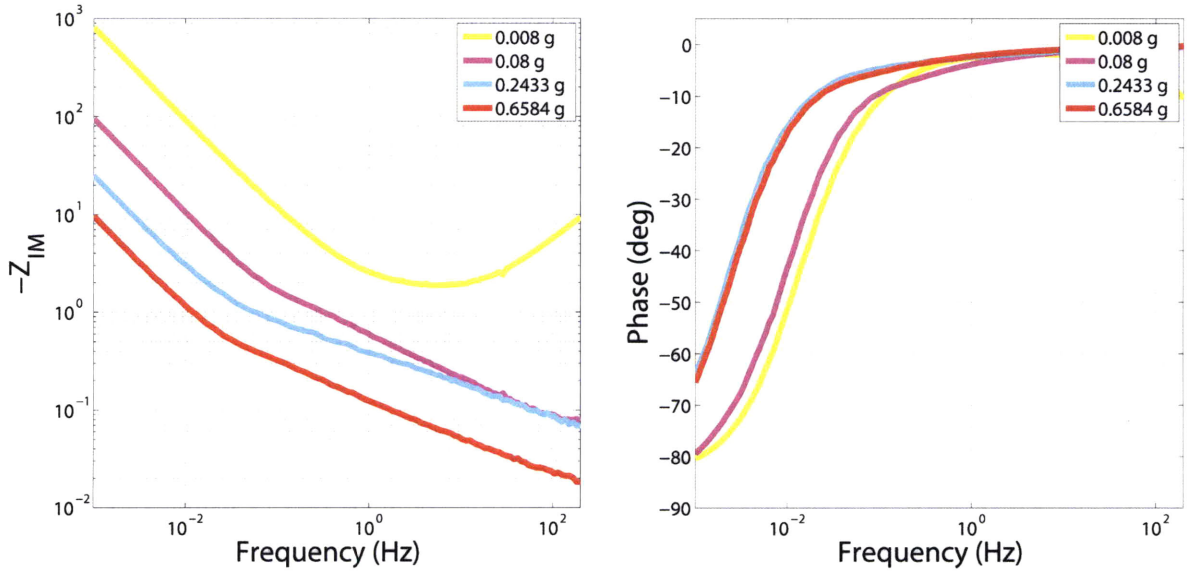

Figure 38: Impedance spectroscopy plots (PEIS) of the imaginary impedance and phase for flexible, polypyrrole supercapacitors of varying masses.

A second source of variation is the ratio of the area of the electrical contacts that charge the capacitor to the area of the capacitive substrate. For example, the smallest capacitor had 2 mm gold strips attached to each polypyrrole plate, occupying about 1/15 of the total surface area. The largest capacitor had 7 mm gold strips attached to the plates, which occupied about 1/45 of the total surface area. The current flux requirements for the large capacitors therefore may have affected the results.

From Figure 38 several other characteristics of mass-scaled capacitors can be determined. First, the slope of the imaginary impedance is consistent for frequencies below 0.01 Hz. This suggests that the capacitive behavior of polypyrrole is independent of mass at low frequencies. The variation at higher frequencies may be due to the fact that capacitance in polypyrrole redox

supercapacitor is, in part, a diffusion limited process. The phase information from Figure 38 suggests that as the mass decreases, the phase approaches -90° more rapidly. This may again be attributed to the charging time of the capacitors and the limits of diffusion. For the frequency ranges tested, none of the capacitors reach -90°. Such phase behavior was observed for all flexible supercapacitors, and can be attributed to the ability of the electrical contacts to charge and discharge the substrate rapidly and uniformly. Removing the metallically backed rigid substrates does not necessarily change polypyrrole's ability to store charge over time, but it does affect the charging rate.

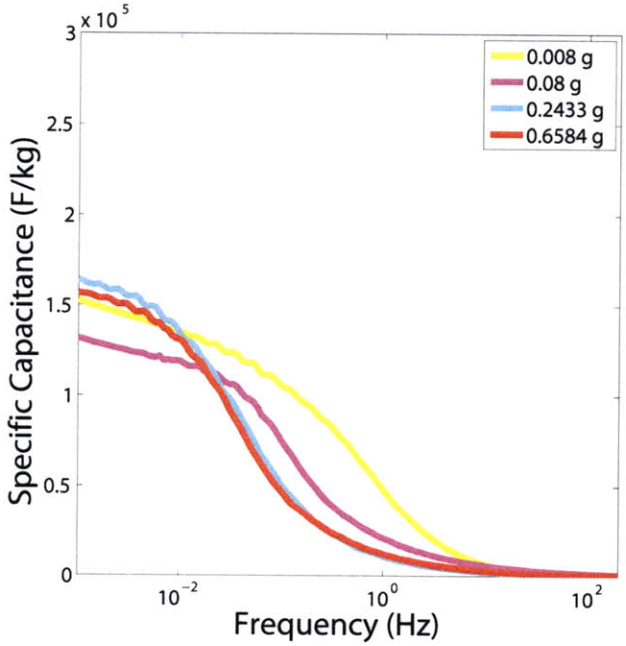

Figure 39: Specific capacitance of polypyrrole supercapacitors as a function of mass. Results show that specific capacitance (F/kg) scales with mass.

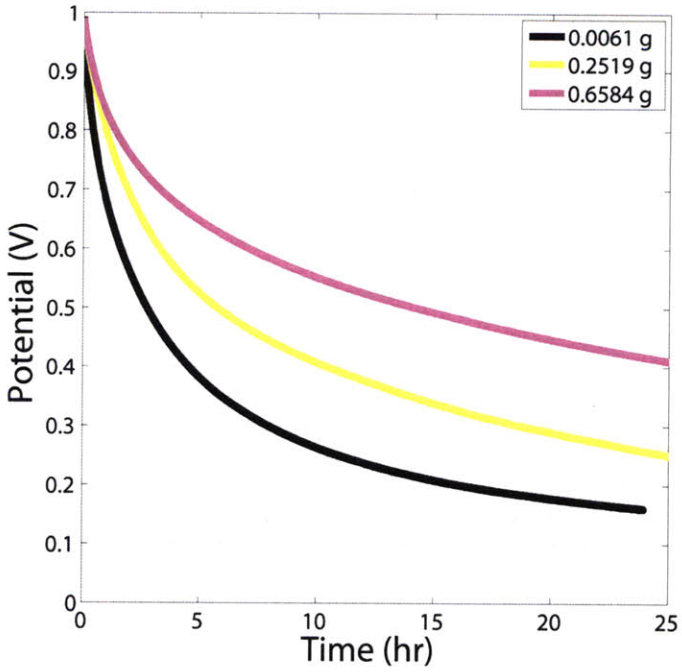

Figure 40: Self-discharge of flexible polypyrrole supercapacitors for various masses. More massive substrates hold their charge for longer periods of time.

The self-discharge behavior as a function of mass was also examined, the results of which are shown in Figure 40. The testing protocol consisted of charging the polypyrrole supercapacitors to 1.0 V until the charging current dropped below 100 μA. The applied voltage was then removed, and the potential difference across the plates was continuously monitored for 24 hours. Both series resistance and the total mass of the capacitor will affect the rate at which self-discharge occurs.

6.5.2 Electrolyte Dopant Matching

With polypyrrole actuators, previous studies have shown that matching polymer dopant and the ions in the electrolyte can significantly change actuation behavior. This concept of ion-pair matching was applied to polypyrrole redox supercapacitors as well, with the intent of quantifying how different dopants and electrolytes affected overall capacitive performance. Three different

dopants, tetrabutylammonium hexafluorophosphate (TBAP), tetraethylammonium hexafluorophosphate (TEAP), and tetramethylammonium hexafluorophosphate (TMAP) were chosen because all three dopants have the same counterion (PF^-6), and have similar molecular compositions. The three chemical structures of TBAP, TMAP, and TEAP are shown in Figure 41.

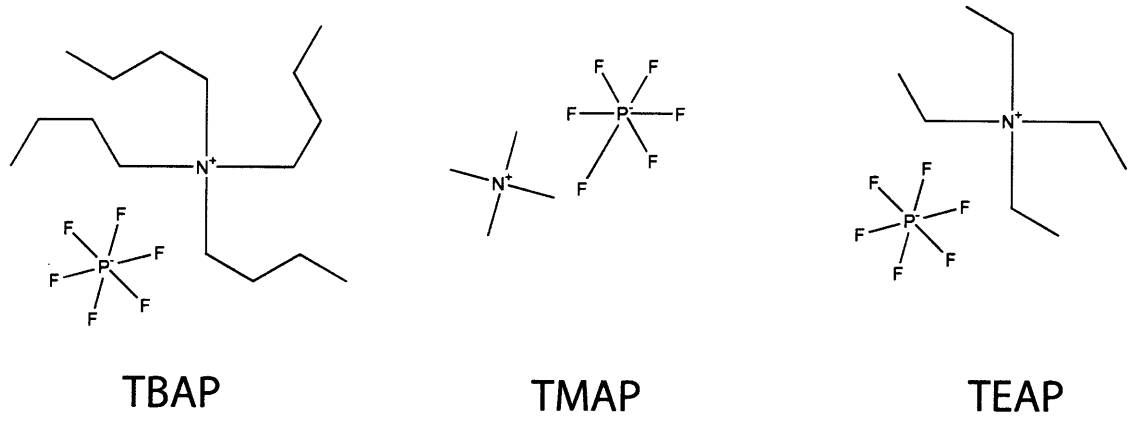

Figure 41: Chemical structure of dopants used in the electropolymerization of polypyrrole substrates that make up polypyrrole supercapacitors, and the dopant used in the electrolytes.

Polypyrrole supercapacitors were grown with each dopant, and each polypyrrole doped substrate type was paired to the three different electrolytes. From a comparison of PEIS tests (Figure 42), results show that matching the dopant ion with the ion in the electrolyte results in higher capacitance values at lower frequencies. The capacitive behavior of the system, indicated by the phase information, shows relatively consistent results for all tests except for the TBAP and TEAP doped polymers with TMAP electrolyte.

The self-discharge characteristics of the different ion-pair matching capacitors are shown in Figure 43. In terms of how ion-pair matching affects the self-discharge behavior of the capacitor, no obvious correlation was found between the impedance measurements of PEIS and the self-discharge characteristics. Nonetheless, polypyrrole capacitors that were doped during

electrochemical deposition with TMAP and soaked in a TMAP electrolyte were exceptionally capable of holding charge over extended periods of time. In most tests performed in this work, cell voltages dropped below 100 mV within 24 hours. With the TMAP/TMAP combination, the cell held 150 mV for 192 hours.

6.5.3 Geometry Effects

The effects of geometry were also investigated to determine whether changing substrate configurations affected the capacitive behavior of the polypyrrole. Both PEIS and discharge tests were performed on two pairs of TBAP doped polypyrrole supercapacitors. Each pair had the same mass, but one was rolled (Figure 35), while the other was encapsulated in the flat configuration without a metallic backing (Figure 34). PEIS plots of rolled capacitors showed aberrant behavior, where the phase remained above 45° for the majority of frequencies (data not shown). Rolled polypyrrole supercapacitors, nonetheless, were able to store charge. Figure 44 shows a comparison of self-discharge characteristics for rolled and flat polypyrrole supercapacitors. In the rolled configuration, the polypyrrole supercapacitors showed significantly less self-discharge over a 24 hour period. This ability to store charge longer may be due to the rolling geometry, the compressive force that rolling exerts on the polymer electrodes, or the change in separation distance between opposing electrodes because of the compressive force that rolling exerts on the porous membrane.

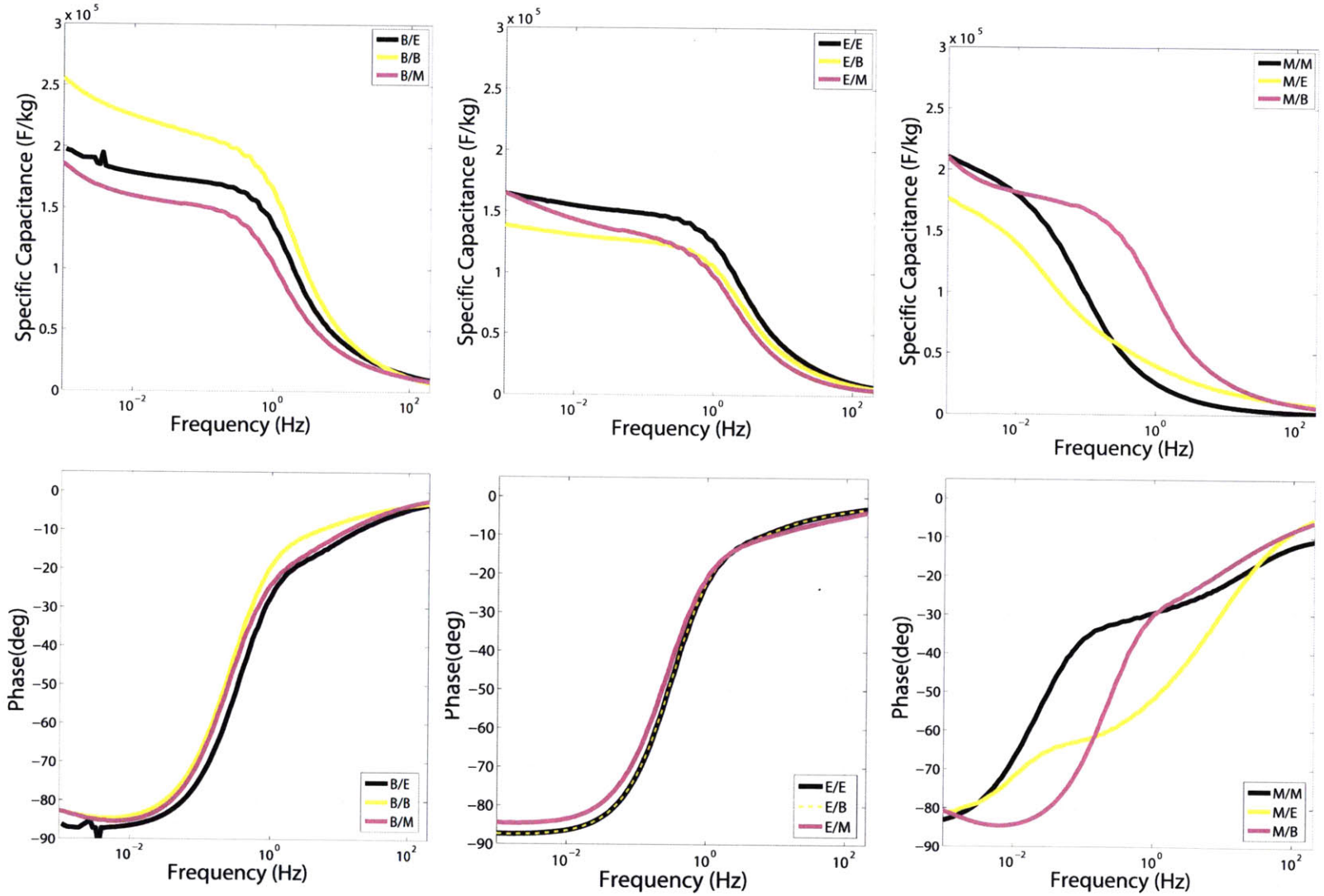

Figure 42: Specific capacitance of various polypyrrole dopants matched with various doped electrolytes. The results suggest that matching the dopant of the polymer with the dopant of the electrolyte consistently yields the highest specific capacitance at low frequencies.

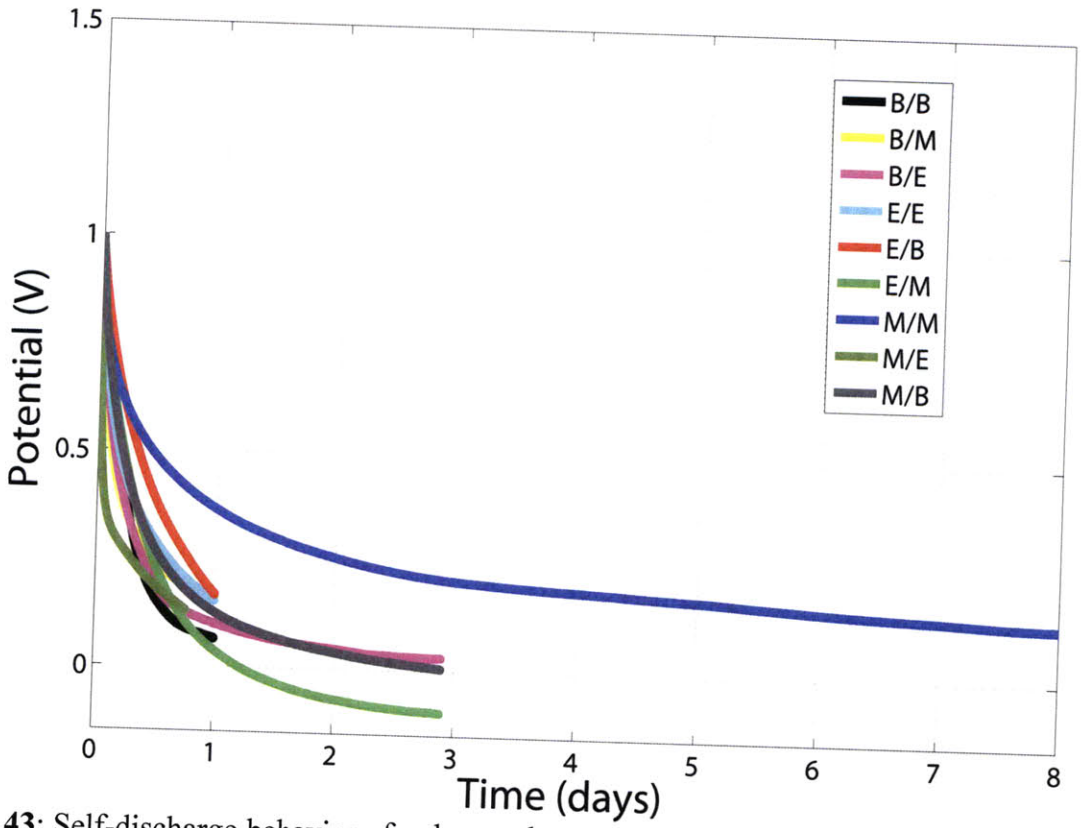

Figure 43: Self-discharge behavior of polypyrrole supercapacitors for various doped polypyrrole films and electrolytes. (E), (B), (M) legend entries represent TEAP, TBAP, and TMAP.

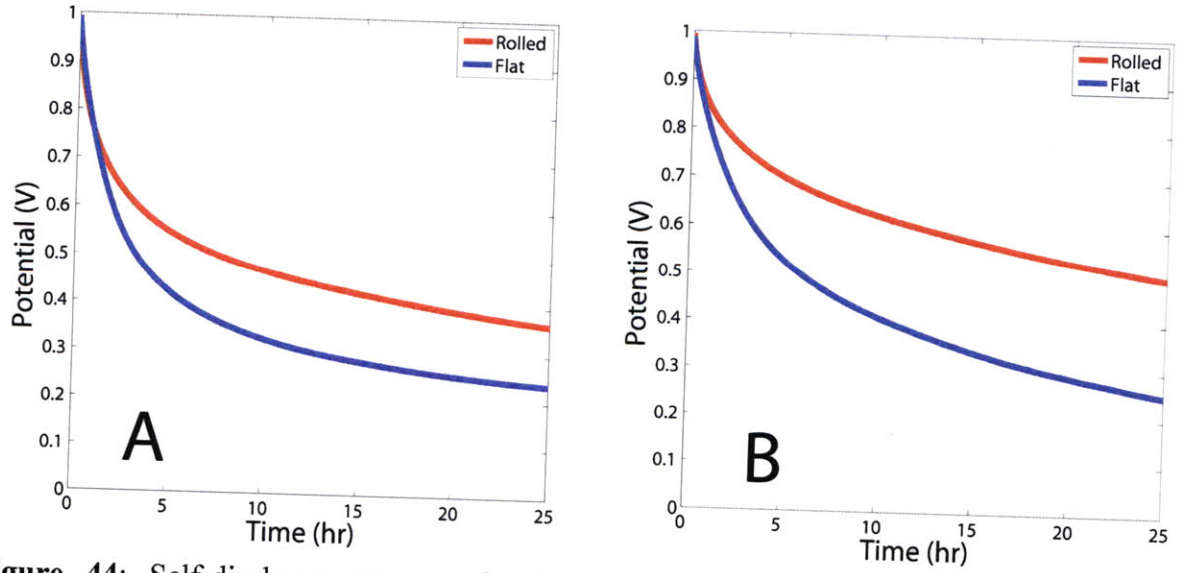

Figure 44: Self-discharge curves of polypyrrole supercapacitors in the rolled and flat configurations. Both supercapacitors in (A) had masses of 0.08 g. Both supercapacitors in (B) had masses of 0.245 g. Supercapacitors were charge to 1.0 V and then the open-circuit voltage was monitored over a period of 24 hours. Rolled capacitors are shown to hold charge for longer periods of time than flat capacitors of the same mass.

6.5.4 Galvanostatic Charge-Discharge Tests

From a series of galvanostatic charge discharge tests, the discharge capacitance, energy density, power density and columbic efficiency can be estimated. Table 1 summarizes these metrics for a TBAP doped polypyrrole supercapacitor with TBAP electrolyte. Galvanostatic charge-discharge testing was performed between the voltage limits of ±1.0 V at various current densities.

Table 5: Capacitance, energy, and power metrics of polypyrrole supercapacitors.

Mass (mg)	Discharge Capacitance at 1.0 V; ($\cdot 10^4$ F/kg)	Energy Density (kJ/kg)	Power Density (kW/kg)	Coloumbic Efficiency (%)
9.20	1.81	18.10	0.73	74
9.20	1.39	13.87	3.49	56
9.20	1.20	12.02	12.80	37
8.40	1.91	19.12	0.69	78
8.40	1.71	17.07	3.03	61
8.40	1.45	14.53	14.82	37

The results shown in Table 5 indicate that as the rate of charge and discharge increases, the power densities increase while the energy densities and columbic efficiencies decrease. Such considerations need to be taken into account when designing artificial muscle systems. For example, for a given power requirement, polypyrrole supercapacitor masses can be increased, so that they can provide an equivalent amount of power as a smaller supercapacitor (discharged at a faster rate), but with higher efficiency.

From galvanostatic charge-discharge cycling, the lifetime of the capacitor can also be estimated, as shown in Figure 45. A small amount of degradation is visible in this TBAP doped polypyrrole supercapacitor after 1000 cycles of charging and discharging. This degradation is

apparent by examining the reduction in the amount of time it takes to charge and discharge the capacitor.

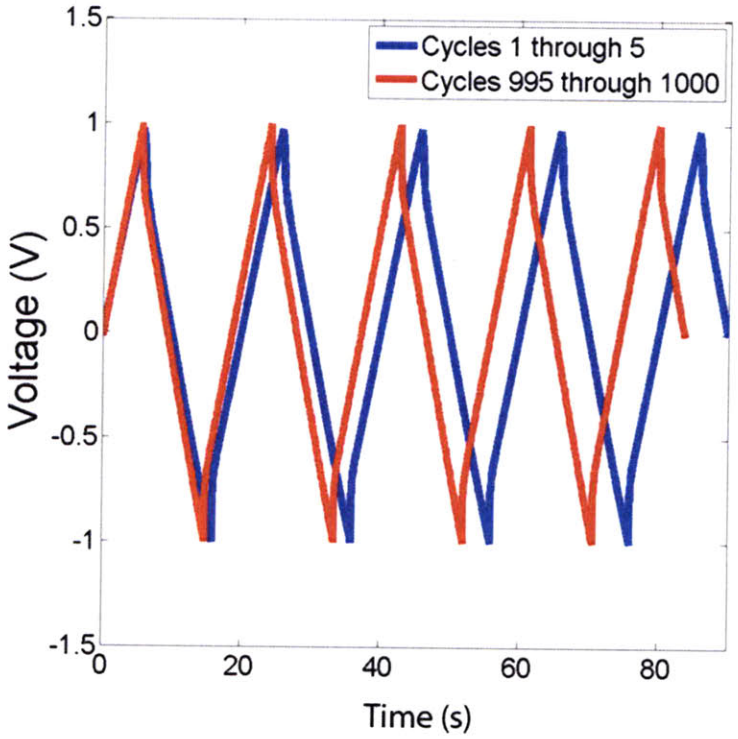

Figure 45: Change in charge-discharge characteristics of polypyrrole supercapacitor that is subject to continuous charging and discharging.

From continuous cycling, the change in capacitance can also be determined. Figure 46 shows this change in capacitance as a function of cycle number using Equation 6-8. These results suggest that initially during charging and discharging (~ first 500 cycles), the supercapacitor loses some of its ability to hold charge. After this period, the capacitance remains relatively constant for over 3,500 cycles.

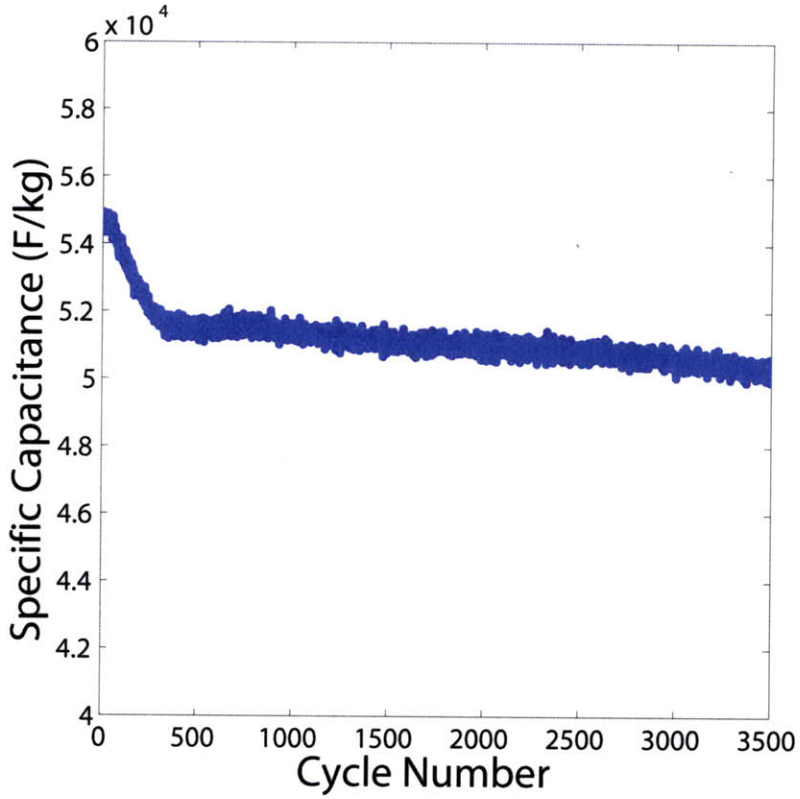

Figure 46: Change in capacitance of a TBAP doped polypyrrole supercapacitor in TBAP electrolyte as a function of cycle number.

Chapter 7 Fabrication Techniques

7.1 Introduction

Combining the various functionalities of polypyrrole onto a single substrate requires several important mechanical, electrical, and chemical considerations. Actuators and length sensors need to have mechanical attachments that do not impede the performance of the components themselves, yet enable coupling between components. Power sources must able to conform to the geometry of the substrate, and be distributed locally next to components which require energy. Components should be built in such a way that they can eventually be scaled in lateral, radial, or longitudinal directions. Recalling the geometric and functional relationships of the complex, compact mammalian skeletal muscle and the neuromuscular system, attempting to mimic this geometry presents a significant manufacturing challenge.

In the search for suitable manufacturing techniques and functional interfacial materials between active and passive components, several processes and substrates were considered. The investigation of mechanical attachments, electrical insulators, and multicomponent fabrication technologies are presented. The first four component, all-conducting polymer, single substrate actuation system is fabricated. In Chapter 8, an investigation into how these techniques affect the overall system performance is also addressed.

7.2 Polypyrrole Growth Techniques

7.2.1 Standard Polypyrrole Synthesis Protocols

For the majority of electrodepositions performed in this work, polypyrrole was polymerized according to a recipe developed by Yamaura [58, 59]. Modifications made within

the BioInstrumentation Laboratory over the past decade have also been taken into account [24, 29]. Unless otherwise stated, depositions occurred in a solution of 0.05 M tetraethylammonium hexafluorophosphate (Sigma), 1% vol/vol water, and 0.05 M pyrrole (Sigma) in a propylene carbonate. Pyrrole, being sensitive to light, oxygen, temperature, etc., was normally distilled once every six to eight weeks and sealed in airtight, light-free containers at -20 °C before use. All other chemicals where used as received, unless otherwise noted.

The majority of films were grown on cylindrical glassy carbon crucibles of dimensions: diameter = 70 mm, height = 50 mm, thickness = 3 mm. Glassy carbon crucibles were produced by HTW Hochtemperatur-Werkstoe GmbH using their SIGRADUR® G grade material, with conductivities near $2.2 \cdot 10^4$ S/m.

Unless otherwise indicated, the counter electrode was a 0.5 mm sheet of copper foil (McMaster-Carr), whose surface area was at least two times the size of the working electrode. Films were deposited galvanostatically at current densities ranging from 0.1 to 1.0 A/m^2, using a Princeton Applied Research VW2, 16 channel, multichannel potentiostat, running EC-Lab® software, version 9.55, from Bio-Logic® Science Instruments Inc. The temperature was maintained at -40 °C during depositions using a Cincinnati Sub-Zero temperature chamber.

Polyimide tape (McMaster-Carr) was used to mask sections of glassy carbon crucibles onto which depositions were not targeted. Deposition times ranged between 5 to 12 h, depending on the application and desired film thicknesses. Resulting films thicknesses ranged between 5 and 25 μm. Films were air-dried, passively or through convection, for anywhere between 12 hours and 7 days following deposition. An example glassy carbon crucible electrodeposition of polypyrrole is shown in Figure 47.

Figure 47: Example deposition of polypyrrole deposited onto a glassy carbon crucible.

7.2.2 Gold Plated Silicon Wafers

The growth of polypyrrole on silicon wafers was explored as a means of obtaining geometrically acceptable polypyrrole substrates that could be easily used in conventional micro-electro-mechanical-systems (MEMS) manufacturing processes. Highly doped silicon wafers without substrate modifications were explored as a target deposition surface. Highly conductive metals deposited onto wafer surfaces were also investigated.

The electrodeposition of polypyrrole directly onto silicon yielded poor results. The first films were brittle, significantly less conductive (10^2 to 10^3 S/m), and contained a significant number of bubbles (Figure 48(a)). Such films were unusable for actuators, lengths sensors, and would make low-quality supercapacitors because of their low conductivities and non-uniform surfaces. One possible reason for such poor film growth was the low conductivity of the target silicon substrate (~ 25 S/m). Another possible reason is that silicon is not electrochemically inert, and when subject to galvanostatic growth conditions, may interact with the electrolyte and the polymer.

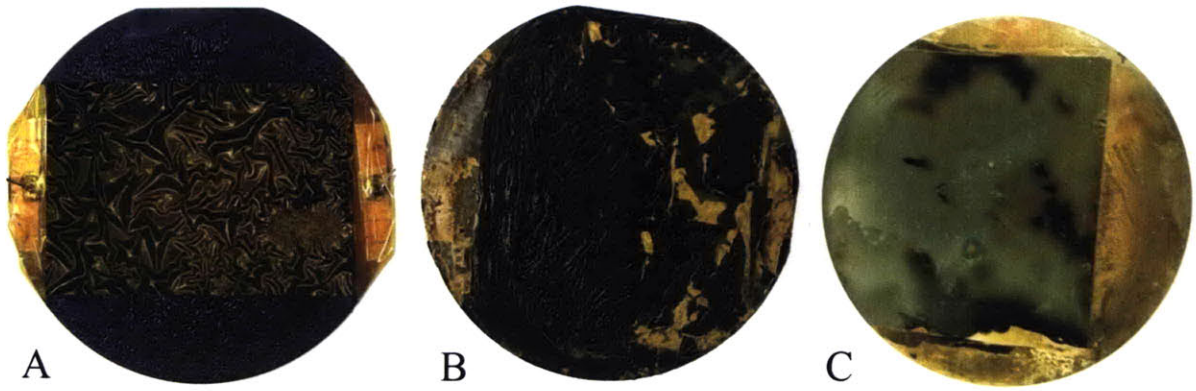

Figure 48: Experimental depositions onto silicon substrates. (A) Shows a deposition onto untreated silicon, resulting in dry, uneven films. (B) Shows a deposition onto gold (sputter coated) silicon wafers. After the deposition, the polypyrrole films are shown to peel off. (C) Shows titanium-gold coated silicon wafers. The resultant polypyrrole film is smooth, and has high conductivity values.

To mitigate this problem samples were subsequently grown onto gold plated silicon wafers. Gold was deposited (50 nm) through sputter coating (AJA Orion 5) before electrodeposition (see Figure 48(b)). Sputter coated substrates yielded significantly better films. Films were more conductive (10^3 to 10^4 S/m) and were uniformly flatter on the surface. After drying the depositions, however, films became wrinkled.

The increase in film conductivity for sputter-coated silicon can be attributed to the higher conductivity of the target surface, plus the masking effect the gold had over the silicon, by reducing any electrochemical reactions that might occur with an exposed silicon surface. The wrinkling was found to be attributed to two steps of the manufacturing process. First, gold deposited directly onto silicon substrates through sputtering can be easily scraped or peeled off. Secondly, as depositions were grown at -40 ^{o}C, when they were removed from growth conditions and dried at room temperature, film volumes shrunk significantly enough to cause detachment between the gold-silicon interface.

To maintain higher conductivities while improving the film quality, a thin layer of titanium (10 nm) was deposited onto the silicon substrates before depositing gold. The titanium helped to keep the gold from peeling off the underlying substrate. Through this process, polypyrrole was able to be electrodeposited with film smoothness and conductivities values in the same range as standard glassy carbon crucible depositions (Figure 48(c)).

7.2.3 Carbon Fiber Paper (untreated and gold coated)

Initial experiments with polypyrrole supercapacitors were made on polypyrrole coated carbon fiber papers. Carbon fiber papers were unmodified (AvCarb^{TM} P50, Ballard Material Products), or a thin layer of gold was electrodeposited onto the surface of the carbon fiber papers at a current density of 0.5 A/m^2 for 10 minutes. Gold depositions were shown to be uneven, and easily flaked off the substrates. Gold surface coatings did nonetheless affect the overall surface qualities of the subsequent polypyrrole deposition. Scanning electron micrographs (JOEL 6060) of these substrates are shown in Figure 49. For polypyrrole grown directly onto the carbon fiber paper, more bubbles appeared on the surfaces than with gold-coated substrates. While this may seem undesirable for polypyrrole used in actuators or length sensors, it may be a desirable characteristic for supercapacitors, since bubbles can significantly increase the cumulative surface area, allowing for faster charging and perhaps, occupy more volume.

7.2.4 Gold Plated Microscope Slides

Similar growth techniques were used with gold plated microscope slides. The absence of silicon, which has its own electrochemistry, resulted in smooth films and film conductivities identical to those grown on glassy carbon substrates. One minor disadvantage to gold substrates, however, was that during film drying, films would sometimes unpeel because the roughness of the deposition surface was relatively smooth.

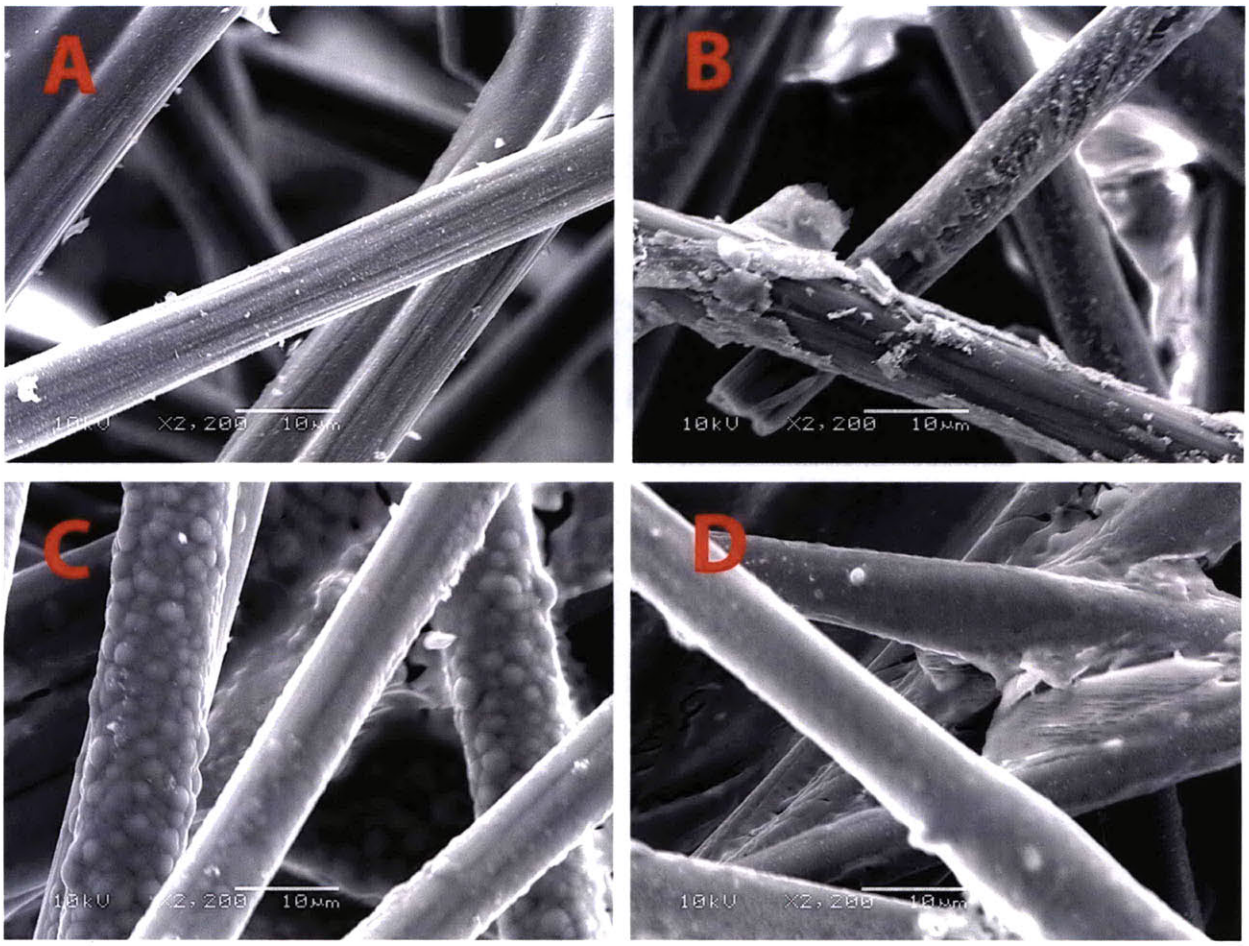

Figure 49: Polypyrrole deposited onto carbon fiber paper substrates. (A) Untreated carbon fiber paper. (B) Electrodeposited gold on carbon fiber paper. (C) Electrodeposited polypyrrole on untreated carbon fiber paper. (D) Electrodeposited polypyrrole on gold coated carbon fiber paper.

7.2.5 Gold-Plated Copper Surfaces

For patterned depositions, gold plated copper printed circuit boards (PCBs) were investigated. These boards were made of G10 (McMaster-Carr), and had a thin layer of copper (~0.5 mm), with an additional surface coating of gold (~0.1 µm). The advantage to gold-plated PCBs surfaces was that patterns could be easily integrated onto the growth substrate by conventional milling manufacturing techniques. One such pattern is shown in Figure 50. The

particular substrate shown in Figure 50 was one plate of a polypyrrole supercapacitor. Films that grew on these substrates were remarkably smooth and had conductivities equal to those grown on glassy carbon. One drawback of these substrates, however, was that when subsequent electrochemical tests were performed to measure capacitance metrics, the electrochemistry from the underlying copper affected the overall results. Gold plated PCBs can therefore be used to grow patterned polypyrrole materials, but such materials must be subsequently removed before being used for electrochemical actuation or energy storage.

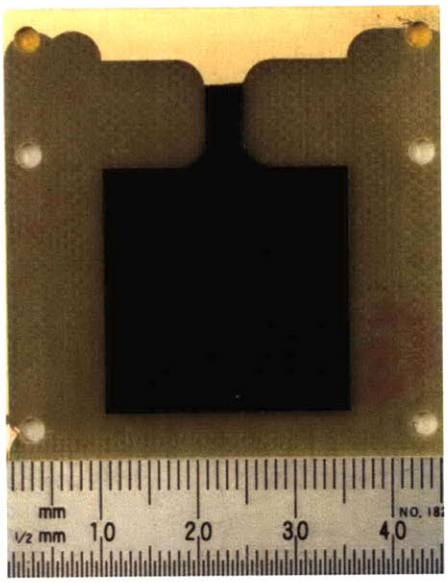

Figure 50: Polypyrrole grown onto a gold plated printed circuit board that was patterned using conventional milling to form the shape of a square, polypyrrole supercapacitor. Films grew exceptionally well on this semi-rough, gold plated copper surface.

7.3 Inter-component Mechanical Attachments

7.3.1 Plasma-aided Polystyrene

Plasma-aided polystyrene deposition was tested as an interfacial material to insulate and join polypyrrole films to one another. Polystyrene films were deposited for times between 10 to 60 minutes, to yield film thickness between 0.1 μm and 1 μm. One advantage to vapor

deposition techniques such as plasma-aided polystyrene is that the surface coating will conform to the geometry of the substrate. A photo of a 1 μm coating of polystyrene on polypyrrole is shown in Figure 51.

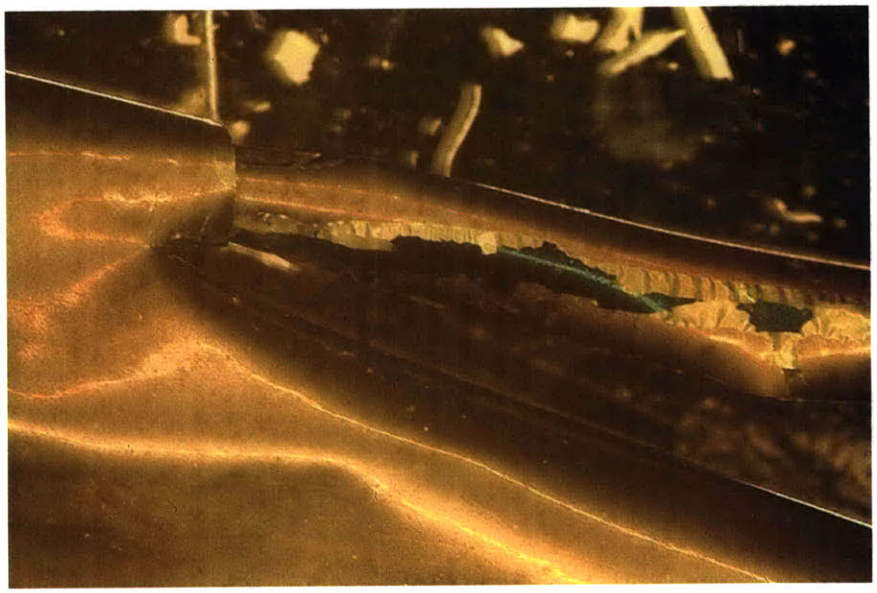

Figure 51: Plasma-aided polystyrene deposited onto free-stranding polypyrrole film. Cracking and peeling of the polystyrene is visible along the center ridge of the photo.

Several effects of the polystyrene deposition process, however, made this process unsuitable. First, for polypyrrole films, extended exposure to vacuum environments caused the films to lose their moisture, and become more brittle. The heat of the polystyrene during deposition also affected the quality of the film. Finally, while polystyrene initially conformed well to film surfaces, after a 48 hour period the outer layers of polystyrene began to peel as it dried out.

7.3.2 Parylene

Parylene was also tested as an interfacial material due to its resistance to solvents and electrical insulation properties. Parylene is similar to polystyrene in that it subjects polypyrrole

films to heat and vacuum environments, but unlike polystyrene, it can be deposited through vapor deposition to yield significantly thicker layers. Greater control over layer thickness ultimately leads to more robust film coatings, and this was observed for the Parylene coated samples of polypyrrole, as shown in Figure 52.

Figure 52: Parylene-coated polypyrrole sample. Although Parylene initially conformed well to polypyrrole surfaces, after cooling down and drying out, Parylene coatings could be peeled away.

Polypyrrole films that were grown on silicon wafers and subsequently Parylene coated (Paratech Lab Top Coater, 3 g, 3 hours) yielded consistently thick films that were electrically insulating. Parylene coatings were less brittle than polystyrene, and did not flake off. Parylene films, however, were easy to mechanically separate after a period of drying, normally between 24 and 48 h. The ease at which they separated suggests that the Parylene-polypyrrole interface is less of a mechanical adhesion, and more of a temporary conformal attachment. Figure 53 shows the peeling edge of a Parylene coated polypyrrole sample.

Figure 53: The peeling edge of a Parylene coating, beginning to detach from a polypyrrole sample.

7.3.3 Polyimide

Polyimide is a processing material commonly used in the silicon manufacturing as an adhesive or an insulator. Depending on the curing temperature, the flexibility and hardness of the polyimide film will change. At low temperatures (90 to 110 °C) polyimide cures to form a soft, flexible film. Although polyimide does not attach permanently to many metallic and plastic substrates, a series of experiments were performed to see whether polyimide could be used as an inter-component adhesive layer for polypyrrole. All films were spin coated using a Solitec Spin Coater, using a custom calibrated curve in which polyimide (Sigma), was deposited for 60 to 90 s at speeds between 500 and 4000 RPM.

Initial tests with polyimide presented several attachment issues. First, polypyrrole is a porous material. After coating polypyrrole substrates with polyimide resin, the resin was observed to slowly seep through the film. For a 20 μm film, polyimide would seep through the

entire film in about 20 minutes. The seeping was minimized by curing the polyimide within 60 s of its application.

In initial tests, wet polyimide resin would spread evenly across the film, but during curing, the polyimide would curdle into small beads, as shown in Figure 54. Figure 54 shows an example, where an attempt was made to attach two sheets of polypyrrole using a polyimide interface.

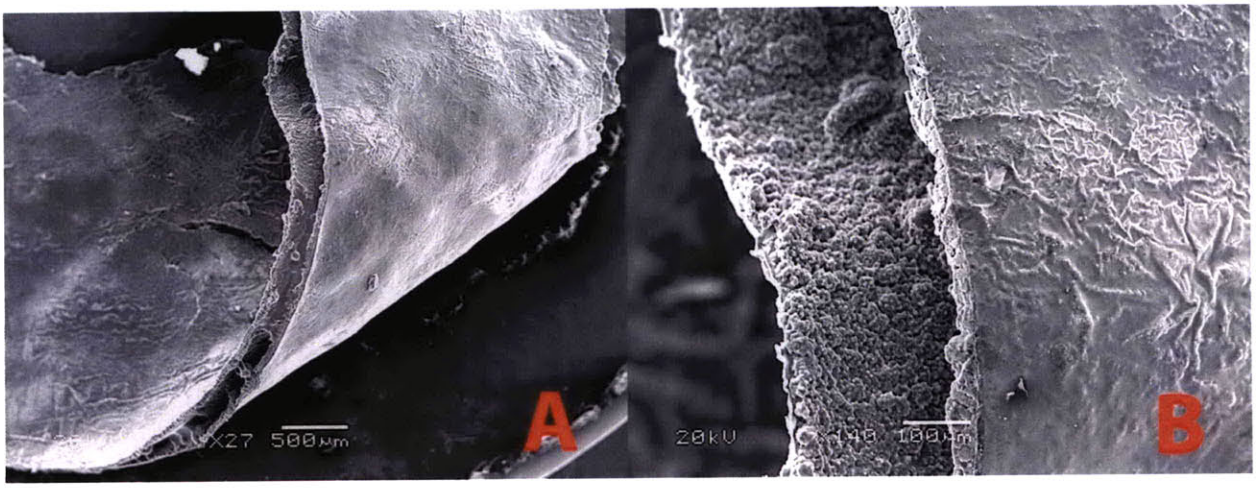

Figure 54: Two free-stranding polypyrrole films surrounding a layer of polyimide. The polyimide did not attach the two films together, but dried in a curdling manner on each respective surface. The poor attachment properties between the polypyrrole substrates can be attributed to the moisture content of the polypyrrole films. (B) is a close-up view of (A). (SEM micrographs from Jeol 6060).

After experimenting with the polyimide thickness, curing temperatures, polypyrrole film thickness and drying time, it was determined that allowing the polypyrrole films to dry on the deposition substrate for at least 48 hours before applying polyimide enabled good mechanical attachment between polypyrrole and polyimide. Polypyrrole is normally dried out for less than 24 hours, so that it maintains some of the solvent and salt solution in which it has been grown. This moisture content enables the film to actuate well. The moisture present after a film's deposition, however, excludes it from being used with polyimide. Moist polypyrrole films

coated with polyimide showed non-uniform curing, and poor mechanical attachment. By drying out the films, polyimide cured more uniformly across the films and could be successfully used as a mechanical adhesive. Figure 55 shows an example of two polypyrrole films, firmly attached by an interfacial layer of polyimide.

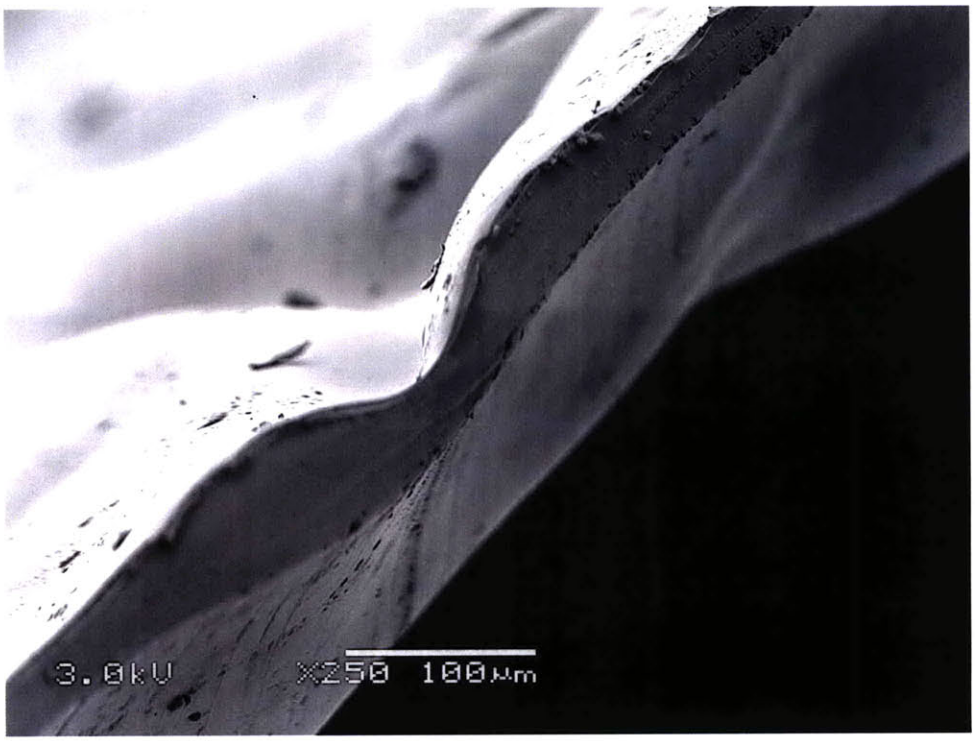

Figure 55: Two free-standing polypyrrole films attached by a thin layer of polyimide. With sufficient drying, mechanical attachments between polypyrrole films are possible. (SEM micrograph from Jeol 6060).

Soft-baked polyimide (90 to 110 °C) takes about 10 to 15 minutes to completely cure. The curing time, however, also depends on the thermal conductivity of the underlying substrate. Polypyrrole samples that were grown on 1 mm glassy carbon plates and subsequently spin coated with polyimide took significantly longer to cure than polypyrrole films grown on gold plated silicon wafers (Figure 57). The longer cure time resulted in more seepage of polyimide into the polypyrrole films. Figure 56 shown the effects of this seepage, where two sheets of polypyrrole were spin-coated using a glassy carbon substrate.

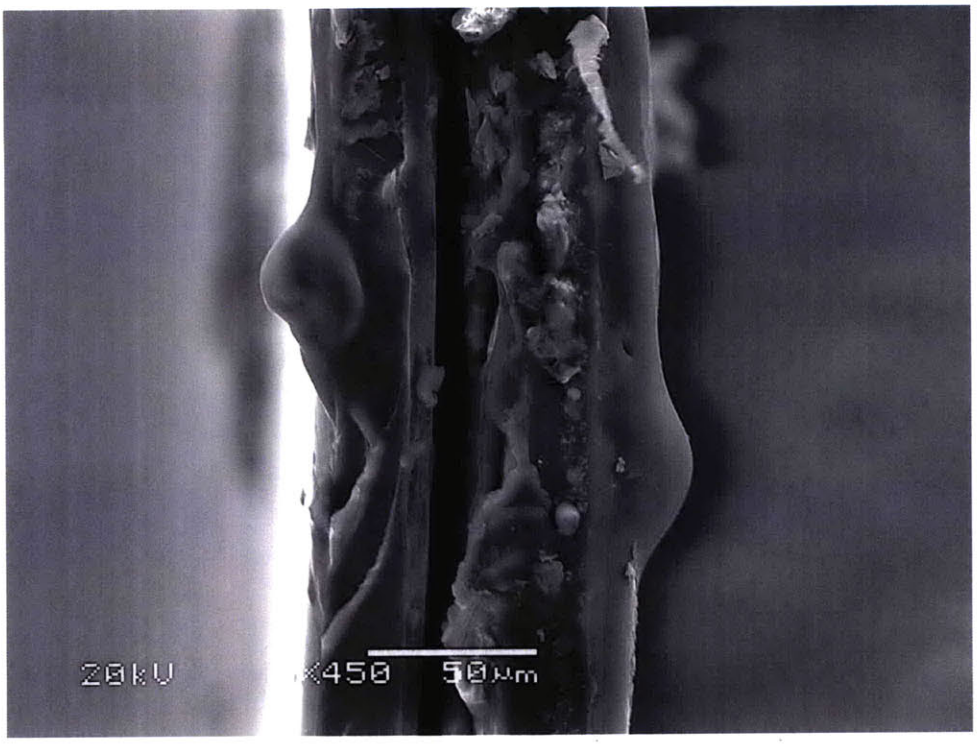

Figure 56: Polyimide seepage at the edges of two samples of polypyrrole films. Seepage is related to the substrate on which curing occurs and the amount of time in which polyimide is allowed to seep into the polymer before being heated. (SEM micrograph from Jeol 6060).

Another issue that arose during polypyrrole-polyimide processing was the thermal-mechanical behavior of polyimide. During the curing process, polyimide shrinks. If polyimide is deposited on top of polypyrrole substrates, during curing the underlying polypyrrole layer will also become deformed. This can be mitigated by changing the deposition order. One option is to deposit polypyrrole on top of polyimide substrates (instead of the reverse), or apply polyimide to localized regions of a pyrrole substrate. In the proceeding sections, both methodologies have been employed to create multicomponent conducting polymer actuation systems.

Changing the layer ordering and the coating thickness will also allow better insulation and adhesion when joining polypyrrole films, with minimal adverse effects from shrinking. The optimal protocol to date was achieved by creating two polyimide layers. The first layer served as

insulation, and could be made as thick as desired. In the current work the insulation layer was kept between 0.5 to 10 μm. After curing the first layer, a second adhesion layer was spin coated on top of the insulation, with a significantly less amount of polyimide (0.15 to 0.5 μm). Polypyrrole films then cut into pre-determined geometries or, layers on as an entire sheet could be deposited onto the thin adhesion layer.

The exposure time of polyimide to polypyrrole was critical to controlling the amount of seepage between the polyimide adhesive and the polypyrrole. Any time over 60 s resulted in significant seepage. Adhesion layers thicknesses were found to have a "happy-medium" solution. Ultra-thin (< 250 nm) polyimide films did not produce a significant amount of adhesion force. Thick films (> 3 μm) took longer to cure and seeped through the polypyrrole, resulting in poorer adhesion as well.

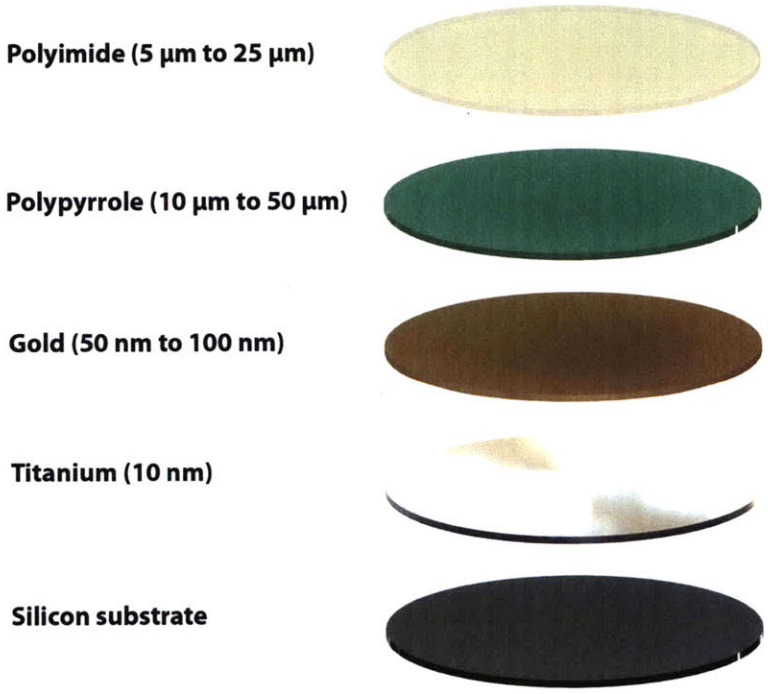

Figure 57: Standard deposition protocol for depositing polyimide onto polypyrrole substrates.

7.4 Inter-Component Electrical Insulation

Mechanical attachments are only one of many criteria that need to be fulfilled to find suitable interfacial materials for building artificial muscle actuation systems. A second and equally critical criterion is the electrical insulation the attaching material provides between different active substrates. A discussion of geometrical considerations in building multi-component conducting polymer systems is addressed in the upcoming section. However, consider briefly that active materials can either be vertically stacked on top of one another, or, laterally positioned next to one another. In the former case, a high insulation material must be placed between two active layers of conducting polymer such that they can perform simultaneously, yet be electrically uncoupled from each other.

Figure 55 showed the mechanical attachment of two sheets of polypyrrole. After this mechanical adhesion was achieved, the films were also electrically insulated from each other. As a more stringent test, and in order to account for the possibility of work in the future, the electrical insulation properties of all of the materials discussed in Section 3 were more rigorously examined by depositing a second conducting polymer, PEDOT, on top of insulation surface coatings. PEDOT can be electrochemically deposited, chemically synthesized, spin coated or deposited through oxidative vapor deposition (oCVD). The latter method, oCVD, enables very thin films of PEDOT to be patterned onto other multi-functional conducting polymer components.

Electrical insulation tests were performed with each insulation material by depositing PEDOT through oCVD onto insulated polypyrrole samples. The deposition procedure, process and technique are discussed in [49].

7.4.1 Plasma-aided Polystyrene

PEDOT coated onto polystyrene showed large globular formations about 25 μm in diameter. A cross-section of a sample of PEDOT-polystyrene-polypyrrole is shown in Figure 58. Though it may be less evident from the figure itself, the PEDOT penetrated through the insulation layer of polystyrene. Resistance values measured across the surface of the PEDOT layer were lower than resistance measurements made across the PEDOT-polystyrene-polypyrrole interface. Essentially, after the deposition of PEDOT, the polystyrene did not insulate the polypyrrole. Instead, the polystyrene became conductive because it was volumetrically coated with PEDOT

Figure 58: PEDOT coated sample of polystyrene insulating a free-standing polypyrrole film.

7.4.2 Parylene

Parylene coated polypyrrole samples were equally poor at withstanding vapor deposited PEDOT. In Figure 59, the cross-sectional view shows the PEDOT visible on all surface areas of the Parylene surface and on the sidewalls made of polypyrrole. In this case, the surface properties of PEDOT were slightly less globular and more uniform than when deposited onto polystyrene. PEDOT, nonetheless, reduced Parylene from an insulator to a conductor.

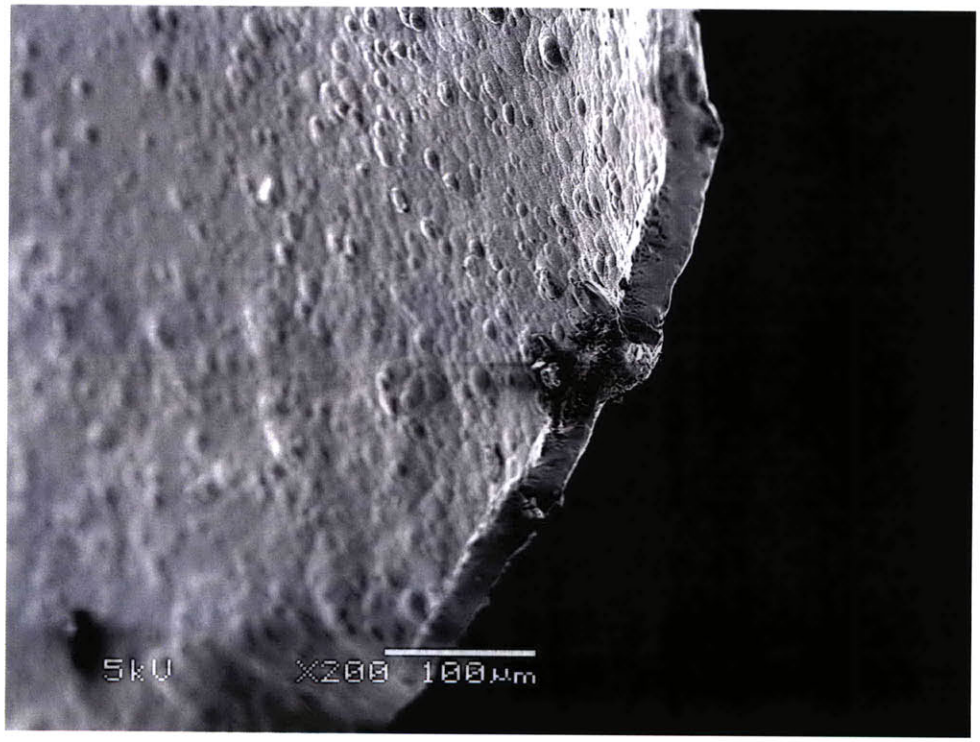

Figure 59: PEDOT coated sample of Parylene insulating a free-standing polypyrrole film.

7.4.3 Polyimide

PEDOT coated on polyimide showed better results depending on the polyimide film thickness. For polyimide layers less than 10 µm, the PEDOT was able to penetrate through the insulation layer. Figure 60 shows PEDOT coated onto a layer of polyimide, which was coated

on top of polypyrrole. From a close examination of Figure 60, one can actually see the penetration depth of the PEDOT by the lightly light coloration along the top of the cross section. From this, the penetration depth was estimated to be between 5 and 7 μm.

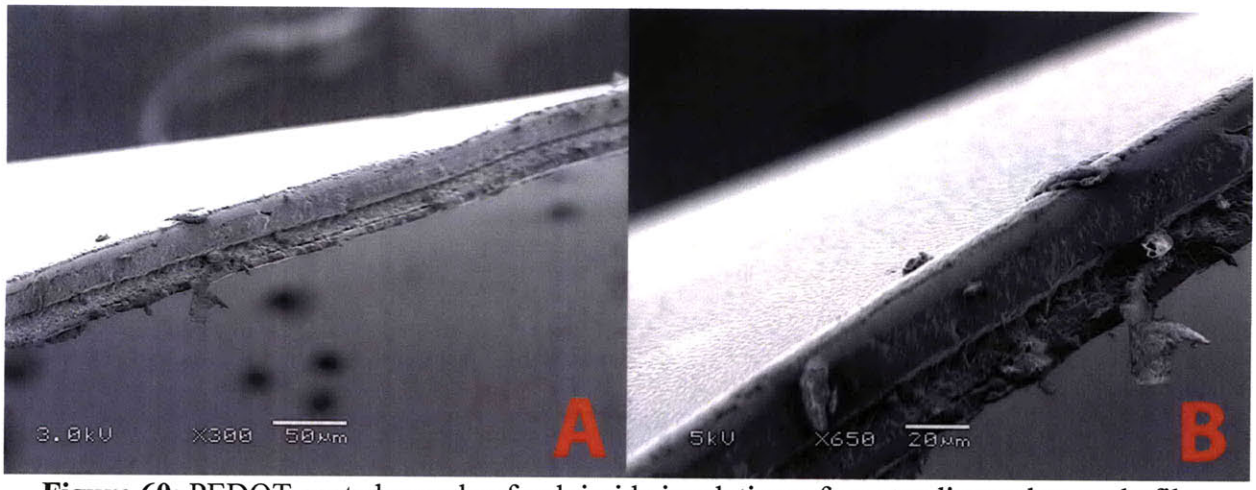

Figure 60: PEDOT coated sample of polyimide insulating a free-standing polypyrrole film.

Figure 61 shows another example of PEDOT coated onto polyimide insulation layers. In this example, polypyrrole was grown off of a gold, sputter-coated silicon wafer. On the inner surface of this stack of materials, flakes of gold that came unpeeled during the removal process can be seen. Again, the polyimide insulation layer is sufficient in electrically insulating the bottom conducting polymer layer from the top one. Table 6 summarizes the electrical resistance properties of the various possible polypyrrole inter-component attachment technologies.

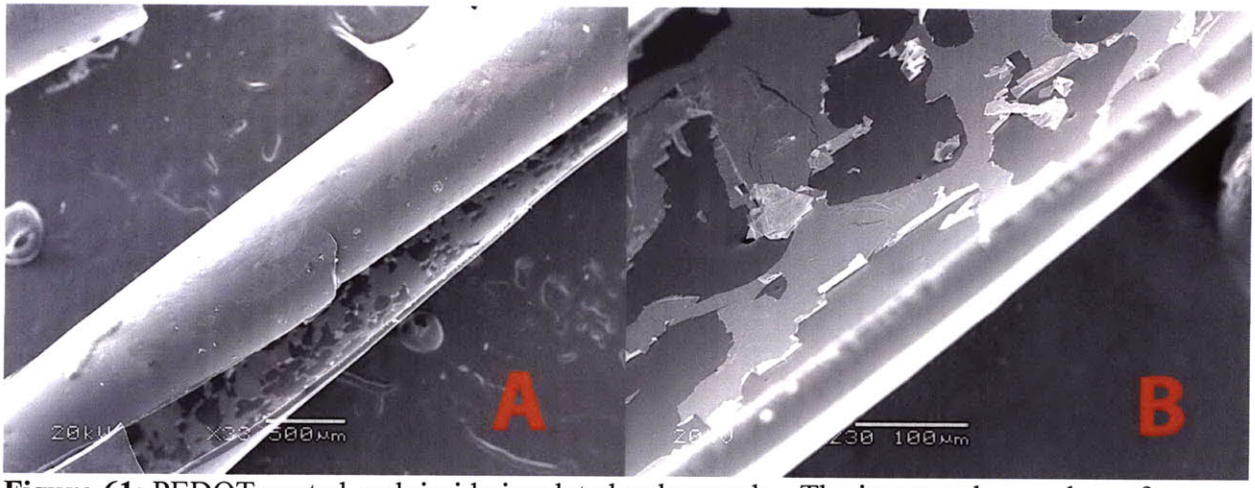

Figure 61: PEDOT coated, polyimide insulated polypyrrole. The inner, polypyrrole surface was coated with gold and shows significant peeling. The outer surface was coated with PEDOT and shows a smooth deposition that is electrically insulated from the underlying polypyrrole and gold.

Table 6: Summary of possible electrical insulators and adhesives for multi-component conducting polymer systems.

	Film thickness	Resistance across layer interface	Comments
Polystyrene	**~500 nm**	**20 MΩ**	**Flakes; Rubs off**
Parylene	**5 um**	**10MΩ - OPEN**	**Good insulation; Poor long-term adhesion**
Polyimide	**~1 um**	**2MΩ - OPEN**	**Good insulation; Good adhesion; Relatively high curing temperature**
Polystyrene/PEDOT	**~500 nm**	**< 100 Ω**	**Does not insulate**
Parylene/PEDOT	**5 um**	**~1 kΩ**	**Does not insulate**
Polyimide/PEDOT	**~10 um**	**OPEN**	**Insulates at sufficient films thickness (> 7μm)**

7.5 Multi-Component Fabrication

With polyimide proving to be a suitable material for both mechanical attachments and electrical insulation between conducting polymer components, two multi-component configurations were explored in the construction of an artificial muscle actuation system. Recalling the hierarchal structure of mammalian skeletal muscle, GTOs are located in series with myofibrils to measure muscle tension, while muscle spindles are located in parallel. Although it is not a requirement to imitate the exact geometry of mammalian muscle, attempts were made to recreate these geometric relationships among components.

7.5.1 Multi-Component Matrices

In order to fabricate length sensors such as muscle spindles in parallel with actuators, a modified version of a polypyrrole-polyimide deposition process was developed. Polypyrrole was grown using the standard protocol, dried out for 48 hours, and then laser ablated (Trotec) such that strips of polypyrrole were cut to the dimensions of desired length sensors. To avoid seepage that occurs at the polypyrrole-polyimide interface, the polyimide electrical insulating layer and the adhesive layer were fabricated in two distinct steps. First, a layer of polyimide was deposited onto a glass or silicon substrate, with a varying thickness between 2 and 20 μm, and cured for 10 minutes at 110 °C. A second, thin layer of polyimide was then deposited onto top of the insulation layer (500 to 1000 nm). This adhesive layer of polyimide provided enough material during curing to attach the polypyrrole strips to the polyimide backing, while at the same time, minimizing the total amount of uncured resin that could seep into the polypyrrole. Reducing the adhesive layer also reduced the curing time to about 7 minutes, which in turn limited the exposure of polypyrrole components to higher temperatures. Figure 62 shows polypyrrole

actuator and strain sensors, cut to dimensions through laser ablation and then mechanically adhered to a thin, polyimide backing.

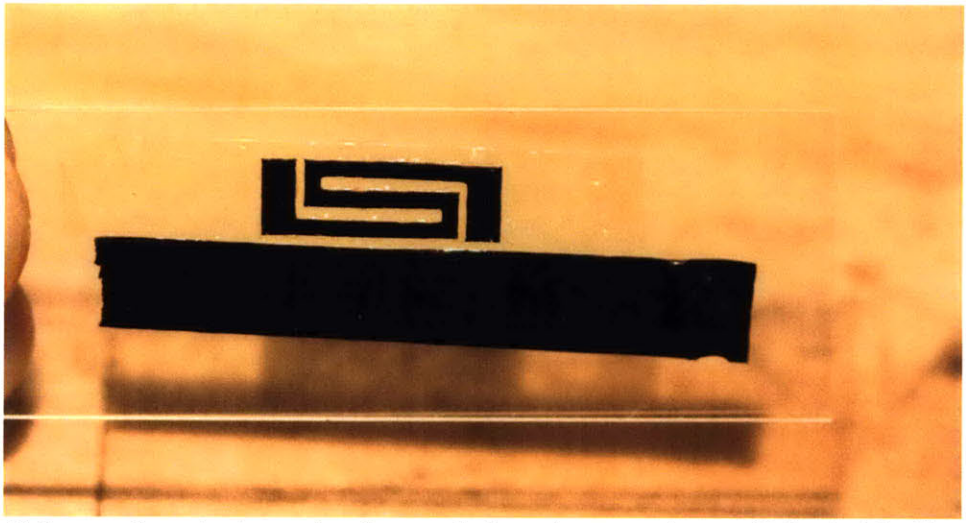

Figure 62: Polypyrrole actuator and polypyrrole length sensor in parallel. A thin (5 μm) layer of polyimide is faintly visible behind the sensor and the actuator. Sample is held between two glass microscope slides.

With this fabrication protocol developed, it was then possible to make arrays or matrices of conducting polymer materials on a single substrate. Figure 63 shows one such matrix, where four actuators and four length sensors are deposited in both series and parallel. This matrix of components could be used simultaneously, or after deposition the substrate could be sliced into separate components.

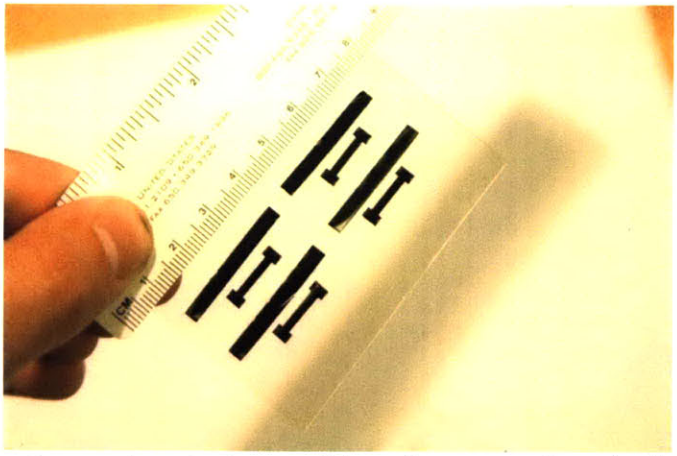

Figure 63: Matrix of polypyrrole actuators and length sensors deposited onto a thin, polyimide backing.

7.5.2 Multi-Component Stacks

Using the polyimide layers as insulators and adhesives, it is also possible to make stacked multifunctional actuation systems. One approach is to layer the actuator and length sensors in parallel, stacked on top of one another as shown in Figure 64. In this case, mechanical coupling occurs through the polyimide insulation layer, such that when the actuators contracts or expands, the polyimide layer contracts or expands as well, as does the strain gage layer above it. This enables the strain of the actuator to be monitored in real-time.

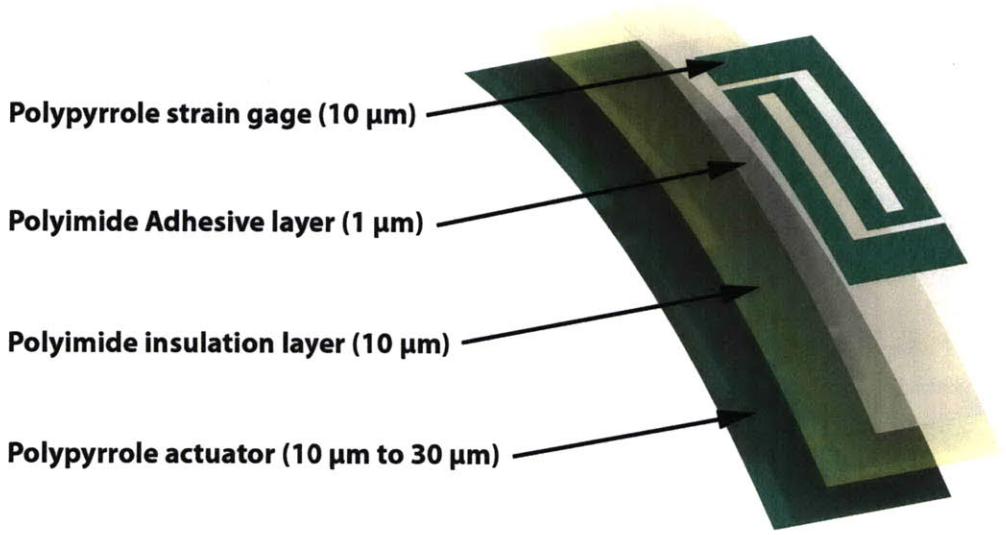

Figure 64: Polymer actuation subunit. An actuator and a length sensor are mechanically attached yet electrically insulated from one another by two thin layers of polyimide.

A set of materials were fabricated according to the model shown in Figure 64. Devices were tested to make sure that the separate layers maintained electrical insulation, as discussed in the previous section. An example polymer stack is shown in Figure 65. Two gold wires, adhered with a silver epoxy paste make electrical contact with the length sensor. The actuator is

visible in the background, as a darkened layer polypyrrole coated with a slightly reflective layer of polyimide.

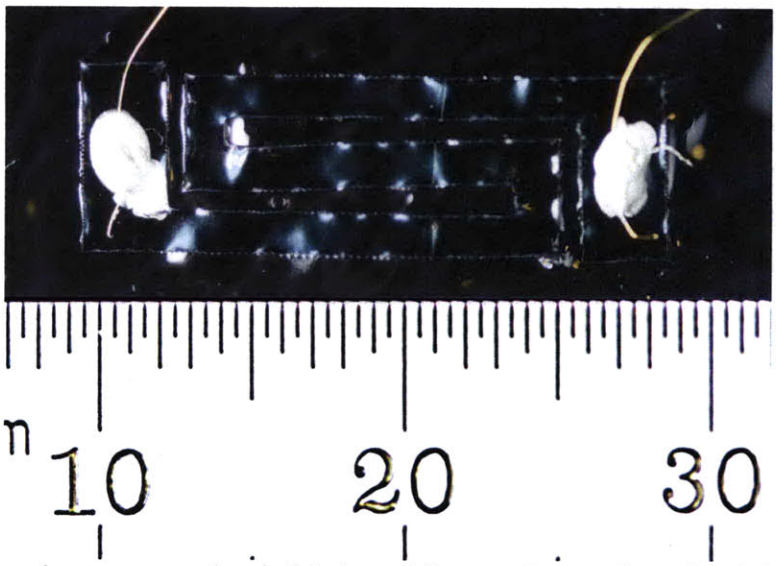

Figure 65: Polypyrrole actuator subunit fabricated from polypyrrole and polyimide. Gold wires, attached by small amounts of silver epoxy adhesive, can be seen in the photo making contact with the polypyrrole length sensor. The polypyrrole actuator is a slightly darker background behind the length sensor. The two components are separated by two thin layers of polyimide.

7.5.3 Three Dimensional Actuation Systems

As a final integration of both flat and stacked systems, multi-component conducting polymer actuation systems were fabricated using a combination of the methods presented in this chapter. Although conducting polymer transistors, for example, were not tested extensively for this work, a series of four-cell electrochemical amplifiers [49] and three-cell electrochemical transistors were fabricated out of polypyrrole and polyimide using a modified protocol of mechanical attachment and adhesion. Figure 66 shows the deposition protocol for the fabrication these transistors. Because polypyrrole cannot withstand the harsh acids normally involved in chemical etching, surface patterns were defined between layers using low powered laser ablation (Trotec). The feature resolution was therefore limited to the beam width and the vaporizing

characteristics of polypyrrole, plus the thermal dissipation of the underlying substrate. With the current setup, troughs as small as 200 μm were possible while features as small as 150 μm were also possible.

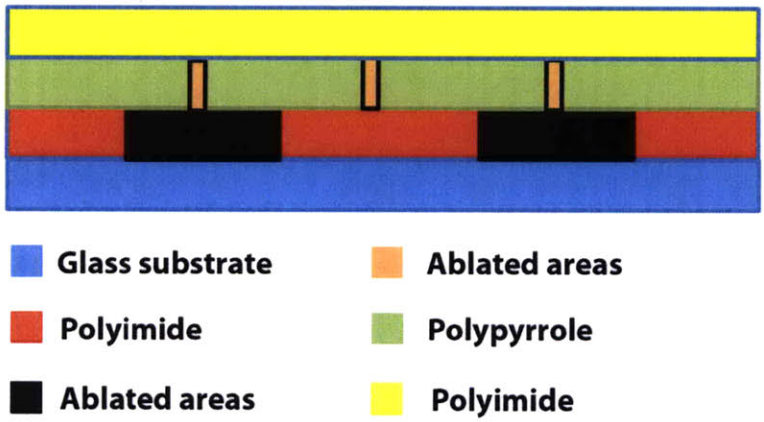

Figure 66: Fabrication technique used to make polypyrrole transistors from polypyrrole and polyimide.

Another possibility in the fabrication of three-dimensional actuation systems is the application of localized attachments between components. While thin polyimide backings minimize the mechanical impedance of the system, if they can be eliminated entirely from substrates which move (i.e. actuators and length sensors), then such components can perform better. Localized inter-component attachments were investigated by applying thin layers of polyimide resin (500 nm) to polypyrrole and polyimide substrates and then providing localized heat with a soldering iron. The tip of the iron was maintained at 110 °C, which was high enough to cause the polyimide to cure, yet low enough to keep the polypyrrole substrate from melting. A heat profile of the localized mechanical attachment method is shown in Figure 67.

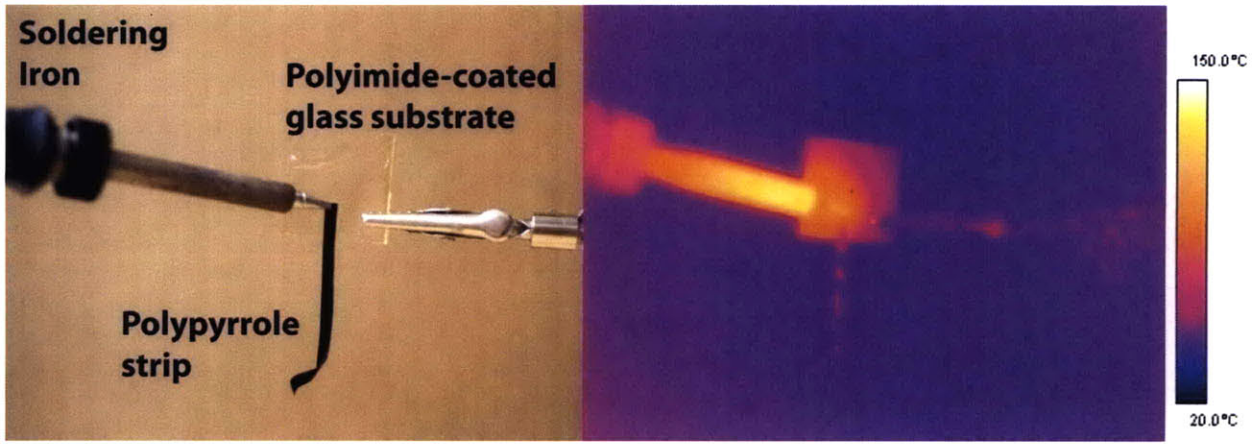

Figure 67: Heat profile of polypyrrole strip being attached to a polyimide coated glass substrate using a soldering iron set at 110 °C.

From the heat profile we see that the thermal dissipation of the underlying substrate (in this case, a 1 mm thick glass plate) was large enough such that heat was applied mainly at the point of contact and not over the polypyrrole strip itself.

Using this technology it was then possible to create multi-dimensional, multicomponent conducting polymer actuation systems like the example shown in Figure 68. Here, four different conducting polymer components have been combined onto a single working substrate: actuators, length/tension sensors, supercapacitors and electrochemical transistors. The final working substrate is flexible, and the materials of the components have remained intact since heat treatment was strictly localized.

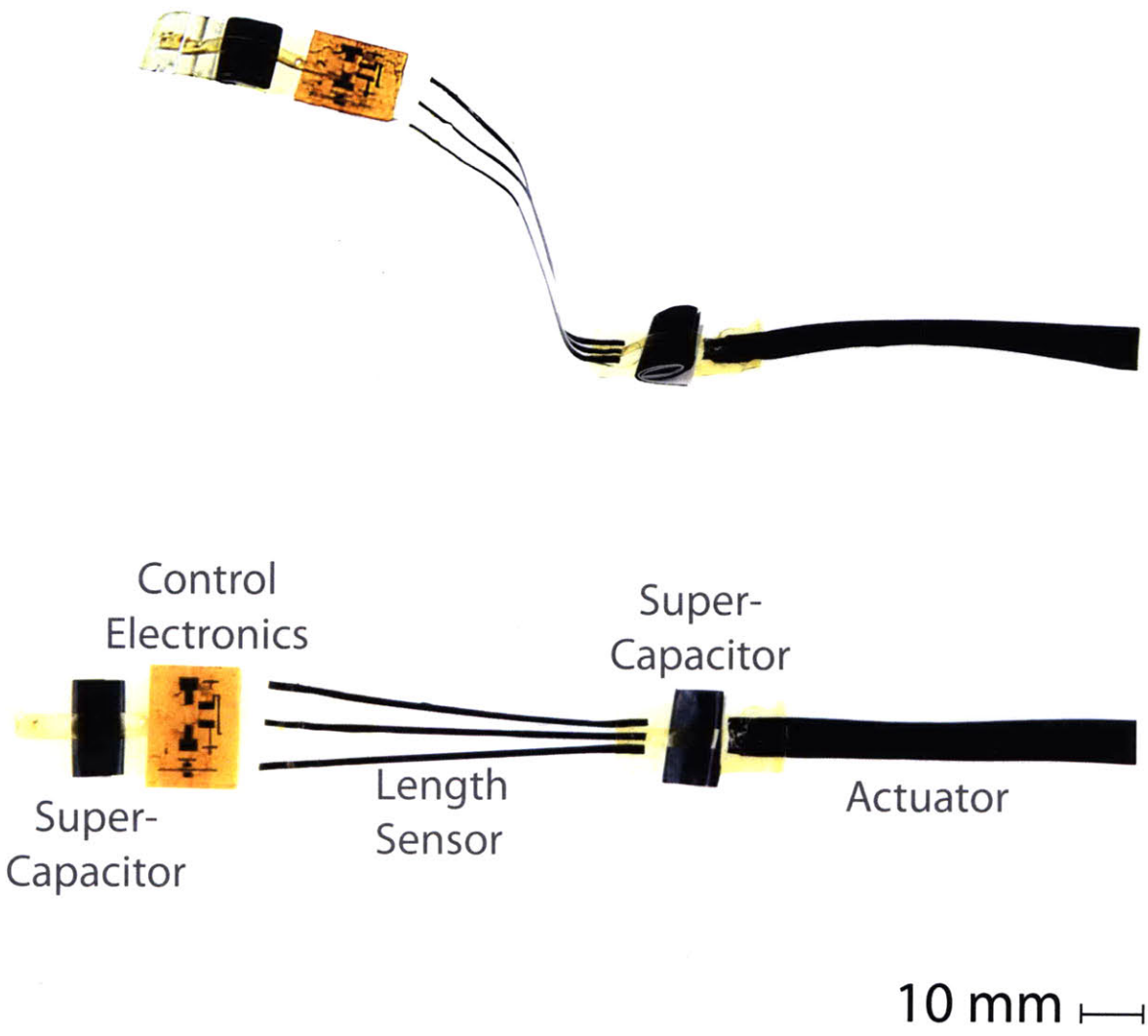

Figure 68: Multi-component conducting polymer system. Four polymer elements (actuator, length sensor, supercapacitor, and transistors) are all attached using localized applications of polyimide.

From this set of fabrication technologies more advanced artificial muscle actuation systems can be produced. The example shown in Figure 68 is one possible configuration. Modifications made to add more electrochemical supercapacitors, reduce the size of each component, and change the order and geometry of the entire system are also possible. For example, one could combine the multicomponent actuation system from Figure 68 to create a set

of agonist-antagonist actuators, length sensors, supercapacitors and control electronics as shown in Figure 69.

Figure 69: Proposed agonist-antagonist set of conducting polymer elements that make up a simple conducting polymer actuation system. The red line (center) indicates the area of motion during actuation.

In Figure 69, the red line (or crossbar) in the center indicates the area of movement of the actuation system, while the outer edges could be fixed to a non-deformable body. On either side of the crossbar, one set of actuators contracts while the other set expands, allowing the crossbar to move both to the left and the right. The sets of length/tension sensors on each side of the actuators monitor the contractile state of the actuators opposite of the crossbar, thereby enabling closed-loop positing control. In the next section, a study of the closed-loop positioning control of polypyrrole linear contractile actuators is discussed.

7.6 Closed-loop Control of Polypyrrole Linear Contractile Actuators

(From 2010 *IEEE International Conference on Robotics and Automation*, Anchorage, AK 2010).

Closed Loop Performance of Polypyrrole Linear Contractile Actuators

Eli Paster, *Student Member, IEEE,* Bryan P. Ruddy, Priam V. Pillai and Ian W. Hunter, *Member, IEEE*

***Abstract*—Conducting polymer actuators such as polypyrrole can generate stresses over 10 times larger than skeletal muscle and have typical repeatable strains between 1% and 12%, making them potential candidates for lightweight, low-cost, robotic applications. Polypyrrole linear actuators under closed loop control have not been previously reported. Here we report the open and closed loop performance of polypyrrole linear contractile actuators evaluated at pre-loaded stresses of 1 MPa to 3 MPa. A standard PI control scheme driving a potentiostat was implemented in conjunction with positioning feedback from a DC/DC linear variable differential transformer (LVDT). A dynamic positioning range of 3400 is reported, with a positioning resolution of 125 nm (0.001% strain) and a maximum repeatable displacement of 427 microns (3.6% strain). The open loop frequency response of actuator strain shows characteristics of a first-order low pass filter with a log gain versus log frequency slope near -1 for frequencies tested between 0.05 Hz to 2 Hz. The closed loop frequency response of actuator strain when tracking a sinusoidal set-point signal of 0.5% strain shows characteristics of a first order system with one zero, with a corner frequency near 0.08 Hz and an operating bandwidth up to 1 Hz. Step responses at various controller output maximum voltages show a reduction in contractile response times by a factor of four, where higher voltages yield faster contractile responses.**

I. INTRODUCTION

THE conducting polymer polypyrrole can be used as a linear actuator when operated within an electrochemical cell. Because of its low voltage operation (1 V to 2 V), low-cost, relatively high force output [1], and ability to produce repeatable strains up to 12% [2], polypyrrole is seen as a potential candidate for artificial muscle applications in robotic, industrial and biomedical fields.

The application of polypyrrole actuators has been demonstrated in various real world devices. Polypyrrole's ability to operate in liquid environments makes it a potential candidate for use in maritime and aquatic devices. Polypyrrole fish fins mimicking the conformational shapes of the bluegill sunfish pectoral fin have demonstrated similar thrust patterns to that of the actual biological organism [3]. A variable camber foil for use in ship propellers has been shown to provide adequate strain for modifying propeller shape underwater [4]. The use of polypyrrole in biomedical applications is also possible, where specific synthesis protocols can be modified to create bio-compatible materials that can actuate *in vivo* [5]. Polypyrrole actuators have also been used in a variety of miniature devices such as micro-positioners [6], pumps [7], and micro-grippers [8]. As performance, speed, force output and material characteristics continue to improve, the use of these actuators in closed loop robotic and micro-robotic applications becomes more and more viable.

Conducting polymer actuators are generally produced, tested, and integrated into systems in one of two configurations: bending actuators [9] and linear contractile films [2]. A design trade-off exists between these two configurations, with the former offering large displacements at the expense of lower force output and the latter offering high force output, but lower displacements. Both actuator configurations can suffer from relatively slow response times and creep damage over time. By incorporating feedback into polypyrrole actuators and limiting the working range of the actuator over its lifetime, significant improvements to minimize creep and increase speed can be attained. Closed loop feedback control can also offer precise output positioning for polypyrrole's use in a wider variety of applications.

To date, feedback performance studies on polypyrrole and other conducting polymers have been limited to bending configurations [10]. Closing the loop on bending polypyrrole actuators has been shown to both improve the response time of the polymer and reduce its positioning error [10]. Evaluating the linear contractile capabilities of polypyrrole within a closed loop system is of equal importance, especially in applications where high force output, precise positioning, or high actuator stiffness is mandated. Closed loop control also offers the possibility of programmable excitation waveforms, where relatively high voltage actuation can be exploited to reduce response times.

Relatively high voltage actuation (> 4 V) can increase the performance of closed loop polypyrrole actuators, but also reduce its operating life-cycle. Polypyrrole actuators operated at low voltages (< 1 V) and low pre-stresses (< 20 MPa) have shown strain reductions as little as 0.5% after 32,000 cycles [11]. At higher voltages and similarly low frequencies, this operating life-cycle is drastically reduced. At higher voltages (up to 10 V) and higher frequencies (above 1 Hz), however, 120,000 cycles of actuation at 0.25%

Manuscript received September 15, 2009. This work was supported in part by the Intelligence Advanced Research Projects Activity under Grant NBCHC080001.

E. Paster is with Massachusetts Institute of Technology, Cambridge, MA 02139 USA (phone: 617-258-0533; fax: 617-252-1849; e-mail: epaster@mit.edu).

B. P. Ruddy is with Massachusetts Institute of Technology, Cambridge, MA 02139 USA (e-mail: ruddy@mit.edu).

P. V. Pillai is with Massachusetts Institute of Technology, Cambridge, MA 02139 USA (e-mail: ppillai@mit.edu).

I. W. Hunter is with Massachusetts Institute of Technology, Cambridge, MA 02139 USA (e-mail: ihunter@mit.edu).

repeatable strain have been reported [12]. The trade-offs between voltage, frequency, and life-cycle are still being investigated to enable the long-term application of relatively high voltage actuation in closed loop polypyrrole actuation systems.

In this paper, the open and closed loop performance of linear contractile polypyrrole films are examined. Closed loop control is shown to significantly improve the positioning capabilities of the polymer films for both static and dynamic set-point targets. Relatively high voltage inputs (up to 9V) increase the polymer's actuation speed, but also reduce its operating life-cycle.

Although the samples studied were limited to operation at frequencies below 2 Hz, their large dynamic range of positions makes polypyrrole a feasible material for task-specific linear positioning devices where low-cost, high positioning accuracy is required.

II. Instrumentation and protocols

A. Polypyrrole Synthesis

Polypyrrole films were synthesized in a propylene carbonate solution of 1% (v/v) deionized water, 0.05 M tetraethyl ammonium hexaflourophosphate, and 0.05M pyrrole (Aldrich). Actuation tests were performed in neat 1-butyl-3-methylimidazolium hexafluorophosphate (EMD Chemicals). All chemicals were used as received, with the exception of pyrrole which was distilled under vacuum before use.

Films were electrodeposited galvanostatically onto a glassy carbon crucible at a current density of 0.5 A/m^2 and a temperature of -40.0 °C. All films were grown for 8 hours, yielding thicknesses near 0.025 mm. After deposition, films were air-dried for 12 hours, sealed, and used within one week. Samples were cut to dimensions (3 mm × 12 mm) and electrical contact was made via 0.030 mm gold wire and silver epoxy paste.

B. Instrumentation and Apparatus

Polypyrrole actuation tests were carried out in a custom built apparatus that allowed both electrochemical excitation of samples and continuous monitoring of both force and position data (Fig. 1). Film samples were held in place with miniature clamps machined from polytetrafluoroethylene. One clamp was statically fixed to a 45 N force sensor (LSB200, Futek) and mounted on the outside of the electrochemical cell. The force sensor was used to determine the initial pre-stress of the polymer under tension, and was excited using a signal conditioning amplifier (2311, Vishay). The other clamp was drawn by a 0.1 mm line of Spectra®

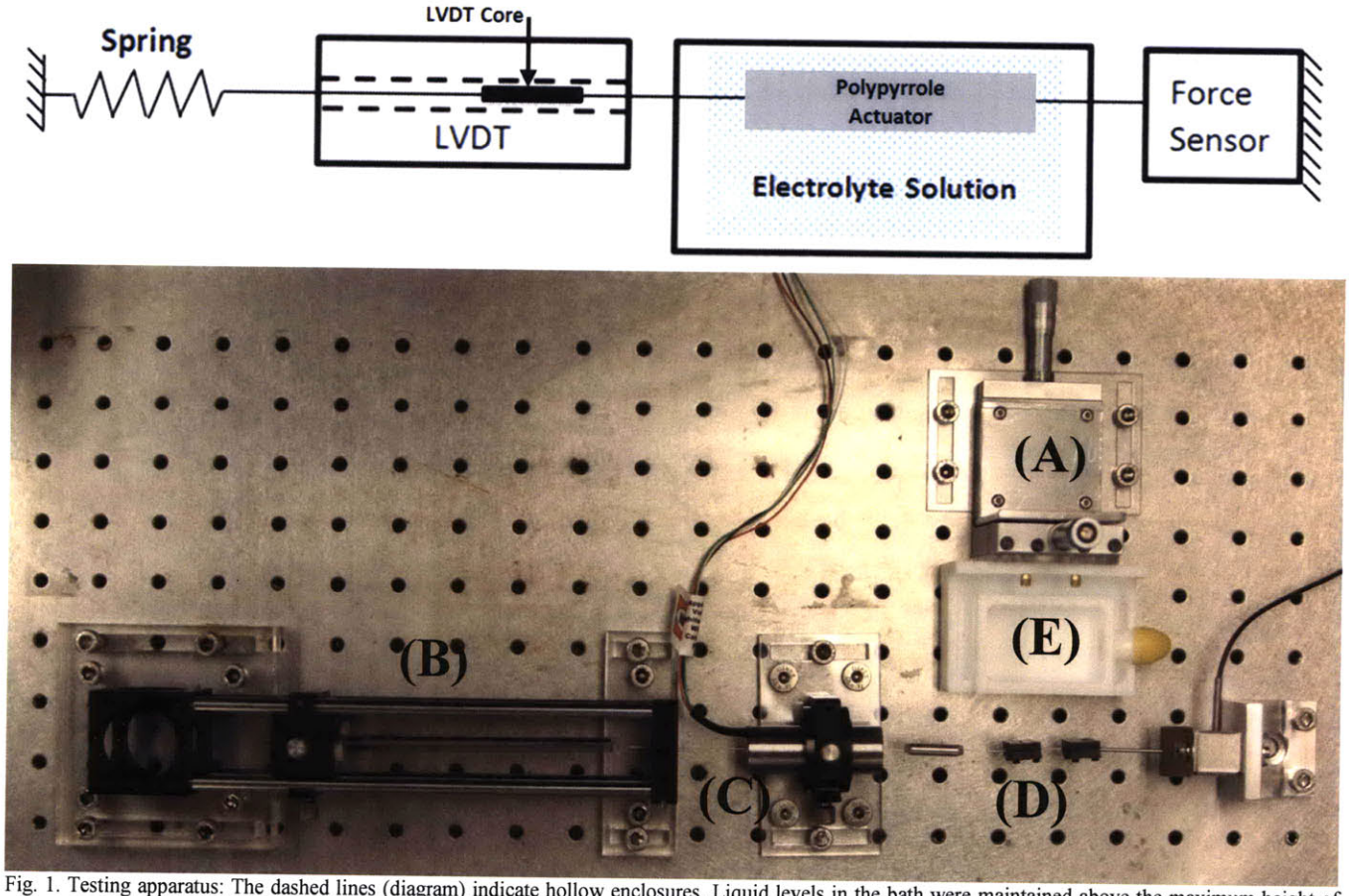

Fig. 1. Testing apparatus: The dashed lines (diagram) indicate hollow enclosures. Liquid levels in the bath were maintained above the maximum height of the sample. All components were fixed to an optical breadboard (below) to reduce vibration. The bath (E) and the outer casing of the LVDT (C) were mounted onto 2-axis positioning stages (A) or concentric optical mounts ensuring adjustments could be made to maintain concentricity along the line of action. The sample can be seen in-between the two clamps at (D). The total system is held under tension by the sliding spring (B).

cable and held under tension by a compliant extension spring (9640K123, McMaster-Carr). The force output from the polymer under contractile conditions was calculated to be at least two orders of magnitude higher than the reaction force exhibited by the spring for the given operating range of displacements that the polymer might undergo. The highly compliant spring thus provided a simple, low-cost, yet effective means of maintaining the polypyrrole linear actuator under quasi-isotonic tensile conditions.

A DC/DC linear variable differential transformer (LVDT) (75S1DC-050SR, Sentech) was axially aligned with the force sensor and the polymer film's contractile line of action. The LVDT core was mounted on the Spectra® cable and used to monitor displacements. Sag in the line from the weight of the LVDT core and the non-fixed clamp was minimized by keeping the clamp mass to a minimum and holding the line under tension.

An electrochemical bath consisting of a main chamber and secondary moat was used to test samples under horizontal tensile conditions. In the linear configuration, polypyrrole actuators were submerged in an ionic liquid during operation. Small holes on the outer walls of the chamber allowed the samples to be held under tension while the Spectra® cable itself never came into physical contact with the walls of the bath, thus eliminating any associated frictional impedances. In a full bath of ionic liquid, the holes on the outer walls were sufficiently small such that any liquid losses occurring over time were minimal compared to the size of the bath reservoir itself.

The main chamber was lined with 0.040 mm thick stainless steel foil which served as the counter electrode within the electrochemical cell. The reference electrode was a silver wire. The working electrode was the polypyrrole sample.

C. Excitation and Control Methods

The diffusion of ions in and out of the polymer leads to the film expanding or contracting volumetrically. This change can be exploited to generate forces or produce motion. Experiments on conducting polymers are usually performed under isotonic or isometric conditions. Under isotonic conditions [13], [14], [15], the polymer film is held fixed at a constant stress, is excited using a potential input, and the strain is independently measured. Under isometric conditions [16], [17], the length of the actuator is maintained constant and the stress output is measured during excitation. For real world applications, isotonic conditions can be approached by using springs or counterweights.

The polypyrrole actuator was driven using a potentiostat. In a standard three electrode configuration, a DC or AC command voltage was input into the potentiostat (2051, Amel Instruments). The potentiostat then drove a current between the counter electrode and the working electrode, such that the potential difference between the working electrode and the reference electrode equaled the input command voltage. As the potential across the actuator changed, the polymer was driven through cycles of oxidation and reduction, leading to the diffusion of counterions from the surrounding ionic solution [14] into or out of the polymer film. This flux of ions yielded actuator displacements.

Control was performed using a real time program developed in LABVIEW®. For the basic control scheme (Fig. 2), the LVDT signal served as the process variable. An output voltage ranging between +/- 10 V was input into the potentiostat to drive the polypyrrole actuator. For the majority of tests, the controller output was limited to +/- 0.75 V with respect to the resting potential of the electrochemical cell, which ranged between 0.20 V and 0.45 V. The LVDT had a ripple voltage of 200 mV, which could be attributed to excitation of the primary and built in signal conditioning circuitry. The ripple voltage frequency (above 4 kHz) was several orders of magnitude higher than the actuation frequencies tested, and was therefore filtered out in post processing. Although the ripple voltage did not allow real-time visual confirmation of tracking performance at low positioning increments, its relatively high frequency with respect to the system response time meant its overall effects on system accuracy were minimal, as they were averaged over time.

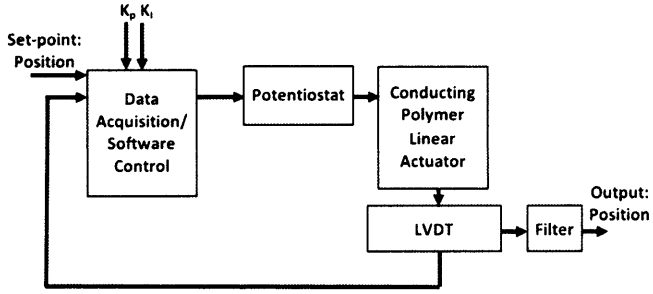

Fig. 2. Control scheme for driving polypyrrole linear actuators. Voltage signals input into the potentiostat drive the polypyrrole actuator between cycles of contraction and expansion. Data acquisition and software control were performed on a computer running Windows XP. A National Instruments PCI Data acquisition card (NI-6289) was used for both acquiring and generating signals.

For all tests, proportional and integral control were used. PI gains were calculated with aid of an auto-tuning algorithm built into LABVIEW® and were maintained constant for the data presented at: P=1466, I=0.049. AC and DC set-point signals were computed in real-time and in buffered configurations.

III. Open loop Control

Open loop control of polypyrrole linear actuators was evaluated by exciting the polymer with a discrete set of sinusoidal inputs between 0.005 Hz and 2 Hz, with a constant amplitude limited to +/- 0.75 V with respect to the resting potential of the electrochemical cell. The output strain was sampled at 100 Hz for each frequency input. A single sine wave fit was computed on each set of strain measurements for the frequencies tested. Actuator strain output, frequency and phase information were

calculated from each fit using a custom script written in MATLAB®. The resultant Bode plot can be seen in Fig. 3.

Open loop performance of the actuator's strain response is similar to the open loop electrical response of polypyrrole previously studied [18]. Similar response characteristics are expected since strain is roughly proportional to charge. Without feedback, the system shows the characteristics of a first-order low-pass filter for the frequencies tested, with a log gain versus log frequency slope of -1. At low frequencies the phase lag is reduced, suggesting that ions have more time to move in and out of the actuator and the response is dominated by electrical and ionic resistance. At frequencies near 0.1 Hz, diffusion becomes the rate limiting phenomenon and the phase remains fixed near -55 degrees.

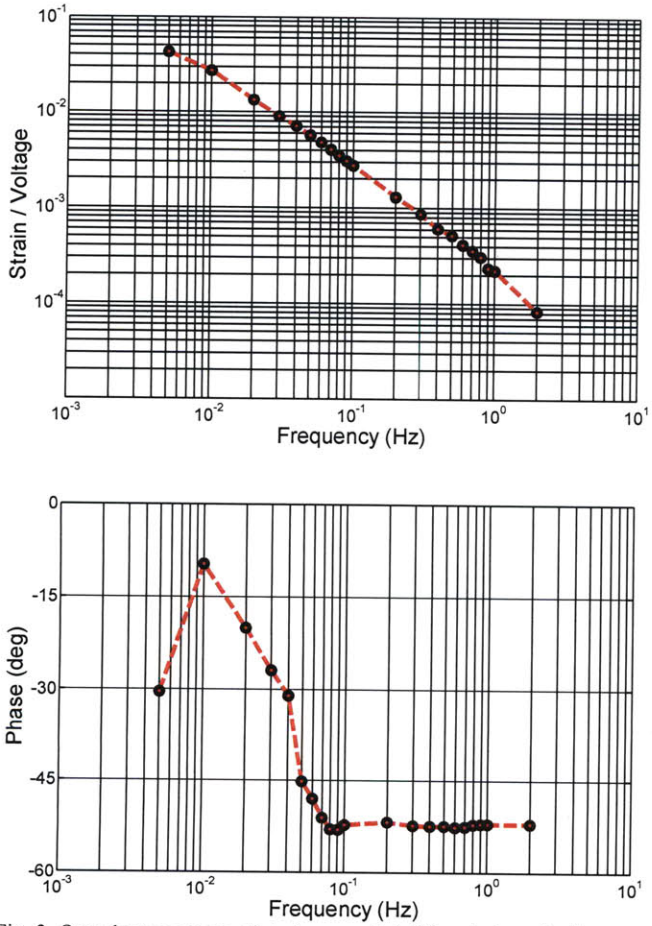

Fig. 3. Open loop response of strain per volt (ε/V) and phase for linear contractile polypyrrole. The data points represent the discrete frequencies tested. The line was drawn using nearest neighbor interpolation.

Because polypyrrole actuation is a diffusion limited process, output strain decreases for a given input amplitude as the frequency increases. This can be attributed to the fact that there is less time for ions to enter and leave the polymer. Faster responses can be achieved by increasing the potentiostat's maximum output voltage [12], decreasing the polymer's thickness dimension, or modifying the deposition protocol to increase conductivity [2], [19]. Under such modifications, the curve in Fig. 3 would shift to the right. Studies are still undergoing to see if such modifications would enable moderate strains above 1 Hz to be achieved.

Open loop control of conducting polymer actuators can be used in situations where oscillation or relative motion is required, rather than absolute positioning. Because the polymer exhibits creep over time [11], without feedback there is no way of maintaining steady positions over long periods of time. Fig. 4 shows one example of an open loop strain response to a 0.03 Hz, +/- 0.75 V sine wave. The phase offset between the two signals has been removed and the outputs have been normalized to compare the shapes of the waveforms. The general shape of the output strain matches the input for the low frequency being examined, but under an open loop configuration, polymer creep becomes an issue. Creep is observed in Fig. 4 only over a few cycles. Over the lifetime of the polymer, errors between the input and output may increase dramatically.

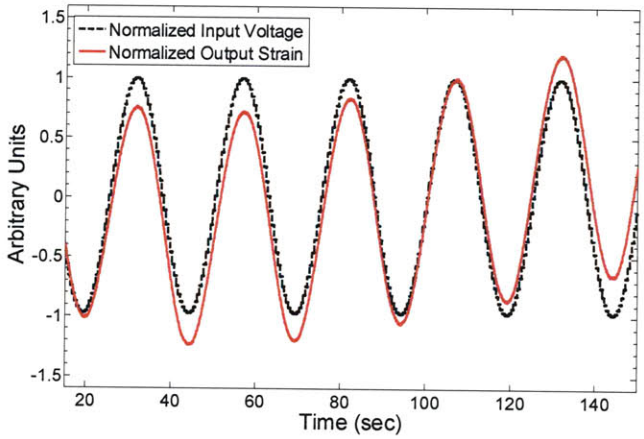

Fig. 4. Open loop response to a sinusoidal input, 0.03Hz, +/-0.75 V, 0.219 V offset (cell resting potential). The phase shift has been removed and the curves were normalized for comparison. The y-axis is both a measure of normalized voltage and normalized strain. The output response shows a similar shape to that of the input, but creep is apparent in the increasing mean of the output strain.

IV. Closed loop control

A. Frequency Response

Closed loop performance was evaluated in both the frequency and time domains by incorporating the LVDT as positioning feedback within a PI control scheme.

A sinusoidal signal of 0.5% strain was used as a set-point target. The maximum controller output ranged from +/- 0.75V with respect to the resting potential of the cell. The actuator's strain was measured using the same sampling and fit parameters as described in Section III. The resultant Bode plot is shown in Fig. 5. The closed loop system response has characteristics of a $1/(s + \tau)$ integral response, with unity gain at low frequencies, a

corner frequency near 0.08 Hz, and a slope near -1 for frequencies above 0.1 Hz.

Like the open loop configuration, modifications made to the polymer's composition, dimensions, or maximum controller output would increase the actuator's response capabilities and shift the curve to the right. For smaller target set-points, the usable operating range would also increase.

B. Non-periodic Set-point Tracking

An arbitrary waveform was also used as a set-point signal to evaluate the strain response over time for non-periodic signals. In Fig. 6 a series of intermittent triangular and DC signals were randomly created to generate an arbitrary set-point target. The total signal output was adjusted so that the target maximum strain remained below 0.5%. The actuator output plot shows the strain following the waveform. Because the system is comparably slow (on the order of seconds), the actuator has time to reach the set-point and maintain tracking. Long-term tracking of DC signals (data not shown) can also be performed under a closed loop configuration.

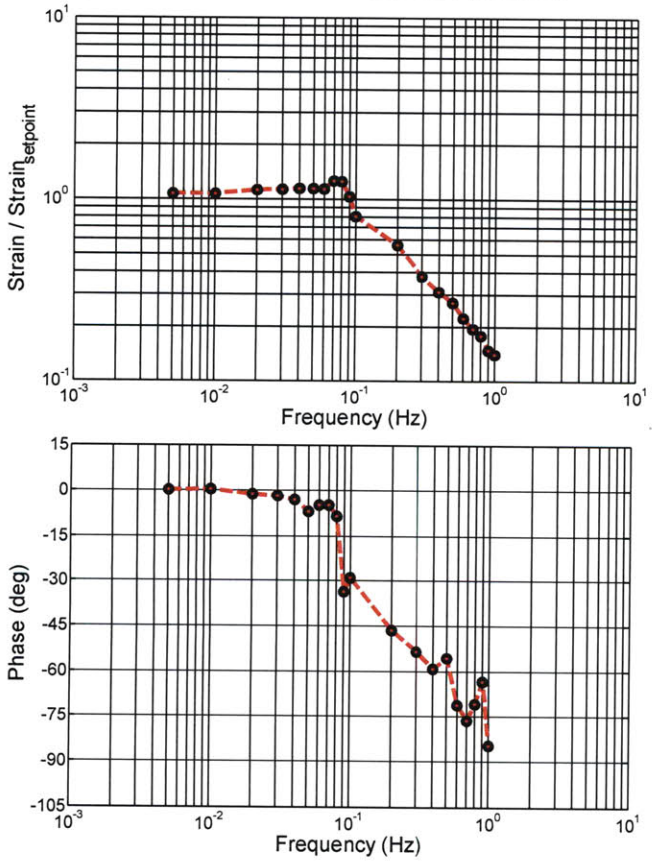

Fig. 5. Closed loop response strain (δ) normalized about the set-point. The data points represent the discrete frequencies tested. The line was drawn using nearest neighbor interpolation.

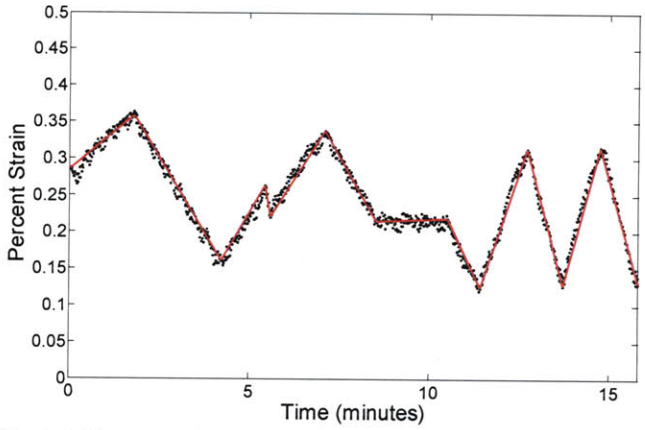

Fig. 6. Arbitrary waveform tracking composed of a series of triangular inputs of various slopes and intermittent sections of DC values. Strain was limited to 0.5% over the total operating range. Potentiostat current was limited to 1 A. The initial strain offset has been removed.

C. Incremental Positioning Resolution

Polypyrrole's closed loop positioning resolution was evaluated by setting the target set-point to a series of 125 nm incremental steps, spaced over 60 second intervals. Data were collected at 1 kHz. Post-process filtering on the LVDT positioning signal was performed using a moving window smoothing average with a window size equal to that of the sampling rate. A small section of steps is shown in Fig. 7.

The incremental response shows both the controller and the polymer actuator are capable of maintaining high positioning resolution where absolute accuracy is important. The step size of 125 nm corresponds to a strain of 0.001%.

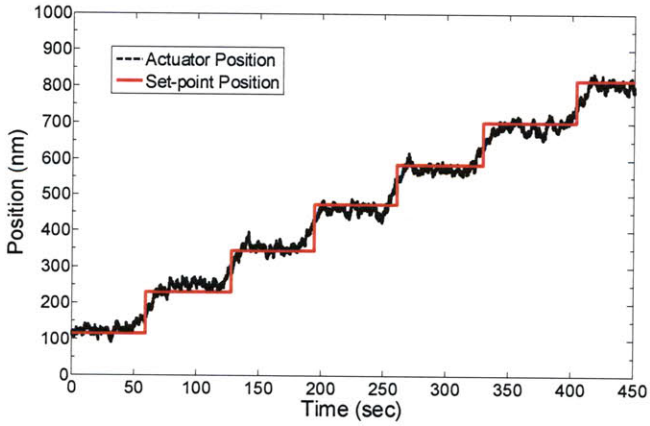

Fig. 7. 125 nm step increments under closed loop control. Set-point and actuator response agreement suggests that high positioning resolution or, slow incremental strains can be generated.

With a maximum displacement of 427 microns (3.6% strain) for the same sample tested at low frequencies, the polypyrrole actuator tested has a dynamic range near 3400. Studies are still ongoing to determine whether or not this resolution is length dependent or is limited by the feedback and processing of the system.

D. Step Responses

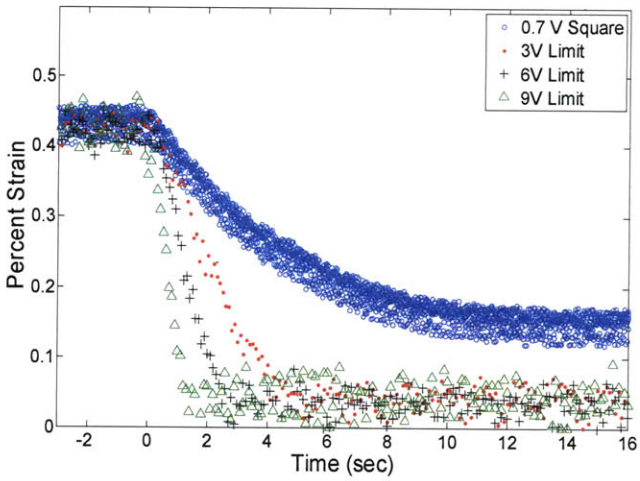

Fig. 8. Polypyrrole closed loop step response at different maximum controller outputs. 0.7 V square is the open loop response. Initial strain offsets have been removed.

The response to a fixed set-point step at various maximum controller voltages was also evaluated to benchmark performance gains in response times of the actuators. Previous studies have shown that relatively high voltage inputs yield fast actuator responses, but at the expense of polymer degradation [12]. Fig. 8 shows the step response of the closed loop system at various maximum controller outputs. For higher maximum controller outputs, the response time is reduced by a factor of 4 between 3 V and 9 V. The difference in responses suggests that the system is not slew-rate limited by the controller itself, but that a non-linearity is introduced by the actuation mechanism of polypyrrole.

V. Discussion

The performance of open and closed loop polypyrrole linear contractile actuators yields several results that can be used as reference when designing or incorporating conducting polymer actuators into robotic applications. The open loop response can be used in part to predict system behavior for the frequency and voltage range tested. Long oscillation times will yield larger strains. As the frequency of the actuator approaches 1 Hz, strain output becomes less useful for any application that requires the actuator to perform work at moderate strains.

In the closed loop configuration, a working bandwidth can be predicted in two ways. First, one can choose a target strain anywhere between the maximum and minimum values of the open loop system. For a smaller target strain, the bandwidth will increase, but at the expense of a limited strain range. Second, one can increase the controller voltage output. This will yield faster actuator response times and therefore a wider bandwidth. Modifying deposition protocols, changing the actuator dimensions, and working with different ionic solutions will also shift the bandwidth in one direction or the other.

Appropriate controller design for polypyrrole actuators will depend on the desired application. For applications where speed is critical, advanced controller design could be exploited to increase the performance metrics in a closed loop system while reducing the temporal exposure of the polypyrrole actuator to higher voltages. For applications where speed is not critical or relatively static set-points exist, an adaptive controller might operate under normal or even lower voltage ranges to conserve power.

The dynamic range of polypyrrole and its ability to output a controllable strain in small increments are useful features for low-cost, precise positioning applications. Whether the positioning resolution of polypyrrole actuators is a function of controller hardware is still being investigated. If it turns out that, like actuator strain, the lower limit of incremental strain is length independent, then scaled versions of linear polypyrrole contractile actuators will have the best of both worlds: larger total displacements without sacrificing the step size.

REFERENCES

[1] Madden, P.G.A., Madden, J.D.W., Anquetil, P.A., Vandesteeg, N.A. and Hunter, I.W., "The relation of conducting polymer actuator material properties to performance," *IEEE Journal of Oceanic Engineering*, vol. 29, no. 3, pp. 696-705, July 2004.

[2] Pytel, R.Z., Thomas, E.L., Chen, Y. and Hunter, I.W., "Anisotropic Actuation of Mechanically Textured Polypyrrole Films," *Polymer*, vol. 49, no. 5, pp. 1338-1349, January 2008.

[3] Tangorra, J.L., Anquetil, P.A., Fofonoff, T., Chen, A.Y., Del Zio, M. and Hunter, I.W., "The Application of Conducting Polymers to a Biorobotic Fin Propulsor," *Bioinspiration and Biomimetics*, vol. 2, June 2007.

[4] Madden J.D.W., Schmid, B., Hechinger, M., Lafontaine, S.R., Madden, P.G.A., Hover, F.S., Kimball, R. and Hunter, I.W., "Application of Polypyrrole Actuators: Feasibility of Variable Camber Foils," *IEEE Journal of Oceanic Engineering 2004*, vol. 29, no. 3, July 2004.

[5] Smela, E., "Conjugated Polymer Actuators for Biomedical Applications," *Advanced Materials*, vol. 15, no. 6, pp. 481-494, March 2003.

[6] Smela, E., Kallenbach, M. and Holdenried, J., "Electrochemically Driven Polypyrrole Bilayers for Moving and Positioning Bulk Micromachined Silicon Plates," *J. Microelectromechanical Systems*, vol. 8, no. 4, pp. 373-383, 1999.

[7] Wu, Y., Zhou, D., Spinks, G.M., Innis, P.C., Megill, W.M. and Wallace, G.G., "A Conducting Polymer Based Microfluidic Pump," *Smart Materials and Structures*, vol. 14, no. 6, 2005.

[8] Smela, E., Inganäs, O., Pei, Q. and Lundström, I., "Electrochemical muscles: micromachining fingers and corkscrews," *Advanced Materials*, vol.5, pp. 630-632, April 1993.

[9] Takashima, W., Pandey, S. and Kaneto, K., "Investigation of bi-ionic contribution for the enhancement of bending actuation in polypyrrole film," *Sensors and Actuators B*, vol. 89, no. 1-2, pp. 48-52, March 2003.

[10] Yao, Q., Alici, G. and Spinks, G.M., "Feedback control of tri-layer polymer actuators to improve their positioning ability and speed of response," *Sensors and Actuators A: Physical*, vol. 144, Issue 1, pp. 176-184, May 2008.

[11] Madden, J.D., Rinderknecht, D., Anquetil, P.A. and Hunter, I.W., "Creep and cycle life in polypyrrole actuators," *Sensors and Actuators A: Physical*, vol. 133, Issue 1, pp. 210-217, January 2007.

[12] Madden, J.D., Cush, R.A., Kanigan, T.S. and Hunter, I.W., "Fast contracting polypyrrole actuators," *Synthetic Metals*, vol. 113, no. 12, pp. 185-192, June 2000.
[13] Spinks, G.M., Truong, V.T., "Work-per-cycle analysis for electromechanical actuators," *Sensors and Actuators A: Physical*, vol. 119, no. 2, December 2005.
[14] Vandesteeg, N., "Synthesis and characterization of conducting polymer actuators," Ph.D. dissertation, Dept. of Materials Science and Engineering, Massachusetts Institute of Technology, Cambridge, MA 2007.
[15] Pytel R., Thomas E. and Hunter I., "Anisotropy of Electroactive Strain in Highly Stretched Polypyrrole Actuators," *Chemistry of Materials*, vol. 18, no. 4, 2006.
[16] Kaneto, K., Fujisue, H., Kunifusa, M. and Takashima, W., "Work behaviors of artificial muscle based on cation driven polypyrrole," *Smart Materials and Structures*, vol. 16, no. 2, June 2007.
[17] Pytel, R.Z., Thomas, E.L. and Hunter, I.W., "In situ observation of dynamic elastic modulus in polypyrrole actuators," *Polymer*, vol. 49, pp. 2008-2013, January 2008.
[18] Madden, P.G., Madden, J.D. and Hunter, I.W., "Parallel Electrochemical Methods to Accelerate Electroactive Material Discovery and Optimization," *Mat. Res. Soc. Symp. Proc.*, vol. 698, 2002.
[19] Fofonoff, T., "Fabrication and Use of Conducting Polymer Linear Actuators," Ph.D. dissertation, Dept. of Mechanical Engineering, Massachusetts Institute of Technology, Cambridge, MA 2008.

Chapter 8 Multi-Component Integration

8.1 Introduction

This chapter is an integration of Chapter 4 through Chapter 7. Conducting polymer actuators, length sensors, and supercapacitors have been evaluated in Chapter 4 through Chapter 6. Here the fabrication technologies developed in Chapter 7 are applied to these components. The resultant performance of polypyrrole actuators as a function of fabrication process is discussed. Multi-component integration is also presented, where conducting polymer actuators and length sensors operate in series and in parallel. A tri-component system in which a conducting polymer length sensor measures the strain of a conducting polymer actuator whilst being powered by several conducting polymer supercapacitors is also shown.

8.2 Fabrication Effects on Actuator Performance

The methods of mechanically joining and electrically insulating conducting polymer materials, as presented in Chapter 7, worked to various degrees of success. Polyimide emerged as the most viable candidate as an inter-component adhesive and insulator. The other technologies could still be used for less demanding tasks, such as encapsulation from contaminants. Therefore, polypyrrole actuator performance was evaluated for each respective fabrication technique.

Figure 70 shows the strain comparison of an untreated polypyrrole actuator in comparison to a polypyrrole actuator subject to a vacuum environment of 0.8 Pa for 1 hour. The results show that extended vacuum exposure does degrade the performance of the actuator

slightly. Vacuum environments were used for both polystyrene and Parylene depositions. In Figure 70, a ~20% degradation in strain is visible. For polypyrrole substrates actually treated with polystyrene or Parylene, the degradation was nearly 95% (data not shown). Both plasma-aided polystyrene and Parylene depositions are done through a vaporization process. One possible explanation for why they caused large strain reductions is that during the deposition process, the vaporized polystyrene or Parylene heated the polypyrrole samples significantly upon contact, thereby subjecting the samples to large heat fluxes for extended periods of time.

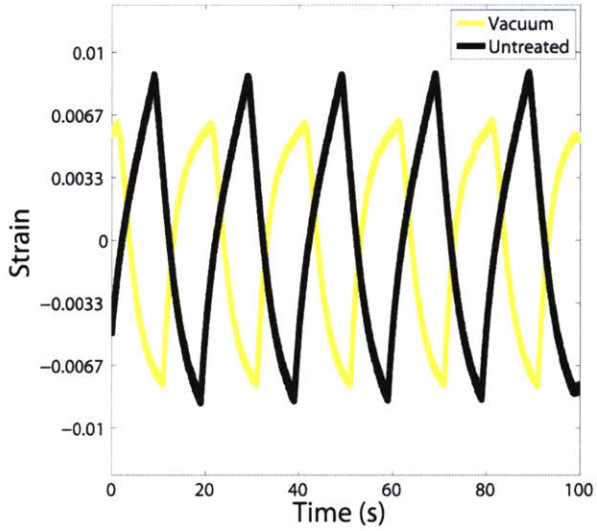

Figure 70: Strain comparison of polypyrrole actuators when subject to vacuum treatment (0.8 Pa; 1 h).

Heat alone, for example, also significantly affects actuator performance. As polyimide cures during a soft bake at 110°C, polypyrrole actuators were held at the same temperature for 15 minutes to simulate curing conditions. Figure 71 shows nearly a 50% reduction in strain output for actuators subject to a 110°C environment. While heat itself may not be degrading the polymer backbone (as discussed in Chapter 4), it does have a significant effect on polypyrrole's ability to actuate.

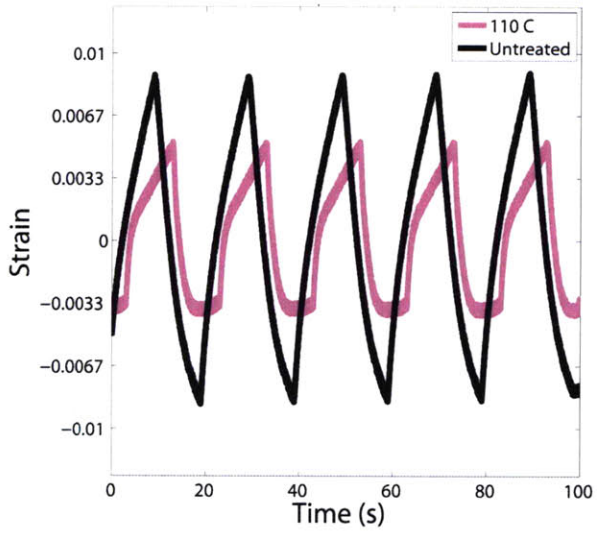

Figure 71: Strain comparison of polypyrrole actuators when subject to heat treatment (110 °C, 15 minutes).

Localized heating, on the other hand, shows significantly better results. The plots in Figure 72 show the strain output of a polypyrrole actuator that was locally attached to two strips of polyimide. The strain reduction from localized heating is still significant, but shows improvement over heating the entire polymer.

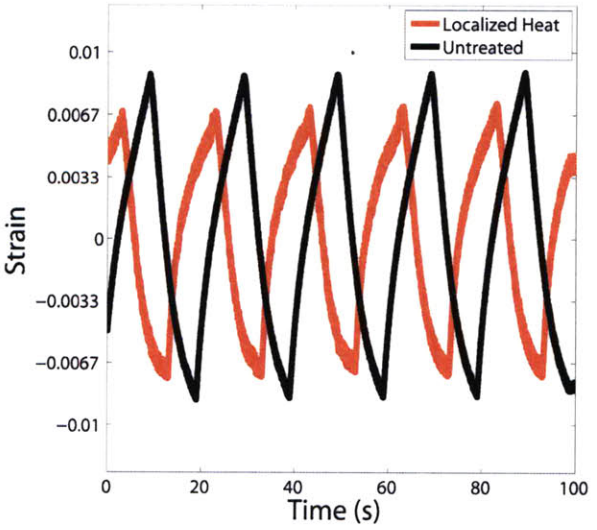

Figure 72: Strain comparison of polypyrrole actuators when subject to localized treatment (110°C applied to out 5 mm of a 20 mm actuator).

Finally, a thick (20 μm) polyimide membrane was attached to the back of a polypyrrole actuator. Figure 73 shows the resultant strain output, compared to an untreated actuator. The drastic reduction in strain can be attributed to two effects: the added mechanical impedance placed on the actuator by the polyimide backing, and, the reduced surface area that the polypyrrole actuator was exposed to electrolyte.

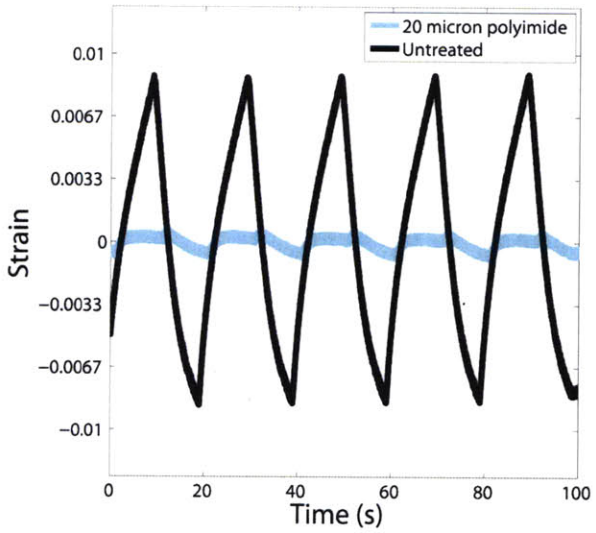

Figure 73: Strain comparison of polypyrrole actuators when attached to a 20 μm polyimide backing.

8.3 Coupled Polypyrrole Actuators and Length Sensors

Coupled polypyrrole actuators and length sensors were tested in three different configurations (stacked, parallel, and series), corresponding to the proposed geometries presented in previous chapters.

A stacked polypyrrole actuator, insulator, and length sensor, identical to the fabrication protocol shown in Figure 64 was tested. One particular issue associated with this design is that the length sensor must be immersed within the electrolyte. During actuation, when currents are maintained between the counter electrode and the working electrode, the polypyrrole length

sensor and the associated signal conditioning amplifier become convoluted with these signals. In order to determine the strain from the length sensors, therefore, the current within the electrochemical cell must be de-convoluted from the signal output of the polypyrrole length sensor. This was done in Figure 74, where a stack of the polypyrrole actuator and length sensor is shown operating in parallel. A major drawback of this configuration is that strain must be determined offline (after computational processing), in order to deconvolve the signals. With the goal of creating a robust, simple, conducting polymer actuation system, these added computational requirements eliminated this design from being further explored.

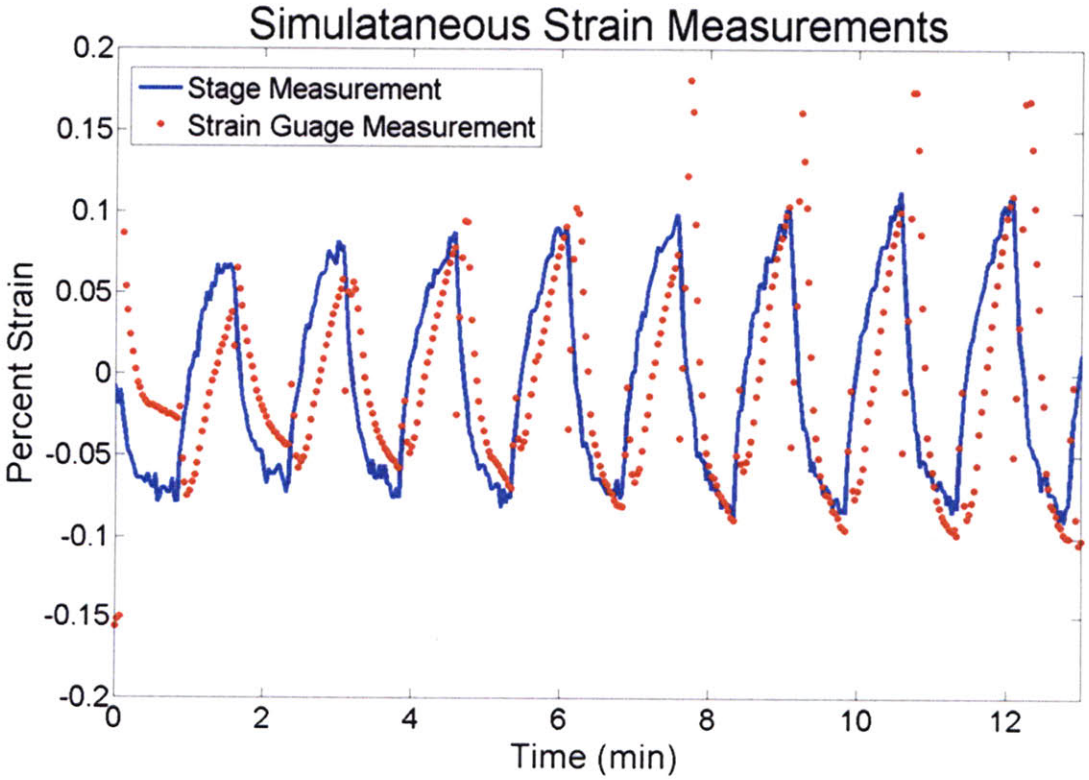

Figure 74: Simultaneous strain and actuator from a stacked, polypyrrole length sensor and actuator positioned in parallel to one another.

A second possibility is to fabricate polypyrrole actuators and length sensors in parallel, but keep the length sensor outside of the electrolyte bath. The parallel-coupled actuator and

length sensors shown in Figure 62 were tested under these conditions, where special clamps were fabricated to keep the length sensor out of the electrolyte bath. Simultaneous strain measured by the LVDT and the length sensor is shown in Figure 75. In this configuration, no additional signal processing was necessary to determine the strain, making this one suitable solution to operating actuators and length sensors in parallel.

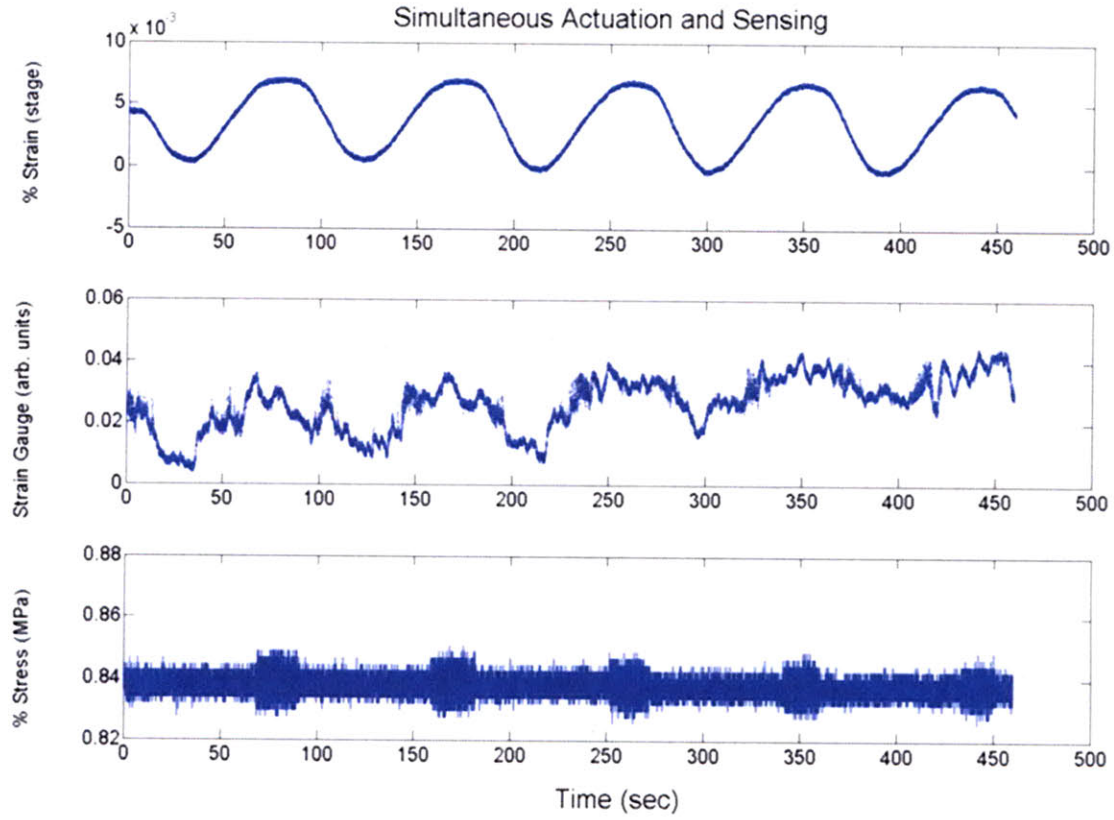

Figure 75: Simultaneous strain and actuation from a lateral, polypyrrole length sensor and actuator, positioned in parallel to one another.

A third configuration involves attaching polypyrrole actuators and length sensors in series. Technically, the length sensor is now operating like the Golgi Tendon Organs, measuring tension. If the length sensor is sufficiently compliant, however, with respect to the actuator, and the two are of similar size, then the length sensor can be used to measure changes in actuation strain while at the same time, keeping the muscle under tension. The simultaneous actuation and

strain measurement under a configuration like that of Figure 65 is shown in Figure 76. While the results of this configuration are not markedly better than the previous two, the feasibility of implementing such a design is much greater because components in and out of the electrolyte bath can be separated more easily.

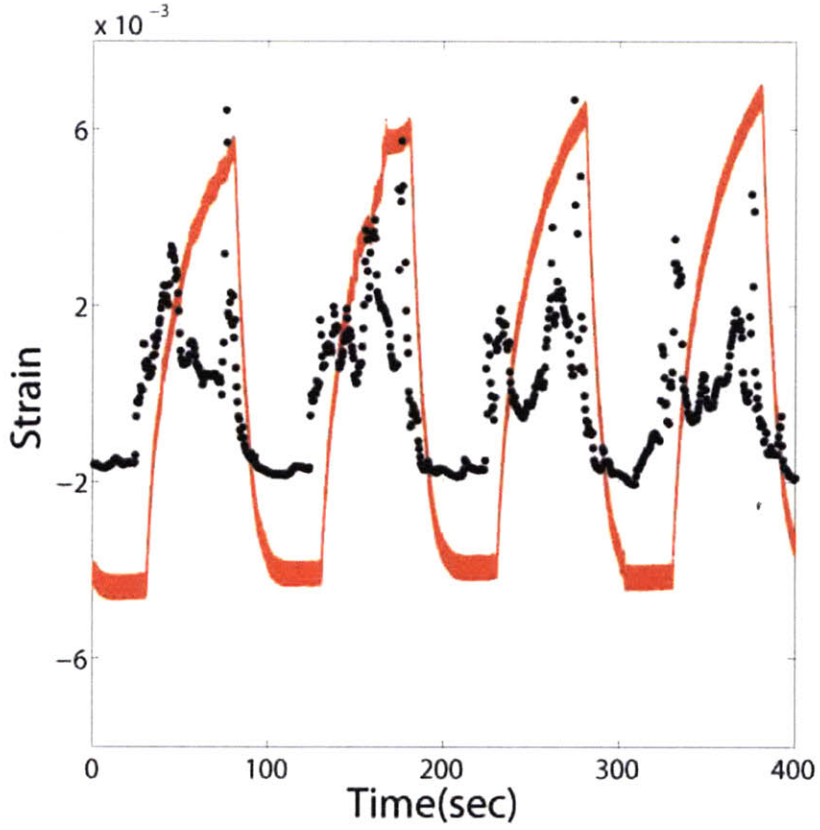

Figure 76: Simultaneous strain and actuator from a polypyrrole length sensor and actuator attached together in series.

8.4 Coupled Polypyrrole Actuators, Length Sensors, and Supercapacitors

In building on the previous section, actuators that were powered by polypyrrole supercapacitors were combined with polypyrrole length/tension sensors acting in series. Figure 77 shows the results of this system. From the plots, one notices that polypyrrole supercapacitors

have sufficiently high power densities to drive polypyrrole actuators. The polypyrrole length sensors, while still inherently noisy, measure the change in strain that the actuator undergoes over time.

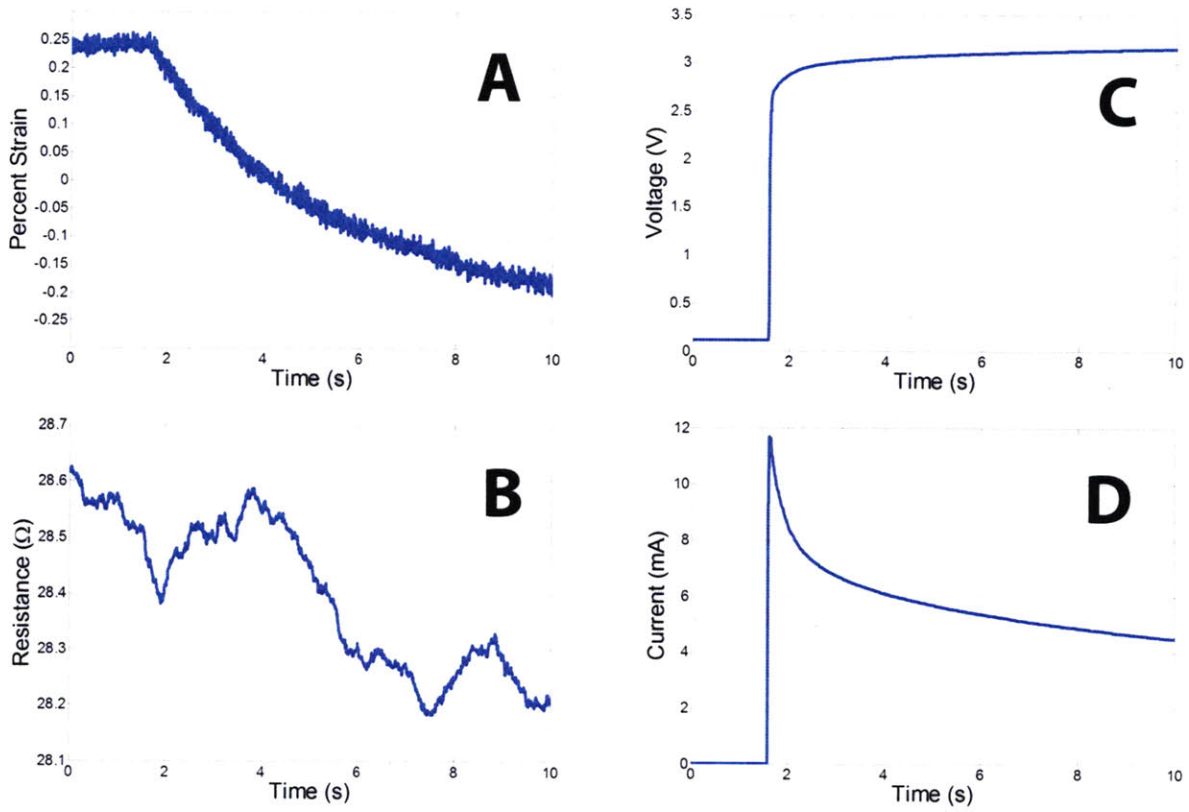

Figure 77: Multi-component, all polymer actuation system performance. A polypyrrole capacitor actuates (A) while its strain is measured with a polypyrrole length sensors (B). The polypyrrole actuators is being powered by several polypyrrole supercapacitors, whose voltage (C) and current (D) are shown during actuation.

Conclusion

Polypyrrole is a multi-functional material that can be used to build artificial muscle actuation systems. From the strain characterization presented in this work, polypyrrole actuators can produce measurable strains up to 60 Hz and strain rates as high as 8.3%/s. Polypyrrole length sensors can consistently measure changes in length over the same range of frequencies over which polypyrrole actuators operate. The stability of the length sensor measurements at the moment excludes them from being used as steady-state length sensors. Polypyrrole length sensors, however, make excellent candidates for dynamic length sensors. Polypyrrole supercapacitors can provide capacitances up to $2.5 \cdot 10^5$ F/kg, energy densities as high as 18 kJ/kg, and power densities as high as 10 kW/kg. These metrics are more than sufficient for powering polypyrrole actuation systems. Finally, fabrication techniques developed in this work shown means by which polypyrrole components can be mechanically attached and electrically insulated to form complex, three dimensional conducting polymer actuation systems. These three dimensional systems have been shown operating simultaneously, thereby developing a framework for constructing future, multi-component, conducting polymer artificial muscle actuation systems that can operate under open and closed loop control.

Though the ultimate goal of fabricating artificial muscle actuation systems equivalent to mammalian skeletal muscle is still looming on the horizon, many steps, past and present, bring us closer to realizing this target. Improving polypyrrole actuators is a continuous endeavor. With improvements in electrochemical synthesis, the actuation speed and strain of polypyrrole actuators will continue to increase. Higher voltage actuation (> 10 V) and galvanostatic

actuation techniques should be explored, to increase these metrics. Polypyrrole length sensors work suitably for dynamic length sensors, yet an optimal geometry for optimizing strain resolution has yet to be investigated, and system noise still needs to be reduced. Polypyrrole supercapacitors, while showing exceptional promise for polypyrrole and non-polypyrrole power systems, requires that future work improve the self-discharge characteristics and increase energy density.

The future of conducting polymer research involves a broad look into the past 30 years of research, along with the need for radical, bottom-up molecular approaches to harnessing chemical systems that store energy, actuate, and measure. Today, conducting polymers lie at the center of this work. Someday, they may be found at the center of our daily lives.

References

[1] Hunter, I. W. and LaFountaine, S. A comparison of muscle with artificial actuators. *IEEE Solid-State Sensor Actuator Workshop*, (pp. 178-165), 1992.

[2] Rome, L. C. Design and function of superfast muscles: New insights into the physiology of skeletal muscle. *Annual Review of Physiology*, 68 : 193-221, 2006.

[3] Josephsen, R. K. and Young, D. A synchronous insect muscle with an operating frequency greater than 500 Hz. *Journal of Experimental Biology*, 118, 1 : 185-208, 1985.

[4] Hunter, I. W., Doukoglou, T. D., Lafontaine, S. R., Charette, P. G., Jones, L. A., Sagar, M. A., Mallinson, G. D. and Hunter, P. J. A teleoperated microsurgical robot and associated virtual environment for eye surgery. *Presence*, 4 : 265-80, 1993.

[5] Pelrine, R., Kornbluh, R. and Kofod, G. High-strain actuator materials based on dielectric elastomers. *Advanced Materials,* 16 : 1223-5, 2000.

[6] Hunter, I. W., Lafontaine, S., Hollerbach, J. M. and Hunter, P. J. Fast reversible niti fibers for use in microrobotics. *IEEE Micro Electro Mechanical Systems*: 166-70, 1991.

[7] Boothroyd, G. Assembly automation and product design. *Manufacturing engineering and materials processing*. 2nd ed. Vol. 66. Boca Raton, FL: Taylor & Francis/CRC Press, 2005.

[8] Madden, J., Madden, P., Anquetil, P., Yu, H., Swager, T., and Hunter, I. Conducting Polymers as Building Blocks for Biomimetic Systems. *Materials Research Society Symposium Proceedings*, 2001.

[9] Bloom, W. and Fawcett, D. W. *A textbook of histology*. 10th ed. Philadelphia: Saunders, 1975.

[10] Kandel, E. R. and Schwartz, J. H. *Principles of neural science*. New York: Elsevier North Holland, 1981.

[11] Jennett, S. *Human physiology*, Churchill Livingstone, 1989.

[12] Binder, M. D. and Mendell, L. M. *The segmental motor system*. New York: Oxford University Press, 1990.

[13] Kabsch, W., Mannherz, H. G., Suck, D., Pai, E. F. and Holmes, K. C. Atomic structure of the actin: DNase I complex. *Nature*. 347, 6288: 44, 1990.

[14] Rayment, I., Holden, H. M., Whittaker, M., Yohn, C. B., Lorenz, M., Holmes, K. C. and Milligan, R. A. Structure of the actin-myosin complex and its implications for muscle contraction. *Science*. 261, 5117: 58-65, 1993.

[15] Huxley, A. F. and Simmons, R. M. Proposed mechanism of force generation in striated muscle. *Nature*. 233, 5321 : 538, 1971.

[16] Boyd, I. A. The isolated mammalian muscle spindle. *Trends in Neurosciences.* 3 : 258-65, 1980.

[17] Schmidt, R. F. and Thews, G. *Human physiology*. Berlin, New York: Springer-Verlag, 1983.

[18] Crago, P. E., Houk, J. C. and Rymer, W. Z. Sampling of total muscle force by tendon organs. *Journal of Neurophysiology.* 47 (6): 1069-83, 1982.

[19] Shirakawa, H., Louis, E. J., MacDiarmid, A. G., Chiang, C. K. and Heeger, A. J. Synthesis of electrically conducting organic polymers: Halogen derivatives of polyacetylene,(CH) x. *Journal of the Chemical Society, Chemical Communications*. 16: 578-80, 1977.

[20] Heeger, A. J., MacDiarmid, A. G., and Shirakawa, H. Nobel prize in chemistry 2000. The Nobel Foundation, 2000.

[21] Zotti, G., Schiavon, G. and Comisso, N. Anion effects on conductivity of isomorphous polypyrrole charge pinning by nucleophilic anions. *Synthetic Metals*. 40, 3: 309-16, 1991.

[22] Kaynak, A. Effect of synthesis parameters on the surface morphology of conducting polypyrrole films. *Materials Research Bulletin*. 32, 3: 271-85, 1997.

[23] Joo, J., Oblakowski, Z., Du, G., Pouget, J. P., Oh, E. J., Wiesinger, J. M., Min, Y., MacDiarmid, A. G. and Epstein, A. J. Microwave dieletric response of mesoscopic metallic regions and the intrinsic metallic state of polyaniline. *Physical Review B*. 49 (4): 2977-80, 1994.

[24] Pytel, R. Z. *Artificial muscle morphology: Structure/property relationships in polypyrrole actuators.* PhD Thesis, Massachusetts Institute of Technology, 2007.

[25] Vandesteeg, N. A. *Synthesis and characterization of conducting polymer actuators*. PhD Thesis, Massachusetts Institute of Technology, 2007.

[26] Pei, Q. and Qian, R. Protonation and deprotonation of polypyrrole chain in aqueous solutions. *Synthetic Metals*. 45 (10): 35-48, 1991.

[27] Saez, M. A. *Fabrication and Characterization of Conducting Polymer Microwires.* SM Thesis, Massachusetts Institute of Technology, 2009.

[28] Ge, D., Wang, J., Wang, Z. and Wang, S. Electrochemical synthesis of polypyrrole nanowires on composite electrode. *Synthetic Metals.* 132, (1): 93-5, 2002.

[29] Madden, J. D. W. *Conducting polymer actuators*, PhD Thesis. Massachusetts Institute of Technology, 2000.

[30] Chen, M. Printed electrochemical devices using conducting polymers as active materials on flexible substrates. *Proceedings of the IEEE.* 93 (7): 1339-47, 2005.

[31] Chen, M., Nilsson, D., Kugler, T., Berggren, M. and Remonen, T. Electric current rectification by an all-organic electrochemical device. *Applied Physics Letters.* 81 (11): 2011-3, 2002.

[32] Skotheim, T. A. and Reynolds, J. R. *Handbook of conducting polymers.* CRC Press. 2007.

[33] Tangorra, J., Anquetil, P., Fofonoff, T., Chen, A., Zio, M. D. and Hunter, I. The application of conducting polymers to a biorobotic fin propulsor. *Bioinspiration & Biomimetics.* 2: S6. 2007.

[34] Carpi, F. and Smela, E. *Biomedical applications of electroactive polymer actuators.* Chichester, West Sussex: John Wiley & Sons, 2009.

[35] Tendick, F., Sastry, S. S., Fearing, R. S. and Cohn, M. Applications of micromechatronics in minimally invasive surgery. *IEEE/ASME Transactions on Mechatronics.* 3 (1): 34-42, 1998.

[36] Madden, J. D., Cush, R. A., Kanigan, T. S. and Hunter. I. W. Fast contracting polypyrrole actuators. *Synthetic Metals.* 113, (1): 185-92, 2000.

[37] Madden, P. G. A. *Development and modeling of conducting polymer actuators and the fabrication of a conducting polymer based feedback loop*, PhD Thesis. Massachusetts Institute of Technology, 2003.

[38] Chen, A. Y. *Large displacement fast conducting polymer actuators*, SM Thesis. Massachusetts Institute of Technology, 2006.

[39] Schmid, B. D. *Characterization of macro-length conducting polymers and the development of a conducting polymer rotary motor*, SM Thesis. Massachusetts Institute of Technology, 2005.

[40] Fofonoff, T. A. *Fabrication and use of conducting polymer linear actuators*, PhD Thesis. Massachusetts Institute of Technology, 2008.

[41] Madden, J. D., Rinderknecht, D., Anquetil, P. A. and Hunter, I. W. Creep and cycle life in polypyrrole actuators. *Sensors and Actuators A: Physical.* 133 (1): 210-7, 2007.

[42] Keng, Y. *The Effects of Temperature and Carbon Nanotubes on Conducting Polymer Actuator Performance.* SM Thesis. Massachusetts Institute of Technology, 2010.

[43] Keng, Y., Pillai, P. V. and Hunter, I. W. The effect of ion delivery on polypyrrole strain and strain rate under elevated temperature. *Materials Research Society Symposium Proceedings*. 1222-DD02-10, 2010.

[44] Skaarup, S., Bay, L. and West, K. Polypyrrole actuators working at 2-30 Hz. *Synthetic Metals*. 157, (7): 323-6, 2007.

[45] John, S., Alici, G. and Cook, C. Frequency response of polypyrrole trilayer actuator displacement. *Proc. SPIE.* 69271T, *2008*.

[46] Pillai, P. V. Massachusetts Institute of Technology. 2007. *Conducting polymer actuator enhancement through microstructuring*, SM Thesis. Massachusetts Institute of Technology, 2007.

[47] Spinks, G. M., Liu, L., Wallace, G. G. and Zhou, D. Strain response from polypyrrole actuators under load. *Advanced Functional Materials*. 12 (7): 437-40, 2002.

[48] Hunter, I. W., Lafontaine, S. R., Brenan, C. J. H. and Jones, L. A. Medical robots and micro machines. *Micro Machine and Human Science*, 1995.

[49] Wiedenman, N. *Towards programmable materials-tunable material properties through feedback control of conducting polymers*, PhD Thesis. Massachusetts Institute of Technology, 2008.

[50] Hashmi, S. A., Kumar, A. and Tripathi, S. K. Investigations on electrochemical supercapacitors using polypyrrole redox electrodes and PMMA based gel electrolytes. *European Polymer Journal*. 41 (6): 1373-9, 2005.

[51] Hashmi, S. A., Latham, R. J., Linford, R. G. and Schlindwein, W. S. Conducting polymer-based electrochemical redox supercapacitors using proton and lithium ion conducting polymer electrolytes. *Polymer International*. 47 (1): 28-33, 1998.

[52] Sivakkumar, S. R., Ko, J. M., Kim, D. Y., Kim, B. C. and Wallace, G. G. Performance evaluation of CNT/polypyrrole/MnO2 composite electrodes for electrochemical capacitors. *Electrochimica Acta*. 52 (25): 7377-85, 2007.

[53] Kelly, T. L., Yano, K. and Wolf, M. O. Supercapacitive properties of PEDOT and carbon colloidal microspheres. *Acs Applied Materials & Interfaces*. 1 (11): 2536-43, 2009.

[54] An, H. F., Wang, X. Y., Li, N., Zheng, L. P. and Chen, Q. Q. Carbon and conducting polymer composites for supercapacitors. *Progress in Chemistry*. 21 (9): 1832-8, 2009.

[55] Mi, H. Y., Zhang, X. G., Xu, Y. L. and Xiao, F. Synthesis, characterization and electrochemical behavior of polypyrrole/carbon nanotube composites using organometallic-functionalized carbon nanotubes. *Applied Surface Science*. 256 (7): 2284-8, 2010.

[56] van Schalkwijk, W. A. and Scrosati, B. *Advances in lithium-ion batteries*. Plenum Pub Corp. 2002.

[57] Conway, BE. *Electrochemical supercapacitors: Scientific fundamentals and technological applications.* Kluwer Academic/Plenum Publishers, 1999.

[58] Yamaura, M., Sato, K., Hagiwara, T. and Iwata, K. Memory effect of electrical conductivity upon the counteranion exchange of polypyrrole films. *Synthetic Metals*. 48 (3): 337-54, 1992.

[59] Hagiwara, T., Hirasaka, M., Sato, K. and Yamaura, M. Enhancement of the electrical conductivity of polypyrrole film by stretching: Influence of the polymerization conditions. *Synthetic Metals.* 36 (6): 241-52, 1990.

[60] Tripathi, S. K., Kumar, A. and Hashmi, S. A. Electrochemical redox supercapacitors using PVdF-HFP based gel electrolytes and polypyrrole as conducting polymer electrode. *Solid State Ionics*. 177 (34): 2979-85, 2006.

[61] Muthulakshmi, B., Kalpana, D., Pitchumani, S. and Renganathan, N. G. Electrochemical deposition of polypyrrole for symmetric supercapacitors. *Journal of Power Sources* 158 (2): 1533-7, 2006.

[62] Rudge, A., Davey, J., Raistrick, I., Gottesfeld, S. and Ferraris, J. P. Conducting polymers as active materials in electrochemical capacitors. *Journal of Power Sources* 47 (2): 89-107, 1994.

Appendix

LabVIEW Block Diagrams

High Frequency Test Apparatus Operating Code

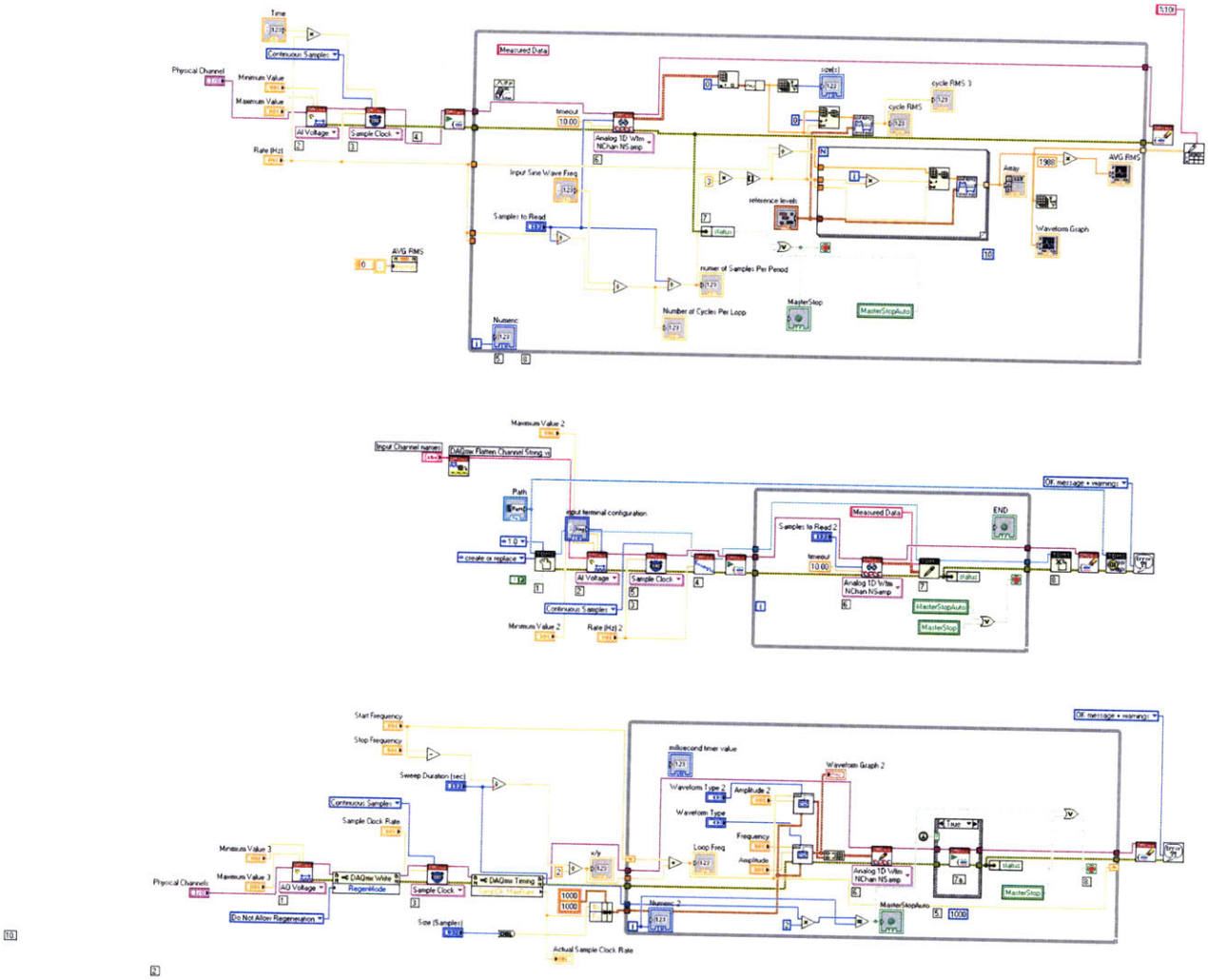

Closed-Loop Test Apparatus Operating Code: